NDKB and Atlastin Structure Endoplasmic Reticulum Membranes

A dissertation submitted to the faculty of Carnegie Mellon University

By

Jeanne Morin-Leisk

In partial fulfillment of the requirements for the degree of Doctor of Philosophy

Carnegie Mellon University

Department of Biological Sciences

Pittsburgh, Pennsylvania

14th November, 2011

Thesis Advisor: Tina H. Lee, Ph.D.

This page left blank on purpose

For my sisters Lili and Cami

Table of Contents

Acknowledgements

My friend and mentor Mark Steckle told me as I was entering graduate school that the single most reliable predictor of my quality of life would be how good a fit my advisor was. He was absolutely right. Tina Lee has been an unimaginably good fit for me. She is an enthusiastic scientist and I have learned how to think, create, and execute experiments from her and I look forward to depending on these lessons forever. I am truly fortunate and grateful to have had such a rich environment to grow in. As I look forward to a post-doctoral position, I hope to find a lab and PI that has even a fraction of the true scientific capability and spirit as Tina's does.

Although in the beginning Tina's lab was small, I have found that as it grew I gained not only in labmates, but also in friends. Kaitlyn, Jaqueline, Sim and Idil have all proved to be dear friends and solid scientists. Their unconditional support, advice, and friendship have gone a long way towards enriching my life and making me a better scientist.

Special thanks go to Adam Linstedt and Debrup Sengupta who made my first rotation a success, initiated my affection for membranes, and who have had consistent and insightful input. Similarly, thank you to the other members of the Linstedt lab especially Smita, Collin, Tim, Cas and Som for their expertise and friendship. Likewise, thanks go to Manoj Puthenveedu and the members of his lab for their advice and critical input. Importantly Manoj Puthenveedu, Mark Macbeth, and Joe Suhan have been inexhaustible technical resources for microscopy, 3D protein analysis, and electron microscopy respectively, and I am grateful for their patient and expert tutelage.

Thank you to my committee members: Adam Linstedt, Tina Lee, Mark Macbeth and especially Meir Aridor, my outside committee member. All of them have had important roles in my growth as a scientist and without them I would not have this opportunity.

My family was the original support system and experimental playground for me and I can say with confidence that without them I would not be where I am. My parents, Camille and William, made science fun in every way - from identifying fresh fish guts to analysis of kitchen 'experiments'. And fortunately for me, my parents executed a few major genetic experiments that resulted in me having two amazing sisters. My roommate and sister Lili has been essential in my success from the beginning. We ran many important experiments together addressing such things as what one would look like without all their hair and what it takes to buy a house. Without her I would always have to do my own dishes, even when I was writing a thesis, and I would never have gotten to realize the dream of being grown-ups together. It is even better than I imagined. Although not residing with us, our younger sister Cami is always in my thoughts and her unflappable faith in me along with a heavy dose of kind words and prescient advice has been a reliable bright spot in my days. Younger in years she may be, but I will always look up to her and strive to match her especially in kindness, compassion and creativity.

My dear friends, especially Jessi Board, Wade Znosko, Sandlin Seguin, Matt Sequin, John Holleran, Katie Holleran, and Biz Hollingdrake have been exceptional resources to me scientifically and personally and there is not enough expressed in a 'Thank You' to suffice, but it will have to do for now.

Abstract

Of the membrane bound organelles in eukaryotic cells, the endoplasmic reticulum (ER) may be the most complex. It is the largest both in terms of surface area and volume. It includes several subdomains: the nuclear envelope (NE) as well as an extensive network of both highly inter-connected fenestrated tubular membranes and flat cisternal sheets (1, 2). While the structure and organization of the ER is thought to be important for the execution of a myriad of essential cellular functions including protein and lipid synthesis and export as well as calcium sequestration and drug metabolism (3), how this membrane system is generated and maintained despite continuous turnover is only just beginning to be unraveled (4). The microtubule cytoskeleton and molecular motors are clearly important for the extension of tubules from the existing network so that they may fuse with nearby ER tubules to generate new three-way junctions (5-8). However, an ER-like network can be generated in vitro in the absence of microtubules (9), which suggests the existence of additional mechanisms for the extension and scaffolding of the ER network. Once the tubular ER does extend out from the existing network the next critical step is fusion. Soluble NSF attachment-protein receptors (SNAREs) were an obvious candidate for this role (10), but ER homotypic fusion events have not yet been found to depend on SNAREs. Recently, a member of the dynamin super-family of large GTPases, atlastin, was implicated in ER homotypic fusion. An in vitro fusion assay (11) and knockdown experiments (12) in conjunction with the crystal structures of the soluble domains of atlastin (13, 14) have led to a possible mechanism of ER fusion, but this model remains to be tested. In my thesis I will describe two projects. One focuses on the role and mechanism of nucleoside diphosphate kinase B (NDKB) in ER network extension and stabilization. The other focuses on the role and mechanism of atlastin in fusing ER membranes.

NDKB was initially implicated as a stimulator of ER export in permeabilized cells (15). Subsequent work suggested that its effect on ER export might be through an effect on ER network morphology. Through in vitro assays, we found that NDKB not only stabilizes the ER network but also actively promotes ER network extension. In order to perform this function we hypothesized that it might interact directly with ER membranes. Indeed, we found a pair of positively charged residues that mediated direct binding of NDKB to anionic phospholipids. When these residues ware mutated to negatively charged residues, NDKB no longer bound anionic phospholipids and failed to mediate ER extension in our semi-intact cell assay. In order

to gain insight into the mechanism for how NDKB might be performing its ER network extension function we took another in vitro approach. Anionic synthetic liposomes were incubated with NDKB and we found that NDKB was able to arrange these liposomes into large arrays that resembled the ER network. Together these results implicate NDKB and anionic phospholipids in a role for ER network morphology, in particular as a means to stabilize and extend the ER network.

We initially became interested in the atlastin GTPase as a result of an ER overexpression phenotype observed by the Blackstone lab indicating a potential role in ER morphogenesis (16). In strong support for a required role for atlastin in ER structuring, we found that siRNA depletion of atlastin from HeLa cells resulted in a reduction in network density which could be rescued by the addition of an siRNA immune atlastin transgene. This established a structure function assay we could use to dissect the functional domains of atlastin. Concurrent with our identification of key residues required for atlastin function, it was observed by another lab that atlastin could fuse synthetic liposomes (11), suggesting that the ER structuring role we had observed for atlastin might correspond to the membrane fusion step. Simultaneously, structure determinations for the soluble domain of atlastin were reported (13, 14). Together, the collective data suggested the following model for atlastin: GTP dependent dimerization of atlastin leads to tethering and subsequent GTP hydrolysis leads to a large conformational change that drives membrane fusion (13, 14). To test the model, we exploited our identification of a required salt bridge central to the large conformational change proposed to convert GTP-bound tethered atlastin dimers into a postfusion state. We established that although blocking the salt bridge had no effect on GTP binding and hydrolysis, it abolished stable atlastin dimer formation. Then, through a series of crosslinking assays probing the conformational state of the atlastin soluble domain, we showed that atlastin adopts the postfusion conformation in the GTP bound state, without the need for GTP hydrolysis. As a result of our studies, we have modified the current model for atlastin's function. In our revised model, GTP binding is required for atlastin's initial dimerization and begins a cascade of conformational changes that results in the large rearrangement thought to drive membrane fusion. We speculate based on our work that hydrolysis may be necessary to complete the fusion cycle and/or function to disassemble the postfusion complex for multiple rounds of fusion.

In summary, these studies provide both an initial analysis of a protein with an ER network extension role and important insights into the mechanism of ER membrane fusion. It is hoped that this work will add to our understanding of the biogenesis and maintenance of the ER network.

List of Figures

Supplemental Figures

Chapter I. Introduction – Endoplasmic Reticulum Structure and Function

Abstract

The endoplasmic reticulum (ER) is the largest membrane-bound compartment in eukaryotic cells (1). Extending from the nuclear envelope all the way to the plasma membrane, the organelle covers a large cytosolic space which can account for more than 10% of the total cell volume (2). The large size of the ER may reflect the fact that it is the site of a myriad of important cellular functions (supported by a large fraction of total cell protein), ranging from protein and lipid biosynthesis and export to calcium regulation and drug metabolism. Each of these processes may function optimally when the membranes adopt a particular shape or surface to volume ratio. For this reason, it is thought that the ER is further compartmentalized into unique architectural subdomains. Even so, the subdomains of the ER are interconnected so the entire organelle has a continuous intralumenal space and continuity of the membrane is maintained. This may be important for ensuring rapid diffusion of macromolecules and solutes within ER subdomains that may be separated by several or tens of microns (3). Finally, the plastic and dynamic nature of the ER allows it to undergo continuous re-arrangement in order to maintain a constant ER network morphology and organization despite changing cellular conditions (4). How exactly each unique structure of the ER subdomains is achieved, interconnected, and coupled to its functions has yet to be completely unraveled.

Most broadly, the ER can be divided up into the membrane sheets that make up the nuclear envelope (NE) and the peripheral ER, which includes the membrane sheets and tubules that extend out from the NE (reviewed in 2&29). Following is a brief examination of the various important functions and structures of the ER.

1.1 Nuclear Envelope

The NE has a number of features that distinguish it from the peripheral ER. Both membrane leaflets that compose the NE, the inner and outer nuclear membranes (INM and ONM respectively), have subsets of proteins that specifically function at the INM or ONM (30). Over 60 NE trans-membrane proteins have been identified. While not all of the functions of these proteins have been elucidated fully, many of them have been shown to interact directly with chromatin and/or the nuclear lamina (31).

The nuclear lamina, composed of polymerized lamin proteins, underlies the NE and is critical for its architecture (32). Some important INM integral membrane proteins such as emerin, MAN1, LBR, lamina-associated polypeptides-1 and -2β (LAP1, LAP2β) and nesprin-1α bind directly to lamins and in this way are likely to be essential for maintaining NE shape by associating the NE with the underlying laminar meshwork (33, 34). A few other proteins have been proposed to link together the nuclear lamina, the INM and the ONM through the NE lumen. These proteins include UNC-84 and UNC-83 (23, 24), ZYG-12 (28) and nesprins (26). By physically connecting the nuclear lamina to the ONM through the NE lumen and the INM, these proteins may be critical for coupling the nucleoskeleton with the cytoskeleton (33).

The INM and ONM are also connected by nuclear pore complexes (NPCs). And interestingly, lamins and their associated proteins are thought to help regulate the placement and spacing of NPCs (27, 28). However, while NPCs happen to be the junction at which the INM and ONM meet and have been shown to interact with lamins, their most important role is mediating transport between the cytoplasm and the nucleus. This massive protein complex weighs in at about 125 megaDaltons in vertebrates and is responsible for the selective transport of small and large molecules across the NE. Due to the physical membranous connection between the ONM and the peripheral ER, the lumen of the two organelles is continuous, which allows the nucleus access to proteins in the lumen. A classic example of this is Ire1p, an integral membrane protein which is required to sense the accumulation of unfolded proteins in the ER and transduce the message to the nucleus so that the unfolded protein response (UPR) can be initiated (29). Most of the ER lumen, however, is not dedicated to the NE, but is spread out inside peripheral ER throughout the rest of the cell.

1.2 Peripheral ER

The peripheral ER is composed of membranes of a variety of shapes that all enclose a single large luminal space. The peripheral ER can be subdivided into cisternal ER, transitional ER, and tubular ER which will be discussed in more detail below. These membranes, which are arranged into flattened sheets, highly curved tubules, regions specialized to contact other organelles, and membranes somewhere in between, are all highly and dynamically interconnected via three-way

junctions to maintain continuity of luminal space and membranes regardless of whether they are of structurally or spatially distinct subregions. Furthermore, this arrangement of a complex network allows cytosolic proteins to diffuse around this massive organelle (reviewed in 30, 31). In spite of this morphological understanding of the ER, only a handful of factors have been identified as having roles in shaping the ER.

1.3 Cisternal ER

The cisternal ER is commonly associated with rough ER (RER) which is studded with ribosomes that give it its characteristic rough appearance. ER cisternae are large flattened sheets of membrane that are prevalent at the network near the NE. These ER cisternae have been found to be enriched in a number of proteins associated with translation and translocation. These proteins include ribosomes, a component of the translocon (Sec61β), a protein tightly associated with the translocon (TRAPα), and a component of an oligosaccharyl transferase complex associated with the translocon (Dad1). This evidence suggests that cisternal ER corresponds to RER and it is at this location of enriched translation machinery that one of the most well-known functions of the ER takes place: protein biosynthesis.

Secreted, plasma membrane, and organelle proteins often begin at the ER, having been directed there by a signal recognition particle (SRP) (32) which recognizes a signal sequence encoded by the N-terminal amino acids of a that protein as its nascent chain emerges from the ribosome (33, 34). Proteins will then continue to be translated through the translocon on the ER membrane and in the case of secreted proteins, released into the ER lumen upon completion of translation (35). In the case of transmembrane proteins, a slightly more complex process takes place. As reviewed by T. Rapoport in 2004, the transmembrane regions of the protein are recognized and let out of the translocation machinery into the ER membrane so that the rest of the protein may finish being translated and translocated. In the case of a multi-pass transmembrane protein, this process may occur more than once (36). And finally, in the case of a tail-anchored (TA) protein where the transmembrane segment is unrecognizable by the translocation machinery for steric reasons (that is, the transmembrane segment is translated and released before it can be recognized and inserted as a transmembrane domain), a post-translational complex is used to insert the TA protein into the ER membrane (37-40). In all these cases of protein insertion into

or through the ER membrane, the resulting feature of the ER is the studding of the ER membrane with ribosomes that are translating proteins.

The correct folding and arrangement of a protein depends on a great deal more than its proper translation and translocation into the ER. Importantly, drifting in the lumen of the ER alongside proteins destined for the secretory pathway, are ER resident proteins. Some of these ER resident proteins are chaperones which are critical for aiding in the correct folding of newly synthesized proteins (41-43). But even with the help of these chaperones some proteins fail to properly fold. And indeed, some of these same chaperones have been implicated to have additional roles in protein quality control (44).

In the event that despite the help of chaperones a protein fails to fold correctly, the cell must dispose of that misfolded protein to avoid the negative effects that such proteins impart upon the cell. Most notably, misfolded proteins have a tendency to aggregate and disrupt cellular function dramatically, sometimes leading to serious diseases such as Alzheimer's and Parkinsons (45). The ER then, and in particular the RER, as a site of protein translation and folding is the perfect place for the cell to undertake the task of ensuring that the proteins that fold in the ER are in fact folded correctly, and if they are not, to allow for proper folding or destruction of the offending polypeptide. There are two basic pathways that are employed in maintaining protein quality in the ER: The unfolded protein response (UPR) and ER-associated degradation (ERAD).

The unfolded protein response is activated in cases of a broad disruption in protein folding that leads to an accumulation of unfolded proteins in the ER (reviewed in 46). Interestingly, as the ER accumulates unfolded proteins and increases chaperone production, its structure changes to accommodate an increase in protein volume. The ER membranes, cisternal membranes in particular, distend and are sometimes captured by autophagosome-like bodies that may aid in the sequestration of these membranes and ultimately their destruction which likely helps dampen the ER stress of accumulated unfolded proteins (47).

How the ER changes its shape as a result of the activation of the UPR has been the subject of much investigation. One proposed mechanism is mediated by a transcription factor regulated by the UPR, XBP1, which has been linked to ER biogenesis (48-50). As it turns out, XBP1 is also required for the development of secretory cells, which have characteristically expansive

networks of RER (48). XBP1's mechanism of action has yet to be completely worked out, but so far it seems that active Ire1p can initiate the splicing of XBP1's mRNA resulting in a spliceform, XBP1(S) which can, upon overexpression, trigger proliferation of RER (50, 51). This correlates with an upregulation of phospholipid biosynthesis and the expression of many proteins that function in the secretory pathway (48,49). This fits well with XBP1's activity in professional secretory cells and taken all together implies that the UPR can enhance ER capacity by expanding its size. It is still unclear, however, if the ability to modulate ER abundance is a more general property of UPR-regulated factors, or if it is specific to a few proteins such as XBP1(S).

ERAD, on the other hand, is a more specific pathway that leads to the export of particular proteins that have been identified as misfolded and targets them for ubiquitination and degradation by the proteasome (reviewed in 52). Activation of the UPR has been shown to enhance the efficiency of ERAD (53-55), but it remains unclear if ERAD is enriched in an ER sub-domain or if it has a dramatic effect on ER structure.

When the ER is functioning normally however, and the cisternal membranes are not perturbed, they have the notable morphological characteristic of being flat. They have a uniform thickness of about 30nm in yeast (56) and 50nm in animal cells (57) and highly curved edges. In fact, it has been suggested that ribosomes play a direct role in stabilizing the flattened shape of cisternal membranes to create the characteristic sheet-like shape of the cisternal ER (58). It is unclear how significant the contribution of ribosomes is to the flattening of cisternal ER membranes, and more work is required to clarify their role. However, a more mechanistic understanding of the protein Climp63 has given some insight into a possible way in which cisternal membranes may adopt a more flattened morphology. Climp63 is suggested to provide a scaffold that reaches through the lumen from one side of the sheet to the other in a 'hand-holding' model where one molecule of Climp63 on one membrane interacts with another molecule of Climp63 on the opposing membrane, thus connecting the two membranes through the lumen (59). This may help maintain the precise thickness of the cisternal membranes as well as contribute to their flattened appearance.

Climp63 has one more reported function and that is to help limit the mobility of translocon complexes on the cisternal ER by mediating association with microtubules (60). This

observation further led to the speculation that this mechanism may play a role in segregating the RER from the SER (60, 61).

Finally, membrane tubulating proteins such as reticulons are thought to localize to the edges of these sheets in order to help maintain their highly curved boundaries (62, 63).

1.4 Transitional ER

When the ER is functioning normally and proteins are successfully translocated across the ER membrane and folded (often with the help of chaperones, which will be discussed later), the next step for many proteins is their export. Transitional ER (tER) is the subcompartment of the ER that is the site of anterograde transport of proteins from the ER (64, 65). The tER was originally described morphologically as a ribosome-free subdomain adjoining the RER and having protrusions reminiscent of budding vesicles (66, 67). A mammalian cell may have several hundred tER sites (68) that are dynamic and long-lived (69-71). The structures described initially as reminiscent of budding vesicles turn out to be just that: vesicles budding from the ER mediated by coat proteins. Anterograde transport primarily occurs when proteins accumulate at ER-exit sites, are loaded into vesicle buds in the ER membrane that are coated with coat proteins (COP), in this case COPII proteins (72) which bud off from the ER, uncoat, and are trafficked via cytoskeleton and dynein/dynactin where they fuse to form the ER to Golgi intermediate compartment (ERGIC) and may continue their journey from there through the secretory pathway (73). Although the minimal machinery necessary for COPII assembly has been identified, a mechanistic understanding of how the tER remains free of ribosomes and enriched in COPII components is somewhat mysterious. So far, the protein Sec16 has been suggested to play a role in organizing COPII proteins (74). This evidence consists primarily of the fact that Sec16 interacts directly with several COPII components (75, 76) and a missense mutation in yeast Sec16 disrupts tER sites (74). Furthermore, Sec16 has been noted at ER exit-sites even when COPII function is blocked (77).

1.5 Tubular ER

The characteristic subdomains of the ER that have been described so far – the flat sheets of the RER and the smooth tER, devoid of ribosomes but bespeckled with prebudding complexes, have the most obvious correlation between their morphology and their functions. The tubular ER, commonly associated with the smooth ER (SER) is thought to house a number of the other

functions of the ER, although it remains unclear how or if the highly curved tubules arranged into a complex polygonal network enhances the efficiency of these functions. Nevertheless, some of the mechanisms for establishing the highly curved tubules that are characteristic of a lot of SER membranes have begun to be unraveled.

Most famously, Reticulons and Yop1 have been implicated in curving membranes to help form the tubules characteristic of the tubular ER in addition to their role in curving the edges of ER cisternae (78-82 & 74). They were first discovered in an *in vitro* system wherein an ER network could be generated using vesicles form Xenopus laevis eggs and cysteine modification as wells as antibodies against a reticulon (Rtn4a) inhibited network formation (78-82). Interestingly, the conserved region among the family of proteins to which Rtn4a belongs (the reticulons) is a hydrophobic region of about 200 amino acids (82). The depletion of both of the reticulon proteins present in yeast was insufficient to generate a dramatic ER network phenotype (82). But, when another protein that was shown to interact with reticulons, Yop1p, was deleted in conjunction with the reticulons, there was a dramatic loss in tubular ER (82). Interestingly, Yop1p (or Dp1) also has a hydrophobic region of about 200 amino acids. These hydrophobic regions are predicted to adopt a 'hairpin' shape such that they insert into the membrane, wedging into the outer leaflet of the ER membrane and causing asymmetry that leads to membrane curvature (74). Furthermore, the reticulons along with Yop1p/Dp1 have been shown to be able to mediate tubulation of membranes *in vitro* (57). A role for reticulons and Yop1p/Dp1 seems clear from this evidence; however, whether these are the only curvature-inducing molecules important for ER network formation remains an open question.

In spite of this understanding of ER curvature, the evidence for the sequestration of functions to these tubular and/or smooth ER subdomains is somewhat more correlational. One line of evidence for the model that the SER houses a subset of ER functions is that in specialized cell types, such as muscle cells that must rapidly regulate calcium levels, there is an enrichment of smooth ER tubules. This morphology and specialization of the ER of muscle cells is given its own name: the sarcoplasmic reticulum (SR). The function of the SR is primarily to sequester calcium and release it upon stimulation of the muscle cell (83). The highly tubulated features of

the SR in light of its role in calcium sequestration and release suggest that this arrangement is highly efficient for mediating these calcium dynamics.

Another line of evidence to support this model is the observed proliferation of SER membranes as a result of various cellular perturbations. For example, when cholesterol synthesis is inhibited there is a proliferation of SER (84) and similarly animal SER membranes are upregulated in response to exposure to phenobarbital (85), which suggests that the SER is an important site for cholesterol synthesis and drug detoxification. This evidence does not directly indicate that these functions are actively excluded from ER cisternae, but it does suggest that the SER is the preferred site for these activities.

In addition to cholesterol synthesis, phospholipids, fatty acids and triglycerides are also synthesized in the ER and are mediated by a class of transcription factors termed sterol regulatory-element binding proteins (SREBPs) which controls the expression of over 30 genes required for lipid and cholesterol synthesis (86-90). Once lipids and cholesterol have been made, however, they need to be transported to the correct locations in the cell. This can occur either by vesicular transport, and in fact a number of phospholipids are required for the proper targeting of vesicles (91), or by direct contact and lipid mixing of the ER with other membranes, such as with the plasma membrane (92).

Contacts between the tubular ER and the plasma membrane, as well as contacts between the tubular ER and mitochondria have also been shown to be critical in calcium homeostasis (91, 92). As the major reservoir for calcium in the cell, it is reasonable that the ER would likewise have roles in maintaining calcium homeostasis. Indeed, if the contacts between the tubular ER and mitochondria are tightened, a disregulated influx of calcium into mitochondria is observed and the mitochondria become prone to calcium overloading (92).

Other homeostatic mechanisms are also localized to the ER. Many of the large family of cytochrome p450 enzymes are localized to the ER membrane and are responsible for a large portion of organic detoxification both of exogenous substrates, such as drugs and endogenous byproducts, such as bilirubin (93) and as I said above, this is likely in the smooth ER.

All of these functions, critically important for healthy cellular processes, occur simultaneously in a single large membrane-bound organelle. In order to facilitate the efficient execution of all of these processes simultaneously while maintaining efficient diffusional capabilities of both the lumen (important for calcium, for example) and the membrane (important for calcium ion channels, for example) it is thought that the ER adopts its highly interconnected and dynamic network (5). Although the specific role for this network, whether it is simply an efficient way to distribute the ER membranes throughout the cell and to allow for the diffusion of important molecules through the lumen and membrane of the ER while also maintaining efficient diffusion of cytosolic factors around such a large organelle, or whether it has a more specific functional role has yet to be satisfactorily determined. Nebulous as this question may be, the mechanisms for generating membrane curvature and forming these tubules so characteristic of the ER network are beginning to be uncovered and hopefully clarification of their functional role is soon to be forthcoming.

1.6 Microtubule-mediated movement

Another mechanism possibly important in the tubulation of ER membranes is its movement out along microtubules (30). Microtubules were discovered to be important when it turned out that when they were depolymerized using the drug nocodazole, the ER slowly retracted from the periphery of the cell (31). Since then some of the particulars of how the ER utilizes microtubules for extension and remodeling of the network have been unraveled. ER dynamics along microtubules have been described to adhere to two main paradigms. The first is by way of the tip attachment complex (TAC) and the second is by way of ER sliding dynamics (31, 32).

However, since the depolymerization of microtubules induces a comparatively slow retraction of the ER membrane (31), since ER-like networks can be generated *in vitro* in the absence of microtubules (30), and since there is an imperfect correlation between ER tubules and microtubules (31), it seems that there are additional important molecules at play to extend and structure ER networks. In fact, NDKB, a protein I will discuss later, may have such a role (Chapter 2).

Nevertheless, microtubule-mediated movements of the ER network are clearly important and, as stated above, have been described as either movements mediated by TAC or movements mediated by sliding dynamics. In ER movements that are described as mediated by TAC, the ER

attaches to the plus-end of a microtubule through the protein STIM1, which is a multipass transmembrane protein localized to the on the ER with its N-terminus in the lumen and C-terminus in the cytoplasm. STIM1 in turn binds directly to the plus-end-tracking-protein EB1 on the microtubule (32). In this way, the ER may extend out (or shrink back) along actively polymerizing microtubules.

In ER movements that are mediated by ER sliding dynamics, the ER tracks along existing acetylated microtubules via the motor proteins dynein and kinesin1 (94, 95). This sliding along existing microtubules is more prevalent than the TAC that is described above, but the regulation of this activity remains to be completely characterized (32, 94).

1.7 Fusion of ER membranes

As ER tubules extend along with or slide next to existing microtubules, they inevitably come into close proximity to other ER tubules. Homotypic ER fusion has been observed along with the sliding of ER tubules with respect to each other in order to generate and rearrange the polygonal array of the ER network (reviewed in 96). The ER is constantly being remodeled and in spite of the observations characterizing the movements of ER tubules along each other in order to generate and consume 3-way junctions, the regulation of and precise machinery governing these rearrangements are still largely unaccounted for. However, the observations of the generation and consumption of 3-way junctions has been carefully studied and a few conclusions can be drawn.

First, it appears that the ER rarely undergoes fission. Instead, there are two ways that tubules have been observed to consume a 3-way junctions: by sliding of the entire junction until it has relocated outside its original polygon, thus creating a polygon with one fewer vertex, or by the sliding collapse of one tubule into another tubule thus often consuming the entire original polygon (96).

In spite of this description of the rearrangements and presumptive fusion of ER membranes, the proteins required to regulate and execute these functions have been, until recently, speculative. A few recent papers have identified Atlastin as a probable ER membrane fusogen (11, 97). And the crystal structure of the soluble domain of atlastin led to a model for how it might work (13, 14).

1.8 NDKB and Atlastin

The following two chapters will describe the experiments done to try to unravel the specifics of how the ER network is generated and maintained. To that end, our first approach was a biochemical one. Nucleoside diphosphate kinase B (NDKB) had previously been implicated in ER export and facilitation of COP-II assembly (15). We found that in permeabilized and salt-extracted cells where the ER network had been retracted, adding NDKB was sufficient to reconstitute the peripheral ER network. Furthermore, NDKB could bind directly to anionic lipids through its basic surface residues and could scaffold synthetic anionic liposomes (Chapter 2). However, knockdown of NDKB did not show a robust ER phenotype and we were unable to assay the *in vivo* activity of this protein in structuring the ER, so further physiological investigation of NDKB's ER structuring role was not practically feasible.

Given the difficulty of further elucidating the role of NDKB in ER network extension in cells, we decided to try another approach. We generated a candidate list of proteins that we hoped was enriched for proteins likely to be involved in ER network formation based on their localization and predicted topology. Our goal was to use siRNA mediated depletion of the most promising candidates on the list and find an ER network phenotype that we could investigate. Among this list was the dynamin related GTPase atlastin. As described below, the literature at the time made this a particularly compelling candidate (11, 16). Indeed we found that atlastin depletion led to a notable loss of ER network branch points, consistent with its emerging role as a fusion protein. Therefore we embarked on a mechanistic analysis of the protein using a structure function analysis based on the ability of an exogenous atlastin transgene to rescue the effects of the knockdown phenotype. It was at about this time when the crystal structures of the soluble domain of atlastin with their accompanying models came out (13, 14). Having a set of point mutant variants of atlastin that we knew to be nonfunctional, we were in a position to test some of the predictions of the initial model. We found that, surprisingly, and contrary to the model that had been suggested, GTP hydrolysis was not required for the major conformational change in atlastin's soluble domains that is thought to drive fusion. And importantly, we defined a salt-bridge that is critical for the stabilization of this conformational change (Chapter 3).

Together these two chapters present data suggesting a role for a protein in ER network extension and some initial insights into the mechanism of action for an ER membrane fusogen.

Chapter II. Nucleoside Diphosphate Kinase B (NDKB) scaffolds endoplasmic reticulum membranes in vitro

Baughman C, Morin-Leisk J and Lee T. Experimental Cell Research 314 (2008) 2702-2714

2.1 Abstract

The mechanisms that structure the mammalian endoplasmic reticulum (ER) network are not fully understood. Here we show that salt extraction of semi-intact normal rat kidney (NRK) fibroblasts and subsequent incubation of the extracted cells with ATP resulted in dramatic ER network retraction. Under these conditions, addition of a single protein, Nucleoside Diphosphate Kinase B (NDKB), was sufficient to reverse the retraction and to promote ER network extension. The underlying mechanism of membrane extension involved direct lipid binding, as NDKB bound phosphatidylinositol (PtdIns)(4)P, PtdIns(4,5)P_2 and phosphatidic acid (PA); binding to these anionic lipids required clusters of basic residues on the surface of the NDKB hexamer; and amino acid changes in NDKB that blocked lipid binding also blocked ER network extension. Remarkably, purified NDKB transformed a uniform population of synthetic lipid vesicles into extensive membrane networks, and this also required its phospholipid-binding activity. Altogether these results identify a protein sufficient to scaffold extended membrane networks, and suggest a possible role for NDKB-like proteins, as well as phosphoinositides and/or acidic phospholipids, in modulating ER network morphogenesis.

2.2 Introduction

The endoplasmic reticulum (ER) is a dynamic, interconnected network of membrane sheets and tubules that extends from the outer nuclear envelope to the cell periphery (2, 96, 98). Despite the potential importance of the structure of the ER for its varied functions, the molecular mechanisms underlying its morphogenesis remain to be fully worked out (2, 98, 96). Frequent close alignment between the ER network and the microtubule cytoskeleton has long been noted (31) and ER tubules have been observed to extend along microtubules both in vitro (97, 98) and in vivo (99). Significantly though, microtubules are dispensable for ER network formation in vitro (9), and a significant fraction of ER tubules in intact cells are in fact not aligned with microtubules (98,101). The latter observations suggest the existence of multiple, overlapping pathways for the formation and extension of the ER network. Indeed, several distinct proteins

have been implicated in ER morphogenesis. The p97 ATPase, a member of the NSF family of AAA ATPases (102), in association with its cofactor p47 (103) has been shown to be required for the in vitro formation of tubular ER networks from a light vesicle fraction prepared from *Xenopus* eggs (104). Though it is thought to mediate a fusion step, the mechanism by which p97/p47 mediates network formation remains unclear. Depletion of p47 (105) and/or the related p97 adaptor p37 (106) from mammalian cells has been shown to reduce the density of three-way tubular junctions in the ER network, though the ER remains tubular and extended in cells lacking either protein. More recently, in vitro studies in *Xenopus* have revealed a role for rtn4a and related integral ER membrane proteins in generating the high curvature membranes that comprise the tubular aspect of the ER network (107, 108). Rtn4a and the structurally related protein yop1 may shape ER tubules either by their ability to aggregate with one another, or by virtue of their unusual hairpin topology (108). Consistent with a requirement for these proteins in ER tubule formation, deletion of rtn4a in conjunction with yop1 in yeast leads to a loss of peripheral ER tubules (107). In *Caenorhabditis elegans*, a similar depletion of yop1 and the rtn4a homologue ret1 causes a pronounced reduction in ER clustering during mitosis (109). Further, silencing of the endosomal rab5 GTPase in *C. elegans* also inhibits mitotic ER clustering (109), suggesting that rab5 on endosomes might somehow act upstream, in trans, to regulate rtn4a and yop1. Clearly, understanding precisely howeach of these activities contributes to forming and extending the ER network remains an intriguing challenge.

The potential number of distinct reactions that underlie ER network formation remains unknown, but it is likely that multiple reactions contribute to each aspect of ER morphology and dynamics - flattening of membranes to form sheets near the nuclear envelope, generation of high curvature membranes for tubulation of the peripheral ER, extension of new tubules, fusion of tubules with pre-existing membranes, and perhaps a scaffold to stabilize the extended network to prevent its retraction.

Previous work in our laboratory has revealed a role for an abundant and ubiquitous member of the multi-functional family of Nucleoside Diphosphate Kinase (NDK) proteins, NDKB, in the assembly of coat protein II (COPII) transport vesicles from the ER (15). NDKB, one of eight isoforms of NDK in mammalian cells (110), was purified on the basis of its ability to stimulate coat protein assembly on the ER in semi-intact cells. Although the mechanism by which NDKB

promotes ER export remains to be determined, immuno-localization studies have revealed an ER network-like pattern for the protein (15). NDK proteins are perhaps best known for their ability to catalyze the transphosphorylation of nucleoside diphosphates using nucleoside triphosphates as a phosphate donor (111). However, multiple members of the NDK family have been implicated in diverse cellular processes, suggesting that this group of proteins may possess multiple cellular functions (110).

Here we report a permeabilized cell assay for mammalian ER network extension, and use this and additional in vitro assays to uncover the capacity of NDKB to bind, scaffold and extend anionic phospholipid-containing membranes, thereby inducing the formation of stable, extended networks. Membrane binding, as well as membrane morphogenesis, depended upon the ability of NDKB to bind anionic phospholipids such as PtdIns(4)P, PtdIns(4,5)P_2, or phosphatidic acid (PA). Together, the results suggest a possible role for NDKB and/or NDKB-like proteins in ER membrane scaffolding.

2.3 Materials and Methods

Antibodies and other reagents

His-NDKB was prepared as described previously (15). K56E,R58E His-NDKB was generated by site-directed mutagenesis using the QuikChange kit from Stratagene (LaJolla, CA). Ni^{+2}-NTA beads and the 6-His antibody for immunofluorescence were from Qiagen (Valencia, CA). The 6-His antibody was from Bethyl Labs (Montgomery, TX) and the polyclonal calnexin polyclonal antibody was from StressGen (Victoria, BC, Canada). Fluorophore-conjugated secondary antibodies were from Zymed/Invitrogen (Carlsbad, CA) and HRP-conjugated secondary antibodies were from Biorad (Hercules, CA). All lipids, mini-extruder and accessories were from Avanti Polar Lipids (Alabaster, AL). The lipid dye FM2–10 was from Molecular Probes/Invitrogen (Carlsbad, CA).

Cell culture

NRK cells were cultured in DMEM (Sigma) with 10% FBS (AtlantaBiologicals) and penicillin/streptomycin in a 5% CO_2 incubator.

Two-stage ER network formation assay and quantification

NRK cells grown on coverglasses were permeabilized with 30 μg/ ml digitonin (Roche Diagnostics, Mannheim, Germany) in PB [25 mM HEPES pH 7.2, 125 mM KOAc, 2.5 mM $Mg(OAc)_2$, 5 mM EGTA] and washed with 2× 1 ml cold 1 M KCl/PB for 20 min on ice as described previously (15). After 2× 1 ml washes in TB [20 mM HEPES pH 7.2, 0.25Msorbitol, 70mMKOAc, 1mM$Mg(OAc)_2$], each coverslip was incubated at 37 °C with 50 μl of TB containing 1 mg/ml defatted BSA (Sigma, St. Louis, MO), 1 mM DTT, protease inhibitors (1 μg/ml pepstatin and 1 μg/ml leupeptin) and an ATP regenerating system (0.5 mM ATP, 0.5 mM UTP, 50 μM GTP, 5 mM creatine phosphate, 25 μg/ml creatine hosphokinase, 0.05 mM EGTA, 0.5 mM $MgCl_2$). After 10 min, the coverslips were briefly washed with 1 ml cold TB and further incubated at 32 °C with the indicated components. All second stage incubations also included protease inhibitors, 1mMDTT and 1 mg/ml BSA. After 10 min, cells were fixed with 3% paraformaldehyde and stained as described previously (15) using rabbit antibodies against calnexin. For quantification, all images in a single experiment were captured with a 40× objective (1.3 NA, Zeiss) on a Zeiss Axioplan microscope equipped with a 12-bit CCD camera (Hamamatsu Photonics) using identical exposure times. All images were subsequently opened in Image J (NIH) and thresholded using a single fixed pixel intensity value just below that of the peripheral ER as marked by calnexin staining in control cells. After thresholding, a boundary that encompassed all calnexin-positive structures was manually drawn for each cell and the area of the selected region measured. To obtain the nuclear area of each cell, a duplicate non-thresholded image was opened and the boundary encompassing the nucleus of each corresponding cell was drawn and the area measured. The final ER network area in each cell was obtained by subtracting the nuclear area from the total area occupied by calnexin-positive structures. ≥30 cells were quantified in this manner per condition per experiment.

Liposome binding assay

Chloroform stocks of PC (75%), PE (20%), PS (5%) and test phospholipid (1–10% by weight; additions were offset by corresponding decreases in PC) were mixed (1.25 mg total) and dried down under a stream of argon. After additional drying under vacuum for 90 min, lipids were hydrated in 20 mM HEPES pH 7.2, 125 mM KOAc, 1 mM $Mg(OAc)_2$ at 37 °C for 45 min with occasional vortexing and passed 10 times through a mini-extruder equipped with a 0.4 μm

polycarbonate filter (Avanti Polar Lipids). Extruded liposomes were sedimented by centrifugation (60 k rpm, TLA 100.3, 30 min), resuspended in 50 μl of the above buffer with 250 mM sorbitol and stored at −80 °C in 10 μl aliquots. For the binding assay, each 10 μl aliquot was mixed with 1.5 μg His-NDKB, 50 μg defatted BSA, 0.5mMDTT and an ATP regenerating system in 50 μl at 37 °C. After 10 min, the samples were diluted with 0.45 ml of the above buffer without sorbitol and sedimented by centrifugation (60 k rpm, TLA 100.3, 30 min). Supernatants were precipitated with ice-cold acetone and dissolved in gel sample buffer, while liposome pellets were directly dissolved in sample buffer. Both were resolved by SDS-PAGE, transferred to nitrocellulose, probed using anti-His antibodies and HRP-conjugated secondary antibodies, developed by ECL (Pierce, Rockford, IL) and recorded with a Fujifilm LAS-3000 imaging system (Fujifilm, Japan). Image J (NIH) was used for quantification.

Microsome preparation and binding assay

Rat livers were washed in ice-cold STKM (0.25 M sucrose, 50 mM Tris–HCl pH 7.4, 25 mM KCl, 5 mM $MgCl_2$) and homogenized in 3 volumes of STKM+1 mM DTT+protease inhibitors. Homogenates were subjected sequentially to centrifugation for 13 min at 8700 ×g, for 9 min at 25,000 rpm in a Ti70 rotor, to remove nuclei and mitochondria, respectively. The resulting supernatant was placed onto a 2.5 M sucrose cushion in a Ti70 rotor tube and centrifuged for 60 min at 50,000 rpm. The membrane pellet was collected, adjusted to 30 mg/ml protein, snap frozen and stored at −80 °C. 10 μl membranes were used for each assay. For trypsin-treated membranes, 30 μg membranes were incubated with 375 μg trypsin for 60 min on ice, collected by centrifugation, washed and resuspended in 20 mM HEPES pH 7.2, 125 mM KOAc, 1 mM Mg(OAc)2+0.5 mM DTT+protease inhibitors (above)+1 mM PMSF at the original volume. Binding assays with control and trypsin-treated microsomes were carried out as described above.

Dynamic light scattering and morphological analysis of Liposomes

Chloroform stocks of PC (60%), cholesterol (20%) and PA (20%) were mixed in a glass vessel under argon and dried by rotary evaporation to obtain a thin lipid film. The lipid film was hydrated in 20mMHEPES pH 7.2,150mMKOAc,1mM$Mg(OAC)_2$ at 37 °C for 45 min to give a concentration of 1 mg/ml lipids. After 3 cycles of freezing on dry ice and thawing at 37 °C, liposomes were extruded with 20 passes through a 0.1 μm polycarbonate filter on a 42 °C heat

block. Extruded liposomes were then incubated alone or in the presence of 250 nM or 1 μMHis-NDKB for 15 min at RT. 500 μM ATP was typically included to stabilize NDKB, but similar results were obtained in the presence or absence of added ATP. Dynamic light scattering was assessed in a Malvern Zatasizer Nano ZS (Malvern Instruments, UK) and analyzed using DTS Nano (Malvern Instruments, UK). For morphological analysis, parallel reactions (~5 μl) were either spotted onto a glass slide and viewed directly by phase contrast microscopy using a 100× objective (NA 1.4, Zeiss) or 5 μl of each reaction was mixed with 1 μl of a 7 μM aqueous solution of FM2–10 on a glass slide and viewed through a 63× objective (NA 1.4, Zeiss). Images were captured using a 12-bit CCD camera (Hamamatsu Photonics). For viewing of NDKB protein in the networks, samples were placed on coverglass, fixed with 3% paraformaldehyde, and processed for immunofluorescence staining as described above, using an anti-6His antibody. Images were acquired by confocal microscopy. Finally, for thin section EM analysis, similar reactions were placed on a 13 mm round cover glass, fixed with 2% glutaraldehyde, stained with 2% potassium permanganate, embedded in Epon-Araldite and subjected to thin (100 nm) sectioning. The sections were stained with lead citrate and viewed on a Hitachi H-7100 transmission electron microscope (Hitachi High Technologies, Pleasanton, CA) operating at 75 kV. Digital images were obtained using an AMT CCD camera (AMT, Danvers, MA) and NIH Image software.

2.4 Results

A semi-intact cell assay reveals stabilization of an extended ER network by NDKB. To better understand the mechanisms underlying mammalian ER network formation and/or maintenance, a semi-intact cell assay monitoring the morphology of ER membrane networks in cultured mammalian cells was established. For the assay, normal rat kidney (NRK) cells were incubated with 30 μg/ml digitonin, which has been established to preferentially permeabilize the plasma membrane of cells, leaving intracellular membranes relatively intact (112). This method of permeabilization has been used widely to reconstitute various cellular processes, including reorganization of the actin cytoskeleton by small GTPases (113), and the trafficking of secretory cargo molecules from the ER to the Golgi apparatus (112). As shown in Fig. 1A, cells permeabilized with digitonin and immediately fixed exhibited a fully extended ER network morphology similar to that observed in intact cells (not shown), as evidenced by staining with an antibody against the membrane-spanning integral ER resident protein calnexin (114). Somewhat

surprisingly, extraction of permeabilized cells with a high salt solution at 4 °C following permeabilization did not dramatically alter ER network morphology (Fig. 1B). However, permeabilized and salt-washed cells subsequently incubated for 10 min at 37 °C in the presence of an ATP regenerating system displayed a markedly retracted ER (Fig. 1C). Calnexin positive membranes were only observed in the juxtanuclear region of cells and few cells displayed an extended ER. Importantly, ER retraction in this situation appeared to be nucleotide dependent because it did not occur when the ATP regenerating system was omitted from the 37 °C incubation (Fig. 1D). Thus, the ER in salt-washed semi-intact cells appeared to undergo nucleotide-dependent retraction.

Previous work in our laboratory had shown that NDKB, a ubiquitous and abundant member of the NDK family of proteins in mammalian cells (110), could stimulate ER export in permeabilized cells (15). Because NDKB had been observed not only in the cytoplasm of cells but also closely associated with ER membranes (115) as well as the microtubule cytoskeleton (116, 117), a possible role of this protein in maintaining ER network morphology was tested. Significantly, addition of 500 nM purified recombinant His-NDKB to salt-washed cells resulted in a significant stabilization of the extended ER network whether in the presence (Fig. 1E) or absence (Fig. 1F) of an ATP regenerating system. Quantification of the ER network area under each condition (B, D, C and E) is also shown (Fig. 1G).

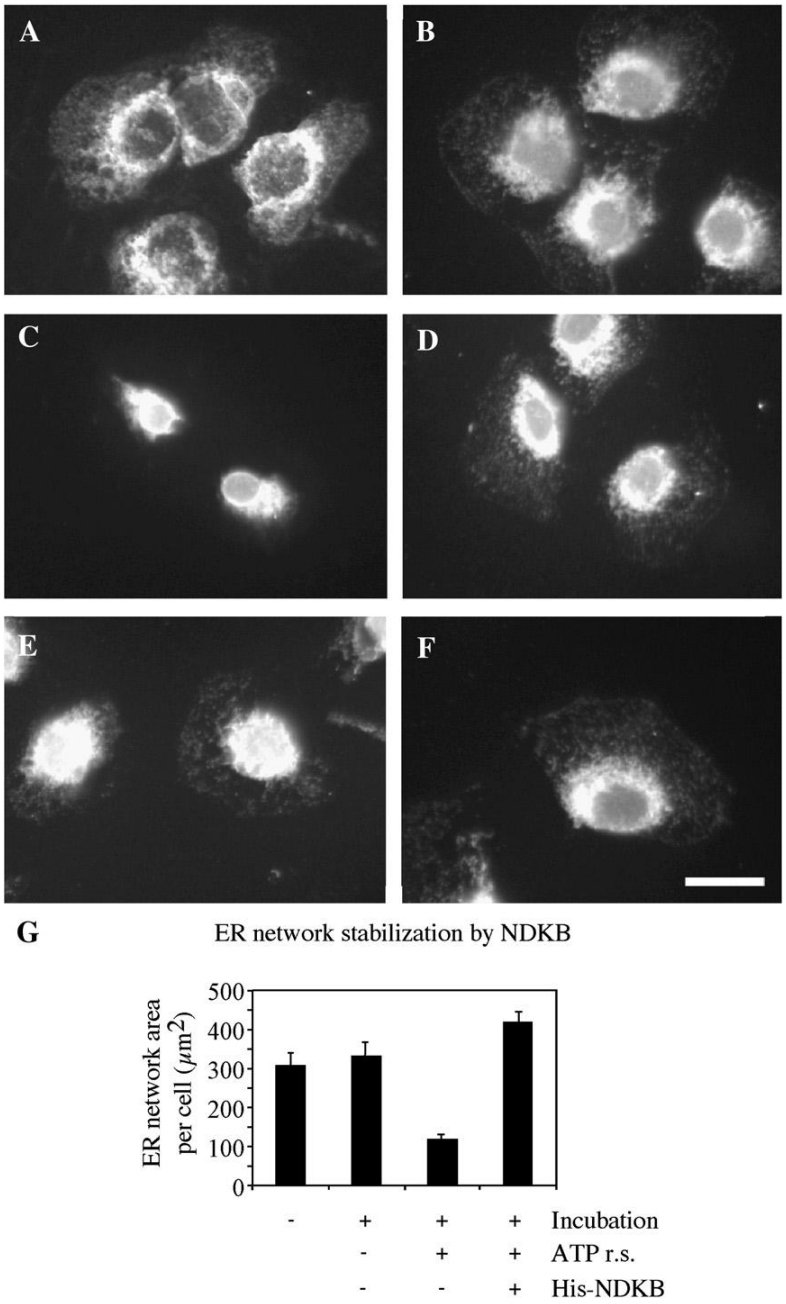

Figure 1. NDKB stabilizes an extended ER network in vitro

NRK cells grown on glass coverslips were permeabilized with 30 μg/ml digitonin in PB and fixed immediately (A) or washed with PB containing 1 M KCl for 20 min on ice prior to fixation (B). In C–F, digitonin-permeabilized cells werewashed with PB/1 M KCl for 20 min on ice, rinsed briefly in TB, followed by incubation in TB plus ATP regenerating system(C), TB alone (D), TB plus ATP regenerating systemplus 500 nMHis-NDKB (E), or TB plus NDKB (F) for 10 min at 37 °C. Cells were fixed and stained using an antibody against the ER marker calnexin. Bar, 10 μm. Quantification of the average ER network area per cell under each condition is also shown (G), average+/−SEM of three independent experiments.

NDKB actively promotes ER network extension

We next set out to distinguish whether NDKB stabilized an extended ER network simply by inhibiting the nucleotide-dependent ER retraction observed above, or whether it might have the capacity to actively promote ER network extension. To distinguish between these possibilities, a two-stage reaction was performed. In the first stage, permeabilized and salt-washed cells were incubated at 37 °C with an ATP regenerating system in the absence of NDKB. This led to ER retraction in the majority of cells as shown above (Fig. 1C). After a brief wash, the treated cells were incubated, in the second stage, either in the presence or absence of NDKB, in the presence or absence of an ATP regenerating system. Incubation in the absence of NDKB, either the presence (Fig. 2A) or absence of ATP regenerating system (Fig. 2B), in the second stage resulted in a retracted ER similar to that seen after the first stage incubation (Fig. 1C). In contrast, addition of 500 nM NDKB during the second stage gave rise to an extensive peripheral ER network whether in the presence (Fig. 2C) or absence (Fig. 2D) of an ATP regenerating system. Thus NDKB appeared to actively promote ER extension. As membrane fusion would be expected to require ATPdependent priming of SNARES (10) or GTP utilization by a yet-to-be identified GTPase implicated in ER–ER homotypic fusion (9), the fact that the NDKB-driven extension of the ER network occurred even in the absence of added nucleotides suggested that the network extension observed under the conditions of the assay might not involve membrane fusion (see below). Interestingly, it was apparent upon quantification of the data, that NDKB-mediated network extension in the second stage was slightly enhanced in the absence of an ATP regenerating system (Fig. 2E). One possibility is that this difference might be due to ongoing retraction of the network in the presence, but not in the absence, of added nucleotides. Finally it was notable that the observed ER extension was not likely to involve the microtubule cytoskeleton as no microtubules were detected at the light microscopic level after the initial cold extraction of permeabilized cells with high salt (not shown). Based on the established cold sensitivity of the microtubule cytoskeleton (119), it is likely that the 4 °C incubation during the salt wash led to the complete or near complete depolymerization of microtubules. In sum, NDKB not only stabilized the ER network in the extended state, but actively promoted extension of the network in a microtubule-independent manner.

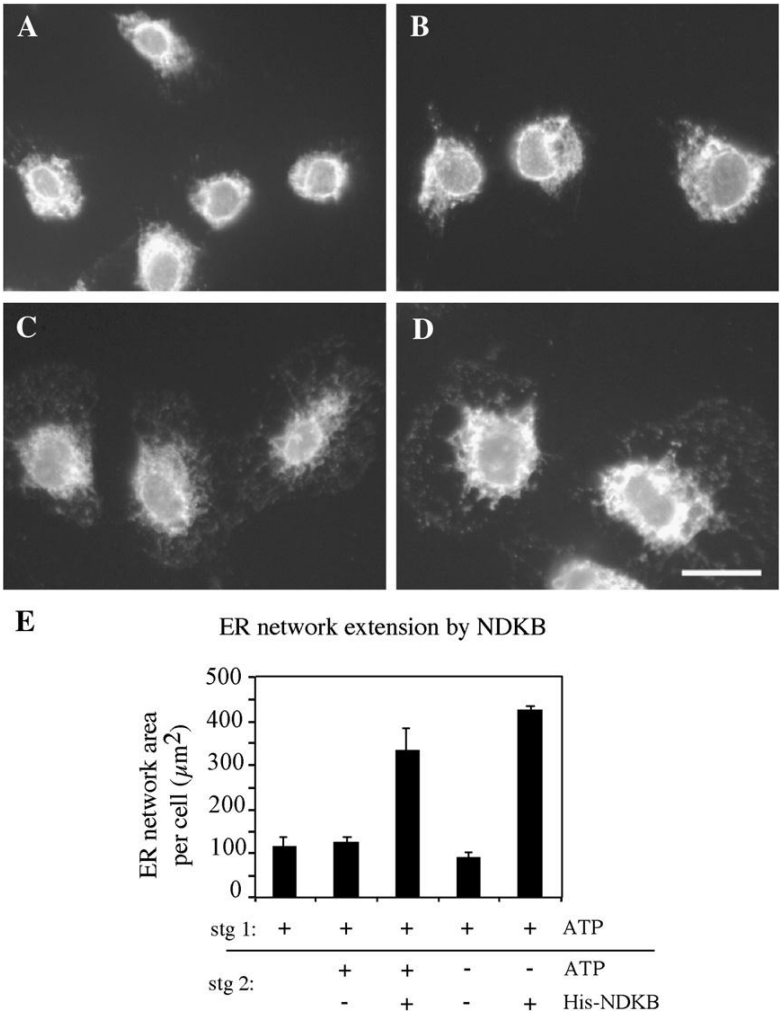

Figure 2. NDKB drives extension of the ER network

Digitonin-permeabilized and salt-washed (1MKCl) NRK cells were incubated in the first stage in TB plus ATP regenerating system at 37 °C. After 10 min, cells were washed briefly in TB and further incubated in the second stage at 37 °C with TB plus ATP regenerating system(A), TB alone (B), TB plus 500 nM NDKB plus ATP regenerating system(C), or TB plus 500 nM His-NDKB (D). After 15 min, cells were fixed and stained using an antibody against calnexin. Bars, 10 µm. (E) The average ER network area per cell under each condition is also shown (E), average +/− SEM of three independent experiments.

NDKB binds PtdIns(4)P and PtdIns(4,5)P2

The observed capacity for NDKB to extend the ER network would be expected to require binding of NDKB, either directly or indirectly, to ER membranes. Consistent with the ability of NDK proteins to interface with membranes, association of NDKB and other NDK isoforms with ER, Golgi and plasma membranes had previously been observed by immuno-EM (115). To characterize the manner in which NDKB might bind ER membranes, a conventional sedimentation assay using a 100,000 ×g centrifugation step to separate membrane-bound NDKB (P) from the soluble pool (S) was employed. As predicted, NDKB was found predominantly in

the pellet fraction when incubated in the presence (Fig. 3A, lanes 3 and 4) but not in the absence (Fig. 3A, lanes 1 and 2) of rat liver microsomes. Surprisingly, binding persisted even after trypsin treatment of the membranes (Fig. 3A, lanes 5 and 6), suggesting that NDKB might bind directly to one or more phospholipid head groups. To address this possibility more directly, liposomes reconstituted from a bovine liver lipid extract were tested for their ability to bind NDKB. Indeed, His-NDKB bound efficiently to these protein-free liposomes (Fig. 3A, lanes 7 and 8), while control proteins (His-GFP or BSA) failed to bind at all (not shown).

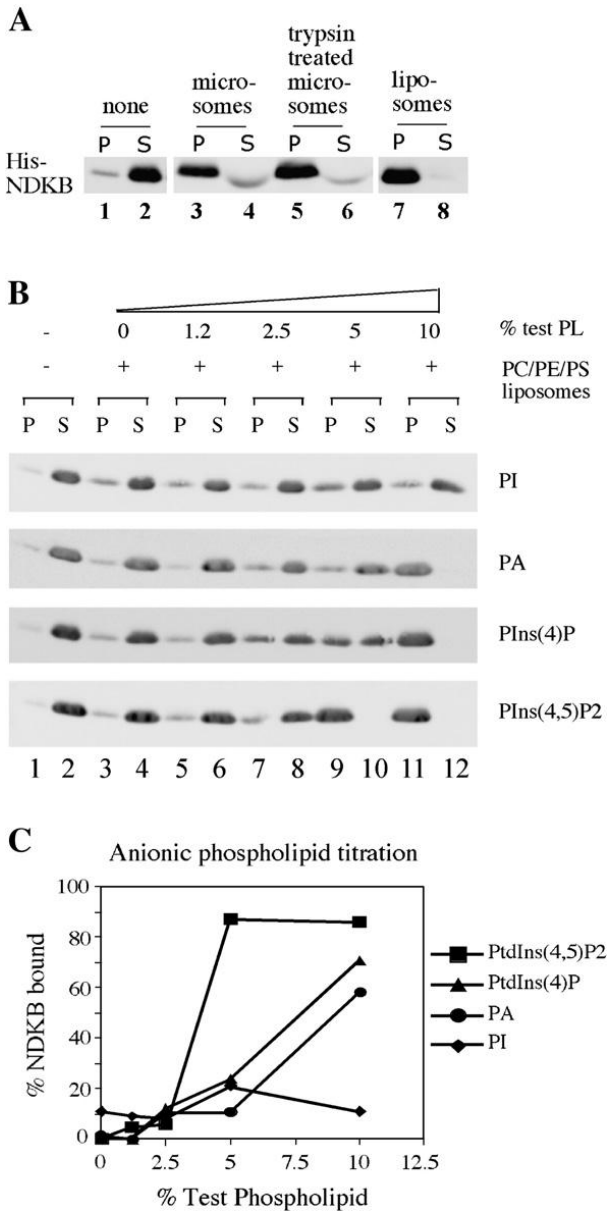

Figure 3. NDKB binds directly to anionic phospholipids

(A) NDKB binds phospholipids directly. 1.5 μg His-NDKB was incubated alone (lanes 1 and 2), with 250 μg rat liver microsomes (lanes 3 and 4),withmicrosomes pre-treatedwith trypsin (lanes 5 and 6), or with liposomes reconstituted from a bovine liver lipid extract (lanes 7 and 8) in a volume of 50 μl. After 10min at 37 °C, samples were diluted10-fold and subjected to centrifugation at 100,000 ×g for 30 min. Supernatants (S) were precipitated with acetone and membrane pellets (P) were dissolved directly in RSB. His-NDKB was detected by using a rabbit anti-His antibody. (B) NDKB binds anionic phospholipids. Co-sedimentation of 1.5 μg His-NDKB in the absence (lanes 1 and 2) or presence (lanes 3 and 4) of 250 μg control liposomes (75%PC:20%PE:5%PS) or liposomes containing 1.2% (lanes 5 and 6), 2.5% (lanes 7 and 8), 5% (lanes 9 and 10), or 10% (lanes 11 and 12) of each indicated test phospholipid (with increases in the test phospholipid offset by corresponding decreases in PC). Supernatants were precipitated with acetone (S) and membrane pellets (P) were dissolved directly in RSB. His-NDKB was detected using a rabbit anti-His antibody. (C) The percentage of NDKB bound to PC/PE/PS liposomes containing increasing concentrations of each of the indicated anionic phospholipids is shown.

To identify the lipid constituents that target NDKB to membranes, differing combinations of pure phospholipids were reconstituted into liposomes and tested for NDKB binding. NDKB binding to liposomes required the presence of an anionic phospholipid head group. No binding to liposomes comprised solely of phosphatidylcholine (PC) and phosphatidylethanolamine (PE) was observed (not shown). In contrast, phosphatidylserine (PS), conferred binding, although the % PS by weight required for binding (25–30%) was relatively high (not shown). Therefore a series of other physiologically relevant anionic phospholipids were tested by introducing increasing concentrations of each test phospholipid into a pre-defined mixture of PC:PE:PS (75:20:5) offset by a corresponding reduction in PC (Fig. 3B). The phospholipid concentrations (PC:PE:PS:test PL=65–75:20:5:1–10) were designed to mimic the composition of rat liver ER membranes (PC:Sphingomyelin:PE:PS:PI=64:4:19:3:9) as previously described (120). Either in the absence of liposomes or in the presence of weakly anionic liposomes, NDKB was recovered predominantly in the supernatant fraction (Fig. 3B, lanes 1–4). However, progressive increases in PA, PtdIns(4)P or PtdIns(4,5)P2, led to increased recovery of NDKB in the pellet fraction (Fig. 3B, lanes 9–12). Notably, PtdIns(4,5)P2 was most effective, followed by PtdIns(4)P and PA. The non-phosphorylated phospholipid phosphatidylinositol (PI) did not increase NDKB binding significantly over background, even though this phospholipid, like PA, has a net negative charge. The quantified results are also shown (Fig. 3C).

Calculation of the molar partition coefficient K (M−1) for NDKB binding to PtdIns(4,5)P2 where % protein bound=K[PIP2](100)/(1+K[PIP2]) and with [PIP2] representing the concentration of PIP2 accessible for protein binding as previously described (121), indicated that the apparent dissociation constant of NDKB for PtdIns(4,5)P2 (KDapp) was ∼30 μM. This

dissociation constant, while comparable to the ~32 μM, 33 μM and 50 μM apparent KD observed for PtdIns(4,5)P2 binding by the PH domains of pleckstrin (122), FAPP1 (123) and diacylglycerol kinase (122), respectively, is significantly higher than the concentration of 0.5 μM NDKB required for ER extension in permeabilized cells. Two potential explanations can be offered for the apparent discrepancy. First, the method of liposome preparation used for this particular binding assay (see Experimental Procedures) was later found to result in predominantly multi-lamellar liposomes. Therefore a high proportion of the phospholipids would have been inaccessible for NDKB binding, substantially raising the phospholipid concentration required to achieve half maximal binding. As a consequence, the ~30 μM KD value should be considered as a conservative upper estimate rather than the actual KD. Second, additional factors, perhaps an integral membrane ER protein, may cooperate with anionic phospholipids in the recruitment of NDKB to ER membranes. In either case, the binding of NDKB to phosphoinositides does not appear to be highly selective, and its targeting to membranes in vivo is expected to depend on the relative abundance of specific phosphorylated phosphoinositides as well as other determinants in native ER membranes.

A pair of positively charged residues on the surface of NDKB mediates PtdIns(4)P and PtdIns(4,5)P2 binding.

The results thus far predicted that a version of NDKB that cannot bind PtdIns(4)P or PtdIns(4,5)P2 would not be properly recruited to ER membranes and would therefore be defective in its ability to drive extension of the ER network in the two-stage assay. To test this hypothesis, an NDKB version defective for phosphoinositide binding was generated by site-directed mutagenesis. Two closely spaced basic residues on the surface of the three-dimensional structure of the homo-hexamer (PDB 1NSK), Lys 56 and Arg 58, were altered to negatively charged residues (Fig. 4A). These changes did not adversely affect protein folding or oligomerization, as the purified preparation eluted as a single peak from a gel filtration column at the same elution volume as did the wild type protein (not shown). Importantly, this version of NDKB (K56E, R58E) lacked the ability to bind either crude liposomes (Fig. 4B, lanes 7 and 8) or liposomes containing PtdIns(4,5)P2 (Fig. 4B, lanes 11 and 12) even though the wild type protein displayed efficient binding to both under the same conditions (Fig. 4B, lanes 5, 6, 9 and 10). Thus, surface positive charges provided by Lys 56 and Arg 58 are required for NDKB binding to membranes. The mapping of the anionic phospholipid binding determinant to Lys 56

and Arg 58 helps to explain the sharp phosphoinositide concentration dependence of NDKB binding to anionic liposomes (Fig. 3C), as three pairs of Lys56,Arg58 dyads lie on each of two opposing sides of the symmetrical homo-hexamer (Fig. 4A). Similar to N-WASP, a regulator of actin assembly that binds PtsIns(4,5)P2 in a switchlike manner through a poly-basic motif (124), cooperative binding by NDKB may represent a mechanism for localizing NDKB to membranes in a manner sensitive to PtdIns(4)P or PtdIns(4,5)P2 density.

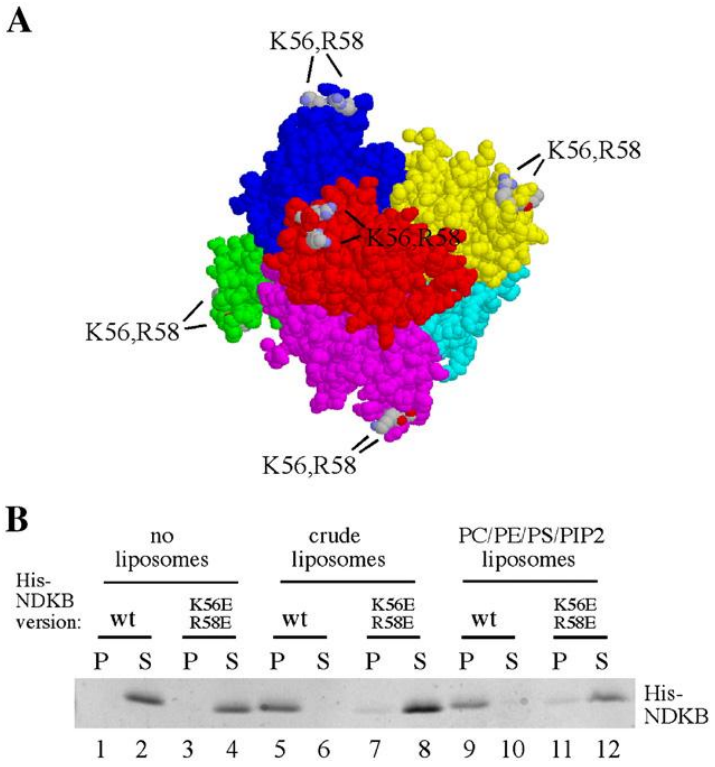

Figure 4. NDKB (K56E, R58E) is defective in anionic phospholipid binding

(A) A space-filling representation of the NDKB hexamer (PDB 1NSK) with the residues required for membrane association indicated. The residues required for phosphoinositide binding on each subunit are colored in CPK and the individual subunits of the homo-hexamer are highlighted by color. (B) Co-sedimentation of 1.5 µg wild type or mutant (K56E,R58E) His-NKDB with no liposomes (lanes 1–4), 250 µg liposomes reconstituted from bovine liver lipids (lanes 5–8), or liposomes reconstituted from synthetic phospholipids PtdIns(4,5)P2:PC:PE:PS=5:70:20:5) (lanes 9–12). Supernatants were precipitated with acetone (S) and membrane pellets (P) were directly dissolved in RSB. Protein was visualized with Coomassie Blue.

Anionic phospholipid binding by NDKB is required for its ER network extension function

To test whether the anionic phospholipid-binding ability of NDKB is required for its ER network extension function in vitro, the activity of NDKB (K56E,R58E) was compared to that of wild type NDKB in the two-stage ER network extension assay. After causing collapse of the ER

network in the first stage (as in Fig. 1C), cells were incubated in the second stage with either buffer, wild type NDKB or mutant NDKB. As seen above, cells incubated with buffer alone in stage two displayed a retracted ER morphology (Fig. 5A), whereas cells treated with wild type NDKB had an extended ER network (Fig. 5B). In contrast, cells incubated with the mutant protein exhibited a markedly retracted ER (Fig. 5C), similar to the predominantly juxtanuclear ER observed in cells incubated with buffer alone (Fig. 5A). The quantified data are also shown (Fig. 5D). Also, a morphological assessment of ER membrane binding confirmed the results of the sedimentation assay (Fig. 4B). That is, wild type NDKB added to gently permeabilized cells decorated the ER network (Fig. 5E), but the mutant protein did not (Fig. 5F). Therefore the ability of NDKB to bind anionic phospholipids is required for its ability to drive ER network extension.

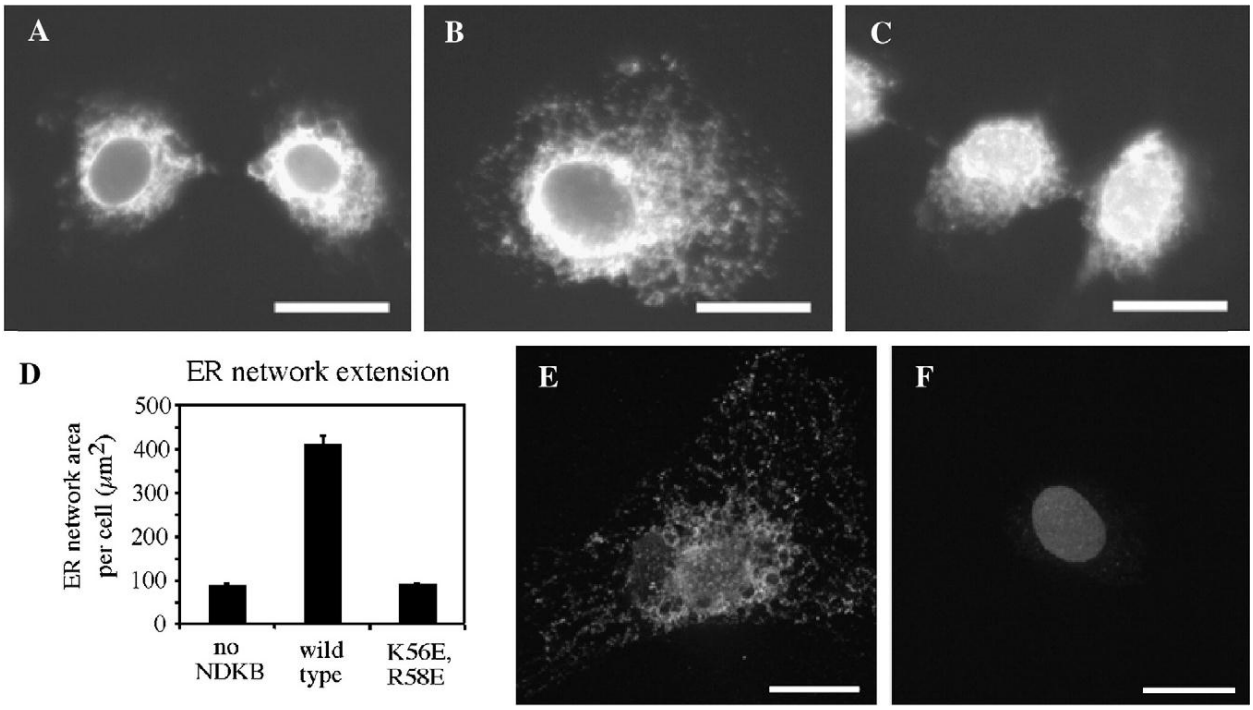

Figure 5. K56E,R58E NDKB is defective in promoting ER network extension

Wild type NDKB (A) but not mutant NDKB (B) can extend the ER network in the two-stage permeabilized cell assay. The quantified data are shown in (C), average+/−S.E.M. of three independent experiments. The ability of wild type (E) and mutant NDKB (H) to bind to the ER network of permeabilized, but not salt-washed, cells is also shown. Bars, 10 μm.

NDKB is sufficient to generate membrane networks

Finally, to address whether NDKB by itself, in the absence of any other protein, might be sufficient to mediate one or more aspects of the ER network extension activity observed in permeabilized cells, the effect of NDKB on synthetic anionic liposomes was examined. Dynamic light scattering measurements indicated that liposomes extruded through 100 nm pore size filters resulted in a relatively uniform distribution of ∼170 nm diameter vesicles (Fig.6A). Intriguingly, addition of 250 nM NDKB to the liposomes shifted the liposome size distribution from a single peak of 170 nm diameter spheres to a bimodal distribution, a population retaining a mean diameter of 170 nm and another with a mean diameter ≥1 μm (Fig. 6B). At 1 μM NDKB, the 170 nm vesicle population was completely lost and only a population of larger structures, with diffusion coefficients representative of N1 μm diameter spheres, were detected (Fig. 6C). Thus NDKB alonewas sufficient to cause an apparent liposome size change. Importantly, the concentrations of NDKB used here, 0.25–1 μM, were identical to those used in the permeabilized cell ER network extension assay, and roughly paralleled the concentration of NDKB in HeLa cells estimated at ∼500 nM by a quantitative immunoblot using pure NDKB as a standard (not shown).

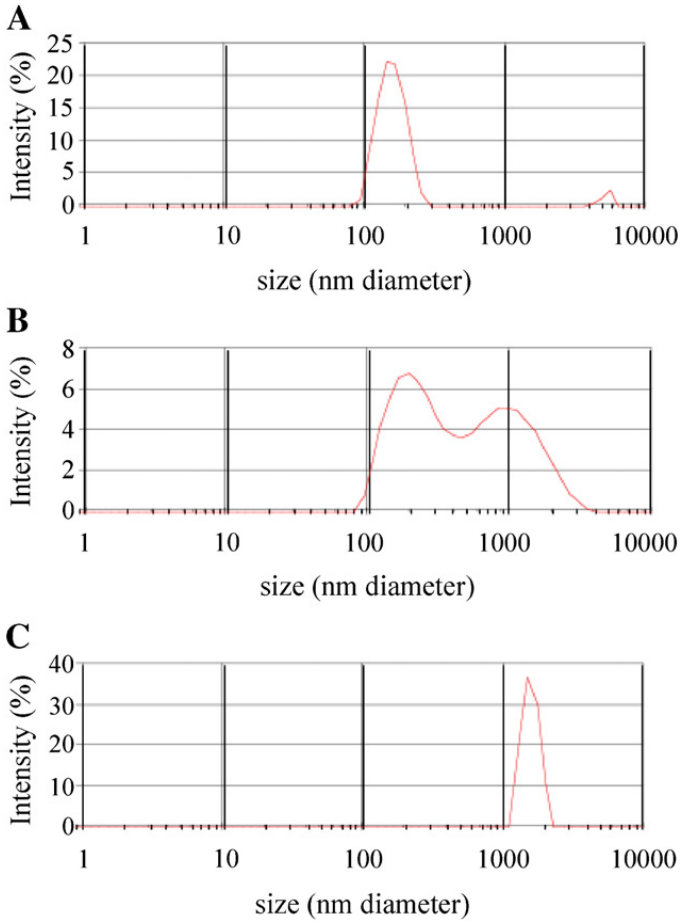

Figure 6. NDKB increases the apparent size of liposomes

Dynamic light scattering measurements were made on liposomes (PC:cholesterol:PA=60:20:20) alone (A), liposomes incubated with 250 nM His-NDKB (B) or liposomes incubated with 1 μM His-NDKB (C). All incubations included 500 μM ATP, but similar results were obtained in the absence of ATP. The size distribution of particles under each condition, representative of three independent measurements, is shown.

One possible mechanism for the apparent NDKB-induced liposome size change could involve an ability of the NDKB hexamer to cross-bridge anionic liposomes. Because the NDKB hexamer is a dimer of trimers with three sets of K56,R58 residues on two opposing faces, the two faces of a single hexamer could bring a pair of liposomes into close proximity, effectively cross-bridging them. In fact, the mitochondrial NDKD isoform has recently been shown to cross-bridge membranes with a composition resembling that of mitochondrial contact sites (125). In the case of simple crossbridging, as has been observed for a number of prot eins (126, 127), the cross-bridged species would be expected to consist of grapelike aggregates of small liposomes without any apparent organization. To determine whether the NDKB-induced size change of the

liposomes reflected simple aggregation of liposomes, or whether it might reflect additional changes in vesicle organization, the resulting membranes were first examined by phase contrast light microscopy. As expected, the bulk of liposomes, estimated to range from 100 to 200 nm in diameter, were too small to be resolved at the light microscopic level, although a few larger liposomes were resolved (Fig. 7A). Also as expected, NDKB alone contained no detectable structures at the light microscopic level (not shown). Notably however, the addition of NDKB to the mostly undetectable liposomes led to the dramatic appearance of large network-like structures (Fig. 7B). In striking contrast, the mutant NDKB protein (K56E,R58E) induced the formation of few if any such structures (Fig. 7C). To confirm that the objects observed by phase contrast microscopy were composed of membranes, the samples were independently stained with the fluorescent lipid dye FM2–10. As shown in Fig. 7D, again no significant structures were observed when liposomes were incubated alone. In contrast, large network-like structures similar to those observed by phase contrast were observed in the presence of 1 μM wild type NDKB (Fig. 7E). Interestingly, lower concentrations of NDKB produced similar network-like structures that were less extensive (not shown), consistent with the smaller mean apparent diameter of objects produced at lower NDKB concentrations, as measured by dynamic light scattering (Fig. 6B). Again as predicted, the mutant protein did not produce such structures (Fig. 7F).

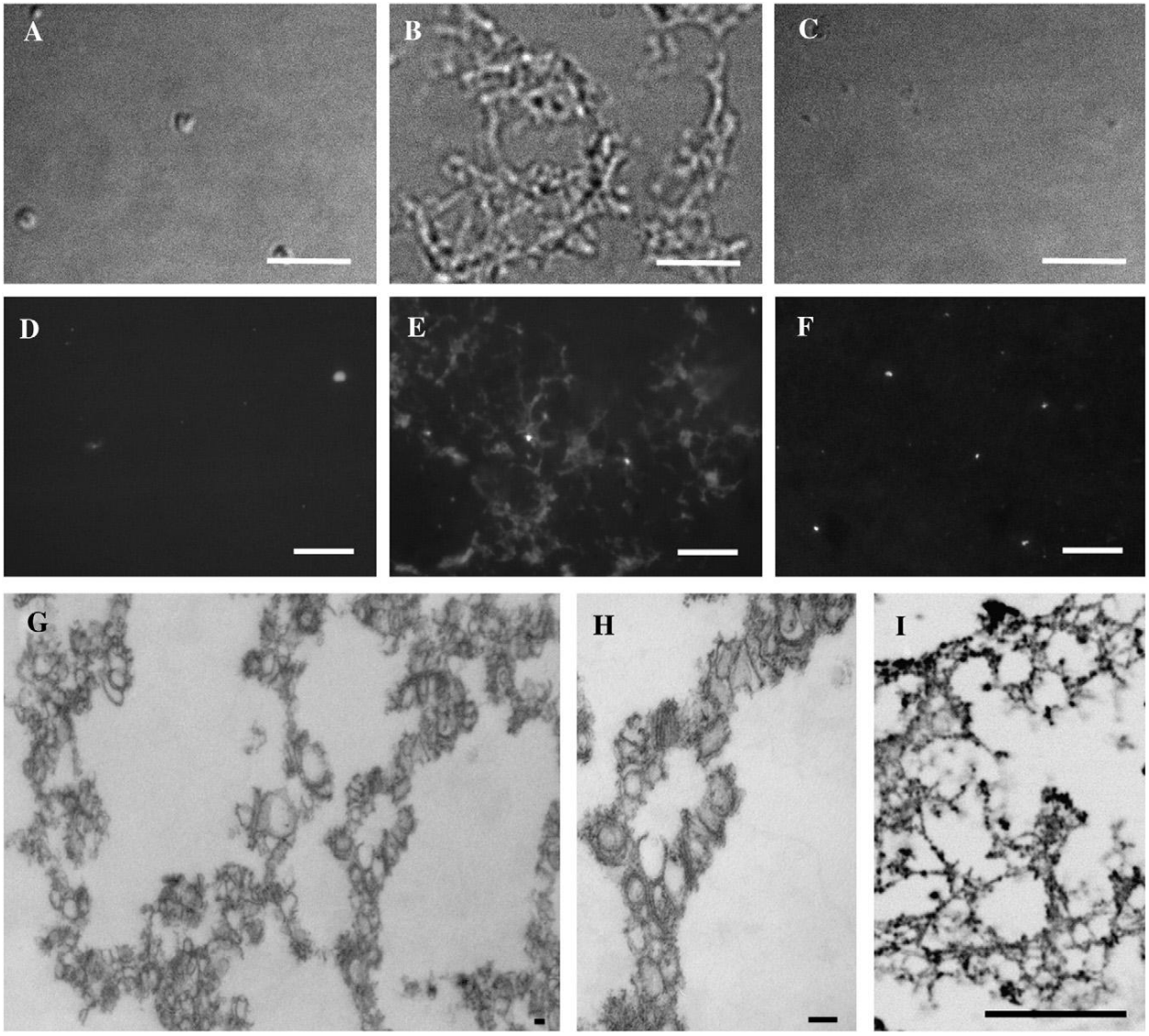

Figure 7. NDKB transforms small vesicles into large network-like structures.

Anionic liposomes were incubated alone (A and D), with 1 μM wild type His-NDKB (B, E and G–I), or with 1 μM K56E,R58E His-NDKB (C and F) and viewed without fixation by phase contrast light microscopy (A–C) and fluorescence microscopy after labeling with the lipid dye FM2–10 (D–F). Samples were also fixed and viewed by thin section EM (G and H), or fixed and stained with an antibody against His-NDKB and viewed by fluorescence microscopy. Scale bars in A–F and I, 10 μm. Scale bars in G and H, 100 nm.

To discern whether formation of networks by NDKB involved membrane fusion or whether the networks were formed by close apposition of individual vesicles, samples were fixed, embedded, sectioned and viewed by electron microscopy. Remarkably, the networks were seen to be composed of linear arrays of closely packed 100–200 nm diameter liposomes (Fig. 7G, enlarged section shown in H). The linear elements of the networks appeared to be roughly 1–3 liposomes in width and apparent branches in the network were occasionally observed. Significantly, the

average diameter of the individual liposomes comprising the large networks was as expected for the average diameter of the starting liposomes, indicating an absence of membrane fusion in the formation of the networks. Thus NDKB appeared to connect individual liposomes into large-scale networks without inducing membrane fusion, thereby functioning like a stabilizing scaffold. To visualize the putative NDKB scaffold, samples were also fixed, extracted with TX100 to solubilize membranes, stained with an antibody against NDKB and viewed by fluorescence microscopy. A filamentous network of NDKB similar in appearance and scale to the membrane networks visualized by FM2–10 staining were observed (Fig. 7I), supporting the idea that the presence of membranes induced assembly of NDKB into a scaffold upon which membranes could be arrayed. No such structures were observed in the absence of added NDKB (not shown). The apparent ability of NDKB to scaffold membranes is consistent with the potent ER network extension activity by NDKB observed above in the permeabilized cell assay, even in the absence of the microtubule cytoskeleton. Moreover, the ability of NDKB to scaffold membrane networks in the absence of membrane fusion is consistent with the apparent lack of requirement for added nucleotide in the permeabilized cell ER extension assay (Fig. 2). Presumably, the changes in ER morphology observed in both assays involve membrane scaffolding and extension, and do not involve membrane fusion. In sum, these results suggest that NDKB or NDKB-like proteins may function to stabilize extended ER networks by providing a proteinaceous scaffold that can interface directly with anionic phospholipids on the surface of membranes.

2.5 Discussion

These results reveal a potential contributing role for NDKB or NDKB-like proteins in ER network extension. First, salt extraction to remove NDKB as well as other peripheral proteins followed by incubation with nucleotides caused a profound retraction of the ER network through an active but unknown mechanism, and then, addition of purified NDKB in the absence of any other factor was sufficient to reverse this retraction and to drive peripheral ER extension in the apparent absence of microtubules. Second, NDKB could bind membranes through a direct interaction with phosphorylated phosphoinositides or PA and moreover the phosphoinositide-(or PA)-binding activity of NDKB was critical for its ability to extend the ER network in semi-intact cells. Third, NDKB alone was sufficient to transform a uniform population of synthetic liposomes into large network-like structures as evidenced by dynamic light scattering, phase

contrast microscopy, fluorescence microscopy using the lipid dye FM2–10, and thin section electron microscopy. The synthetic liposome system is clearly far removed from native ER membranes, with native ER membranes consisting of sheets and tubules, as opposed to vesicles. However, we speculate that the ability of NDKB to scaffold vesicles into linear arrays may reflect an underlying ability of NDKB to scaffold and stabilize an extended ER tubular network in a more physiological setting. Whether the retracted ER membranes acted upon by NDKB, in the second stage of the two-stage semi-intact cell assay, consist of a collapsed network of tubules, or whether they consist of tubules that have collapsed into sheets remains to be determined. The former seems more likely as the tubule-inducing rtn4a and related integral membrane proteins (108) should have been retained in the ER even after salt extraction.

NDK family members perform cellular functions beyond nucleotide homeostasis.

A single gene encodes NDK in bacteria (128) and yeast (129),whereas multiple genes encode NDK in metazoans, ranging from three NDK genes each in C. elegans (Caenorhabditis Genome Sequencing Project) and Xenopus (130), to eight distinct NDK genes in humans (110). NDK family members from diverse organisms exhibit tissue specific expression and even those that are ubiquitously expressed appear to be targeted to distinct sub-cellular locations (110, 115). NDK family members have been implicated in a variety of cellular processes, including cell proliferation, signaling, adhesion, and differentiation (110, 131, 132). Thus, the family, by gene duplication and diversification during evolution, apparently acquired novel functions in addition to its ancient metabolic activity. Although the precise mechanisms by which NDK proteins mediate each of these diverse processes is largely unknown, the mechanisms are likely to include conventional nucleoside diphosphate phosphorylation as well as other unconventional activities. Perhaps most relevant to our work, NDKA, the isoform most closely related to NDKB, affects dynamin- and arf6-mediated endocytosis. A mutant allele of NDKA was identified as an enhancer of the shibirets mutation in dynamin in Drosophila (133), and overepression of the H118C catalytic mutant of NDKA blocks arf6- and dynamin-mediated endocytosis in mammalian epithelial cells (134). In this case, a nucleotide channeling mechanism has been proposed, whereby NDKA maintains a high local concentration of GTP in the vicinity of dynamin by physically interacting with the endocytic machinery. Although this hypothesis has not been directly tested, NDKA does physically interact not only with dynamin but also with arf6

(134, 135). Our study reveals a potentially novel unconventional mechanism of action for NDKB in structuring the ER network - that of providing a structural scaffold for ER network extension.

Is catalysis part of the mechanism by which NDKB extends the ER network?

NDKB-mediated ER network extension in permeabilized cells and its formation of networks from lipid vesicles were both independent of added nucleotide. Thus our assays have, so far, failed to detect a role for phospho-transfer in the proposed ER network extension activity of NDKB. Interestingly, this does not rule out the possibility that catalysis confers an added level of functionality. For example, the liposome networks formed by NDKB failed to fuse, and fusion during ER network formation from a small ER vesicle fraction from Xenopus laevis egg extracts requires GTP (15). Perhaps the presence of NDKB on ER tubules additionally provides a mechanism for locally supplying GTP for the fusion of newly extending tubules with a pre-existing network branch. Or alternatively, nucleotide binding and hydrolysis by NDKB could serve as a mechanism for regulating its assembly onto, and disassembly from, ER membranes, which could be important given the dynamic nature of the ER network in cells.

A role for anionic phospholipids in ER network dynamics?

NDKB has previously been demonstrated to associate with membranes by a variety of biochemical and morphological methods (115,136,137), but the potential membrane receptor(s) that targets the protein to membranes is unknown. This study reveals an ability of NDKB to bind directly to anionic phospholipids, suggesting that lipid interactions, at least in part, mediate NDKB membrane targeting. Although PtdIns(4,5)P2 was most effective at recruiting NDKB to membranes in the biochemical assay, PtdIns(4)P and PA were also effective; thus the precise lipid species that recruits NDKB to membranes in vivo is expected to depend on the relative abundance of each lipid species in native ER membranes. Moreover, although an interaction with acidic phospholipids appears to be required for the binding of NDKB to ER membranes, it may not be sufficient. In this regard, it is noteworthy that FAPP1 (138) and OSBP (123), two PH domain containing proteins that bind PtdIns(4)P in vitro, localize to Golgi membranes in a manner dependent not only on PtdIns(4)P but also on Arf1. Like these and other phosphoinositide-binding proteins, NDKBmay require an additional ER-localized binding interface for proper targeting in vivo. Interestingly, the basic residues required for phosphoinositide binding by NDKB are conserved in NDKA-D, the other ubiquitous isoforms of

NDK in mammalian cells (110). Although NDKA is not yet known to bind phosphoinositides, its targeting to membranes may similarly depend on the coincidence of both plasma membrane lipid and protein determinants (e.g. PtdIns(4,5)P2 and Arf6 or dynamin). Finally, because local pools of phosphoinositides are generated and turned over by specifically localized kinases and phosphatases that are themselves regulated (139), the interaction between NDKB (and possibly otherNDKisoforms) with membranes may be regulated by physiological conditions.

NDKB may scaffold the ER network.

Residues required for phosphoinositide binding by NDKB sit on opposing faces of the hexamer, consistent with the idea that NDKB can cross-bridge membranes. This has also been shown recently for the mitochondrially localized NDKD hexamer (125). Other proteins, such as the C2 domain of synaptotagmin, CTP:phosphocholine cytidylyltransferase (CCT) and annexin, have been shown to cross-bridge vesicles by virtue of a lipid binding domain on multiple individual subunits of a homo- or hetero-oligomer (126, 140, 141). However, the latter proteins aggregate lipid vesicles into clusters, whereas NDKB generated extended network-like structures, implying that the NDKB hexamer has additional properties that account for this unique behavior. Close inspection of the networks by thin section EM revealed linear arrays of closely apposed liposomes with diameters similar to those of the starting liposome population. That is, the linear arrays were typically 1 or 2 liposomes in width. How might NDKB line up liposomes in this manner? One possibility is that clusters of phosphoinositides in the plane of the membrane may increase the local concentration of NDKB to levels sufficiently high enough to promote low affinity lateral interactions.

Redundant mechanisms likely contribute to structuring the mammalian ER network.

NDKB is one of a growing list of factors that have been implicated in structuring the mammalian ER. Other factors implicated in ER network morphogenesis include p97/p47 or p97/p37 (104,105), Rtn4a and yop1 (107), CLIMP63 (142), STIM (143) and the microtubule cytoskeleton (31, 97, 98). Depolymerization of microtubules in intact cells by nocodazole treatment results in perturbation of the ER network, indicating inter-dependency between the ER network and microtubules in vivo (31). However, ER network formation or extension in multiple in vitro systems, including the Xenopus system as well as the permeabilized cell assay presented in this study, appears not to depend on the microtubule cytoskeleton (9). Indeed, the absence of the

microtubule cytoskeleton in these in vitro systems may have helped to reveal additional redundant mechanisms that contribute to forming and maintaining a robust ER network in cells. Consistent with the existence of multiple redundant pathways for ER morphogenesis, injection of antibodies against p47, or siRNA-mediated depletion of the related p97 adaptor p37, leads to a reduction in the density of three-way tubular junctions in cells but does not induce either loss of tubules or ER retraction (105,106). Likewise, defects in overall ER morphology caused by siRNA-mediated knockdown of Rtn4c, CLMIP63 or STIM (143) in mammalian cells have not yet been reported. Finally, siRNA-mediated silencing of NDKB in our hands has failed to produce a discernable ER morphological phenotype, at least at steady state. Because NDKB, NDKA and NDKC are 88% and 65% identical at the amino acid level, respectively (110), it is possible that the three isoforms are somewhat redundant in cells with respect to the ER scaffolding function proposed herein. Alternatively, it is possible that NDKB and more distantly related proteins with structural properties similar to NDKB function redundantly to scaffold the ER network in vivo. For example, a GST fusion protein containing only the PH domain of OSBP (123), which forces dimerization of the PH domain, possesses weak ER extension activity in the permeabilized cell assay (not shown). While OSBP is localized to the trans-Golgi network and hence unlikely to contribute normally to ER extension (123), other abundant ER localized proteins that contain a multimerized anionic phospholipid binding domain have the potential to collaborate with NDKB to extend the ER network in cells. Further work will be required to determine the contribution made by NDKB and NDKB-like proteins in structuring the ER.

Chapter III. An intramolecular salt bridge drives the soluble domain of GTP-bound atlastin into the postfusion conformation.

Morin-Leisk J, Saini SG, Meng X, Makhov AM, Zhang P, and Lee TH. The Journal of Cell Biology 195,4 (2011) xx-xx

3.1 Abstract

Endoplasmic reticulum (ER) network branching requires homotypic tethering and fusion of tubules mediated by the atlastin (ATL) guanosine triphosphatase (GTPase). Recent structural studies on the ATL soluble domain reveal two dimeric conformers proposed to correspond to a tethered prefusion state and a postfusion state. How the prefusion conformer transitions to the postfusion conformer is unknown. In this paper, we identify an intramolecular salt bridge mediated by two residues outside the GTPase domain near the point of rotation that converts the prefusion dimer to the postfusion state. Charge reversal of either residue blocked ER network branching, whereas a compensatory charge reversal to reestablish electrostatic attraction restored function. In vitro assays using the soluble domain revealed that the salt bridge was dispensable for GTP binding and hydrolysis but was required for forming the postfusion dimer. Unexpectedly, the postfusion conformation of the soluble domain was achieved when bound to the nonhydrolyzable GTP analogue guanosine 5′-[β, γ-imido]triphosphate, suggesting that nucleotide hydrolysis might not be required for the prefusion to postfusion conformational change.

3.2 Introduction

The membrane-anchored atlastin (ATL) proteins belong to the dynamin superfamily of large GTPases (144, 145). In humans, the neuron-specific isoform ATL1/SPG3A is enriched in the cis-Golgi apparatus, and mutations in it are linked to motor neurological deficits associated with hereditary spastic paraplegia (144). ATL2 and ATL3, 62 and 60% identical to ATL1, respectively, are expressed in most, if not all, tissues and primarily ER localized (16). SiRNA-mediated depletion of isoforms 2 and 3 from HeLa cells, expressing little, if any, isoform 1 (16), leads to an unbranched ER morphology, implying a function for ATL2/3 in ER network branching (12). This requirement could reflect a role for the molecule in tubule formation, extension, tethering, and/or fusion (96, 101). Though, based on the remarkable finding that the single Drosophila melanogaster orthologue of ATL, purified and incorporated into artificial liposomes, is sufficient to drive membrane tethering and fusion, ATLs have been proposed to

mediate the homotypic tethering and fusion of membranes that underlies the branched ER network (11).

Recently, two groups have solved the x-ray crystal structure of the soluble domain of human ATL1 (13, 14). The structures reveal a globular GTPase head connected through an eight–amino acid linker to a middle domain comprised of a three-helix bundle. As expected, the GTPase domain has an overall fold similar to that of GBP1 (147), the closest relative of ATL1–3 in the dynamin superfamily (14, 14, and 16% identical to ATL1, ATL2, and ATL3, respectively). Dynamin superfamily members undergo conformational changes in a manner dependent on their nucleotide-bound state (148, 149). Accordingly, ATL1 crystallization by both groups was performed in the presence of a variety of GTP analogues. Both groups observed two strikingly distinct ATL1 conformers, indicating that, like GBP1 and dynamin, ATL1 indeed undergoes discrete conformational changes during its reaction cycle. Moreover, both structures showed ATL1 as a head to head dimer, reminiscent of the head to head dimers observed in crystal structures of the GTPase domains of dynamin bound to the transition state analogue GDP + AlFx (149), and GBP1 bound to either guanosine 5′-[β, γ-imido]triphosphate (GMPPNP) or GDP + AlFx (148). Curiously, only GDP was observed in the nucleotide-binding pocket of the structures obtained, possibly because of either slow hydrolysis or increased mobility of the terminal phosphate of GMPPNP and other analogues (13, 14). Therefore, how changes in the nucleotide-bound state of ATL1 relate to changes in its conformation remains to be clarified.

In the first of the two ATL1 dimer conformers (form 2), the monomers interact in a head to head fashion with an interfacial area of 756 Å 2 because of contacts solely between the GTPase domains. The α-helical bundles of the respective middle domains point away from the dimer interface, and although not present in the crystal structures, the trans-membrane segments would be expected to anchor the interacting subunits in opposing membranes. In the second conformer (form 1), a similar head to head configuration is observed as in the form 2 dimer, though additional contacts increase the interfacial area between the GTPase domains to 1,226 Å 2 . In addition, the α-helical bundles of the middle domains are crossed over with respect to the head domains caused by a 90° rotation about a central conserved proline residue in the linker. In this crossed dimer configuration (form 1), a new set of contacts are made between the middle domains and the opposing heads. As a consequence of the crossover, the C termini of the two

subunits of the form 1 dimer are within 14 Å of one another, necessarily placing the trans-membrane segments of the interacting subunits in the same membrane. Based on the orientation of the molecules relative to the presumed orientation of the lipid bilayer, the form 2 and form 1 dimers have been designated pre- and postfusion states, respectively (13, 14, 150). The dimer pairs suggest a compelling model for membrane tethering and fusion. First, head to head dimerization of ATL in trans (form 2) would initiate membrane tethering. Once tethered, crossover of the middle domains would catalyze membrane fusion, presumably by bringing opposing lipid bilayers into tight apposition and deforming them, consequently reducing the activation barrier for membrane fusion (13, 150). In part because dimerization of ATL1 in solution is nucleotide dependent (13, 14), GTP binding has been suggested to form the prefusion dimer for the membrane-tethering step, whereas GTP hydrolysis and Pi release has been hypothesized to trigger the 90° rotation and crossover of the middle domains to achieve the fused state (13). According to this scenario, a cycle of GTP binding and hydrolysis would drive both membrane tethering and fusion, though how the postfusion complex is disassembled for further rounds of fusion remains to be clarified.

If the crossed dimer conformation indeed represents the postfusion state, contacts unique to this conformer should be important for driving membrane fusion. Conversely, inhibiting such contacts should block the conversion of prefusion dimers to the postfusion state. Here, we report a functional analysis of residues within the middle domain of ATL2 in search of ones that might be involved in the prefusion to postfusion transition. We then focus on a pair of residues that appear to mediate a postfusion conformer-specific salt bridge. We show that the salt bridge is not required for either GTP binding or hydrolysis but is necessary for transitioning to the postfusion dimer conformation. Furthermore, although GTP hydrolysis has been suggested to be required for formation of the postfusion conformation of the soluble domain, our results indicate that hydrolysis is not required, at least in the context of the soluble domain. The potential implications of this finding with regard to the ATL fusion mechanism are discussed.

3.3 Materials and Methods

Cells, constructs, antibodies, and reagents

All experiments were conducted on HeLa cells maintained at 37°C in a 5% CO_2 incubator in MEM (Sigma-Aldrich) and 10% FBS (Atlanta Biologicals) with 1% penicillin/streptomycin

(Thermo Fisher Scientific). The N-terminally HA-tagged ATL2 isoform 2 construct was contributed by C. Blackstone (National Institutes of Health, Bethesda, MD). All ATL2 variant constructs were generated by PCR-mediated site-directed mutagenesis (QuikChange; Agilent Technologies). The siRNA-immune HA-ATL2 construct was generated using QuikChange to replace the 21 nucleotides targeted by the ATL2 siRNA 5′-GGAGCTATCCTTATGAACATTCATA-3′ with 5 ′-GGAGCTATCCGTACGAACACTCATA-3′. N-terminally Myc-tagged PRA2 and DP1 constructs were generated by PCR amplification of a HeLa cDNA library and cloning into the pCS2 Myc vector at the EcoRI and XbaI sites and the XbaI site, respectively. All constructs used herein were fully verified by sequencing (Genewiz). An mAb used to detect protein disulfide isomerase (Abcam) and the HA epitope (Sigma-Aldrich) were purchased, and the 9E10 mAb was used to detect the Myc epitope. The rhodamine anti–mouse secondary antibody was also purchased (Invitrogen). GTP, GDP, and GMPPNP were purchased (Sigma-Aldrich), reconstituted to 100 mM stocks in 10 mM Tris, pH 8.0, and 1 mM EDTA, and stored at -80°C.

Knockdown replacement assay

Cells plated on 60-mm culture dishes were transfected with ~5μg of the indicated HA-ATL2 replacement constructs using transfection reagent (jet-PEI; VWR). Myc-tagged PRA2 and Myc-tagged DP1, both ER-localized proteins, served as negative controls. Neither affected either the percentage of cells showing the unbranched ER phenotype or the extent of loss of network branching relative to siRNA treatment alone. 24 h after DNA transfection, cells were trypsinized and replated onto 12-mm glass coverslips in a 24-well plate. siRNA treatment targeting both ATL2 and ATL3 was performed the next day using transfection reagent (Oligofectamine; Invitrogen) according to manufacturer's recommendations. The ATL2 (#1) and ATL3 (#2) siRNAs were identical in sequence to those previously published (16). 72 h after knockdown, cells were fixed in ice-cold methanol and processed for immunofluorescence. In brief, primary (1 h at RT) and secondary (30 min at RT) antibody incubations were performed in a blocking solution consisting of PBS + 2.5% calf serum + 0.1% Triton X-100, and washes were with 5× 1 ml PBS. All images were obtained using a spinning-disk confocal scanhead (Yokagawa; PerkinElmer) mounted on a microscope (Axiovert 200; Carl Zeiss) with a 100× 1.4 NA objective (Carl Zeiss) and acquired using a 12-bit camera (ORCA-ER; Hamamatsu Photonics). Maximal

value projections of sections at 0.2-µm spacing (approximately six per cell) were acquired using Imaging Suite software (PerkinElmer) and imported as 8-bit images into Photoshop (Adobe). Quantification of functional replacement was performed manually on a wide-field fluorescence microscope (Axioplan; Carl Zeiss) with a 40× 1.4 NA objective. Images were acquired using a 12-bit camera (ORCA-ER) and QED software (Media Cybernetics). For quantification of functional replacement, the fraction of cells expressing the indicated HA-ATL2 that showed a loss of ER network branching (among ≥100 cells per experiment) was counted. Some of the HA-ATL2 variants, when expressed at high levels, exhibited a dominant-negative ER phenotype (even without ATL knockdown). For these variants, a threshold level of HA-ATL2 immunofluorescence below which expression of the replacement construct alone did not confer an ER phenotype was determined. Quantification of functional replacement was then restricted to those cells expressing the HA-ATL2 variant below the predetermined threshold.

Protein expression and purification

The 6His-tagged cytoplasmic domain of ATL2 was generated using PCR amplification of nucleotides encoding amino acids 1–467 from HA-ATL2 and cloned into the pRSETB vector at NheI and EcoRI sites. Variants were generated using QuikChange mutagenesis and sequence verifi ed. Protein expression was induced with 0.5 mM IPTG in BL21(DE3)pLysS cells at 23°C for 16 h, and purification used standard protocols for purifi cation of 6His-tagged proteins on Ni^{+2} agarose beads (QIAGEN). Proteins, eluted in 50 mM Tris, pH 8.0, 250 mM imidazole, 100 mM NaCl, 5 mM MgCl 2 , and 10% glycerol, were typically 8–24 mg/ml, >95% pure, fl ash frozen in liquid N 2 , and stored at -80°C.

GTPase assay

Purified 6His-ATL2 variant proteins, dialyzed into SEC and precleared by centrifugation in a rotor (TLA-100; Beckman Coulter) at 100,000 rpm for 15 min, were diluted to various concentrations in the same buffer. GTP at the indicated concentrations was added to the protein and incubated at 37°C for varying times. After quenching with 5 mM EDTA, 160 µl of each reaction was then added to 40 µl malachite green phosphate assay reagent (Accurate Chemical & Scientific Corp.) in a 96-well transparent fl at-bottomed dish (Costar; Thermo Fisher Scientific) and developed for 10 min at 25°C before measuring the absorbance at 650 nm. Phosphate release was calculated using a standard curve according to the manufacturer’s instructions.

KM and kcat determinations

1μM dialyzed and precleared 6His-ATL2 variant proteins were incubated with 5, 10, or 20 μM GTP at 37°C for varying times, quenched, and assayed for phosphate release (see previous paragraph). Initial velocities for each ATL2 variant were plotted against substrate concentration on a double reciprocal scatter plot, and the K M for each ATL2 variant was extracted from the x intercept of its best-fi t line (R 2 = 0.99 1; x intercept = 1/ K M). For catalytic rate constant, k cat , determinations at differing protein concentrations, varying concentrations of 6His-ATL2 variants were incubated with 0.2 mM GTP (determined to be saturating for ≤2 μM ATL2) for 5 min at 37°C. During this time, product formation was predetermined to be linear with time. Samples were quenched and assayed for phosphate release (see previous paragraph). When assaying GTPase activity at high concentrations (3 and 30 μM ATL2), GTP was added at 1 mM in the reaction and incubated for 1 min at 37°C. Thereafter, samples were diluted 10-fold before assaying for phosphate release.

SEC

Purified 6His-ATL2 variant proteins, dialyzed into SEC buffer + 0.5 mM DTT and precleared by centrifugation in a rotor (TLA-100) at 100,000 rpm for 15 min, were diluted to 10 or 30 μM and incubated with or without 2 mM GMPPNP for 30 min at RT. 100 μl of each sample was then injected onto a fast protein liquid chromatography column (Superdex 200; GE Healthcare) preequilibrated in SEC buffer + 0.5 mM DTT and separated at a fl ow rate of 0.5 ml/min at 4°C. 0.5-ml fractions within the included volume of 24 ml were collected, precipitated with TCA using 0.5% Triton X-100 as a carrier, resuspended in reducing sample buffer, resolved by SDS-PAGE, and stained using Coomassie blue. Where indicated, wild-type ATL2 was incubated with 5 mM GDP for 30 min at RT and resolved on the same column, except that 1 mM GDP was also included in the column buffer.

Cross-linking

Purified 6His-ATL2 variant proteins were dialyzed into SEC buffer, pH 7.0, at 4°C and precleared by centrifugation in a rotor (TLA-100) at 100,000 rpm for 15 min. 20 μM of each protein was incubated at RT in SEC buffer, pH 7.0, in the absence or presence of 2 mM GMPPNP, GDP, or GTP. After 30 min at RT, the reaction was diluted five-fold into SEC (to 4

μM ATL2) in the absence or presence of 12 μM BMOE (Thermo Fisher Scientific) and incubated for 1 h at RT. Samples were then quenched with 20 mM DTT for 15 min, mixed with reducing sample buffer, and resolved by SDS-PAGE.

EM

20μM purifi ed 6His-ATL2 in buffer containing 25 mM Tris-HCl, pH 7.5. 100 mM NaCl, 5 mM MgCl 2 , 2 mM EGTA, 5% glycerol, and 0.5 mM DTT was diluted twofold in the same buffer without glycerol in the presence of 1 mM GMPPNP. After 30 min at RT, the reaction mixture was further diluted 30-fold into the same buffer and immediately applied onto glow-charged thin carbon foil grids, blotted with a filter paper, and stained with a 2% solution of uranyl acetate in water. The grids were examined at 120 kV with an electron microscope (Tecnai 12; FEI). Images were recorded with a 2,000 × 2,000 charge-coupled device camera (UltraScanT 1000; Gatan, Inc.) at a nominal magnification of 52,000.

Image processing and model docking

EM images were processed using the EMAN image analysis software (National Center for Macromolecular Imaging; 151, 152). Individual particles were boxed manually with 80 × 80 pixels (2.17 Å/pixel), normalized, and combined to yield one raw image stack file. A total of 571 individual particle images were collected, band-pass filtered, and aligned with respect to their center of mass. To test the likelihood of the conformations that the ATL GTPase could adopt, two simulated 3D density maps were computed with Chimera (version 3; University of California, San Francisco) from the atomic models of two conformers (shown in Fig.6 A), prefusion (Protein Data Bank accession no. 3QOF) and postfusion (Protein Data Bank accession no. 3QNU). These two density maps were then used as initial references for the reference-based projection matching of the particle images followed by the reconstruction of particle images in EMAN2. The iterative refinement cycles were ended when the calculated Fourier shell correlation between the 3D models generated in two consecutive iterations showed no further improvement. This indicated that the 3D reconstruction was converging to a stable optimum, and the final 3D density maps were calculated. For model docking, the atomic models of prefusion and postfusion were fitted into the reconstructed EM density map using the feature Fit model in map implemented in Chimera. Crosscorrelation values between the final density maps and the

simulated 3D density maps from two conformers were calculated. The value was 0.293 for the prefusion conformer and 0.425 for the postfusion conformer, with 55% volume included.

13.4 Results

Loss of ER network branching upon ATL2/3 knockdown is rescued by wild-type ATL2 expression

To identify ATL residues that participate in the interconversion between pre- and postfusion conformers, we used an RNAi knockdown replacement assay. The assay is based on the previously reported requirement for ATL2/3 in ER network branching in HeLa cells (12). As anticipated, treatment of HeLa cells with siRNAs identical to those previously shown to knock down ATL2 and ATL3 (16) resulted in an abnormal ER morphology characterized by a notable reduction in network branch points (Fig. S1, A–C). In contrast to control knockdown cells with 200–400 ER network branch points per cell, ATL2/3 knockdown cells typically had <100 network branch points per cell (Fig. S1, C and D). Also consistent with a previous study, knockdown of both isoforms was required to elicit the unbranched phenotype (Fig. S1 A), indicating that either ATL2 or ATL3 is sufficient to maintain normal network morphology (12). To assess whether the unbranched ER phenotype is a specific consequence of ATL2/3 loss, the ATL2/3 siRNA was cotransfected with either a negative control DNA construct or an siRNA-immune HA-tagged ATL2 replacement construct. Whereas ~50% of cells expressing the negative control construct displayed a largely unbranched network (<100 branch points per cell), few, if any, cells expressing wild-type HA-ATL2 displayed the phenotype (Fig. 8, A and B). Therefore, the unbranched ER phenotype can be attributed specifically to the loss of ATL2/3.

Specific middle domain residues are required for ATL2 activity

As our analysis was initiated before the recent determination of the ATL1 crystal structure, we started with a computationally derived ATL2 structure model based on its similarity to GBP1 (147, 153). Domain boundaries defined by the model were applied to first test the importance of the middle domain. As anticipated, the HA-tagged variant ATL2 Δ377–463 (or ATL2 Δmiddle), lacking the entire middle domain, was stably expressed but failed to functionally replace endogenous ATL2/3 (Fig. 8, A and B). Then, several conserved middle domain residues were screened. RNAi knockdown replacement using ATL2 variants with either single or double amino acid substitutions to alanine revealed required residues within the middle domain (Fig. 8, A and B). Substitutions that blocked ATL2 function include E380A, L384D, K433A, K434A, M435A,

F440A, and Y444A. Most of the residues identified by our analysis are located near the GTPase head (Fig. S2, A and B). Notably, M435 is equivalent to M408 in ATL1, which, when mutated, is associated with hereditary spastic paraplegia (144), though the mutations have been reported to have only modest effects on the GTPase activity of ATL1 (13, 14). Also, E380 is equivalent to residue E328 in the Drosophila homologue, whose charge reversal inhibits the in vitro liposome fusion reaction by 75% (13).

ER network morphology after replacement with the various ATL2 proteins appeared somewhat distinct, not only from one another but also from the morphology seen after knockdown. The exception was ATL2 Δmiddle, whose network morphology was similar to the knockdown. The significance of these differences is unclear but may reflect a differing ability of each variant to engage in the ATL2 reaction cycle, with ATL2 Δmiddle being the least functional. Many of the single alanine substitutions that blocked ER network branching were in highly conserved residues (Fig. S2 A), though substitution of at least one conserved residue, E454, had no apparent effect Fig. 8, A and B). Less conserved or nonconserved surface residues, such as Q447 and S431, respectively, could also be substituted (Fig. 8, A and B).

Finally, many of the nonfunctional ATL2 variants, when expressed at high levels, exerted a dominant-negative effect on ER morphology that could be observed even in the presence of endogenous ATL2/3 (Fig. S2 C). To avoid the potentially complicating effects of such high level expression, only cells expressing each variant below a predetermined threshold level were included for quantification of functional replacement (see materials and methods, Chapter 3.3).

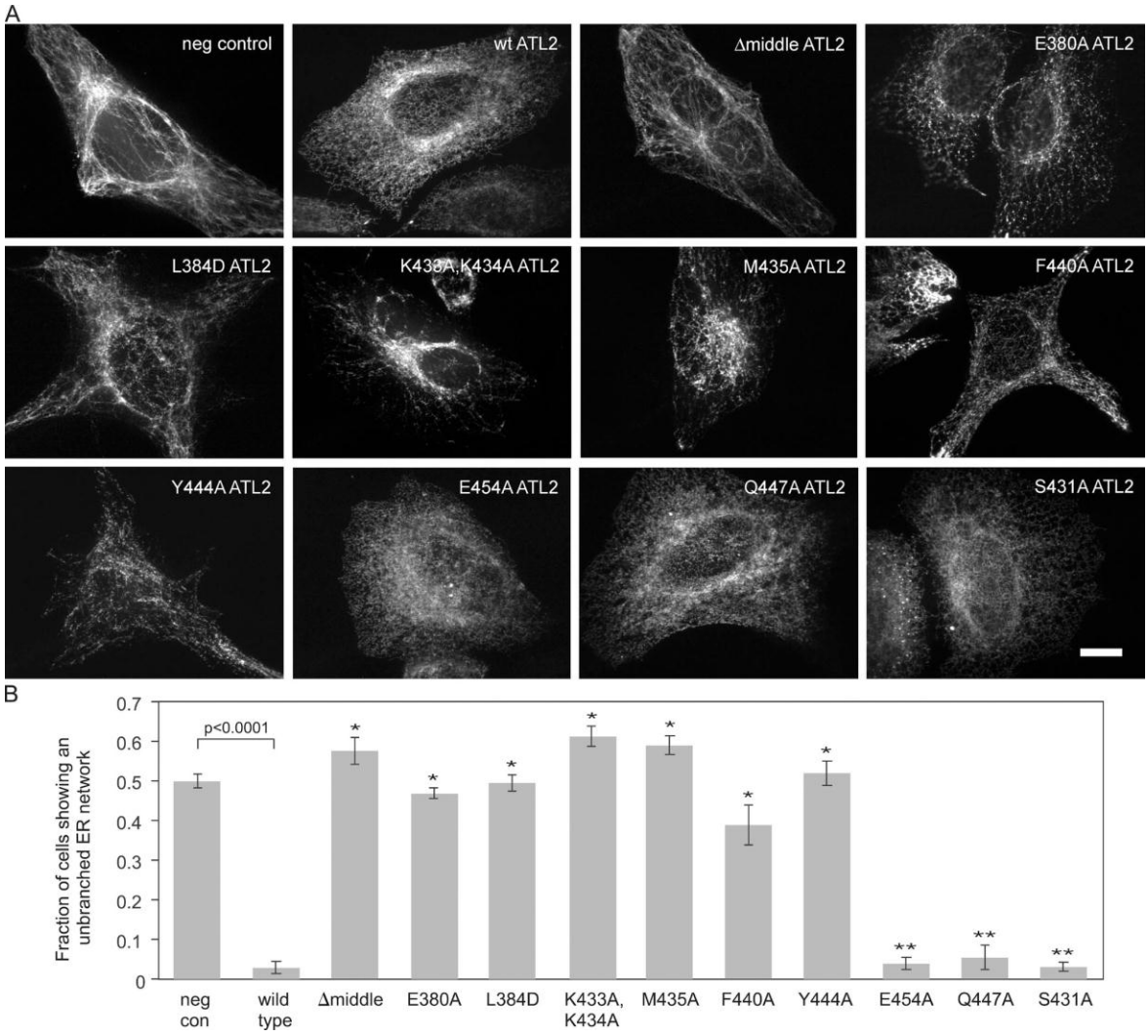

Figure 8. Identification of ATL2 middle domain residues required for its ER network branching function.

(A) Knockdown replacement assay. 48 h after transfection with a Myc-tagged DP1 negative control (neg con) construct, wild-type HA-ATL2, or each of the indicated HA-tagged ATL2 variants, cells were transfected with siRNAs targeting ATL2 and ATL3. 72 h after knockdown, cells were fi xed and stained using an antibody against the Myc or HA epitope and viewed by confocal microscopy. Bar, 10 µm. (B) Quantifi cation of the fraction of cells expressing the indicated proteins that had the unbranched ER phenotype. Values represent the means of three independent experiments ± SD. *, P < 0.0005 with respect to wild type; **, P < 0.0005 with respect to the Myc-DP1 negative control.

Middle domain mutations fall into three classes

The two dimer crystal forms of ATL1 (13, 14) allowed us to analyze the positions of our mutations. Because ATL2 is 73% identical to ATL1 in its cytoplasmic domain, its overall fold is likely very similar to ATL1 with only minor differences in the precise placement of the

backbone and side chains. To aid in the analysis, computational models for ATL2 in both the pre- and postfusion conformation were derived based on the ATL1 structures (153). Inspection revealed that the required residues fall into three categories (Fig. 9, A and B). The first category consists of L384, Y444, and F440 (Fig. 9, A and B, box 1). These residues pack together near the surface of the middle domain in the prefusion conformer, and the packing interactions remain relatively unchanged in the postfusion conformer. The second category consists of K433 and M435 (Fig. 9, A and B, box 2). These residues are in a loop connecting two helices (8 and 9) of the middle domain. In the prefusion conformer, K433 and M435 contact residues within the head domain of the same monomer. In the postfusion conformer, K433 and M435 alter their contacts to residues in the head domain of the opposing monomer. The third and final category, consisting of E380 and K372, was of particular interest, as it pointed to residues appearing to make substantial contacts only in the postfusion conformer (Fig. 9, A and B, box 3). In the prefusion conformer, the nonpolar portion of the E380 side chain may be involved in a set of middle domain packing interactions, and K372 exhibits no obvious contacts. Significantly, K372 is immediately adjacent to the point of 90° rotation that converts the prefusion dimer to the postfusion dimer conformer, and in the postfusion conformer, it becomes involved in a salt bridge with E380.

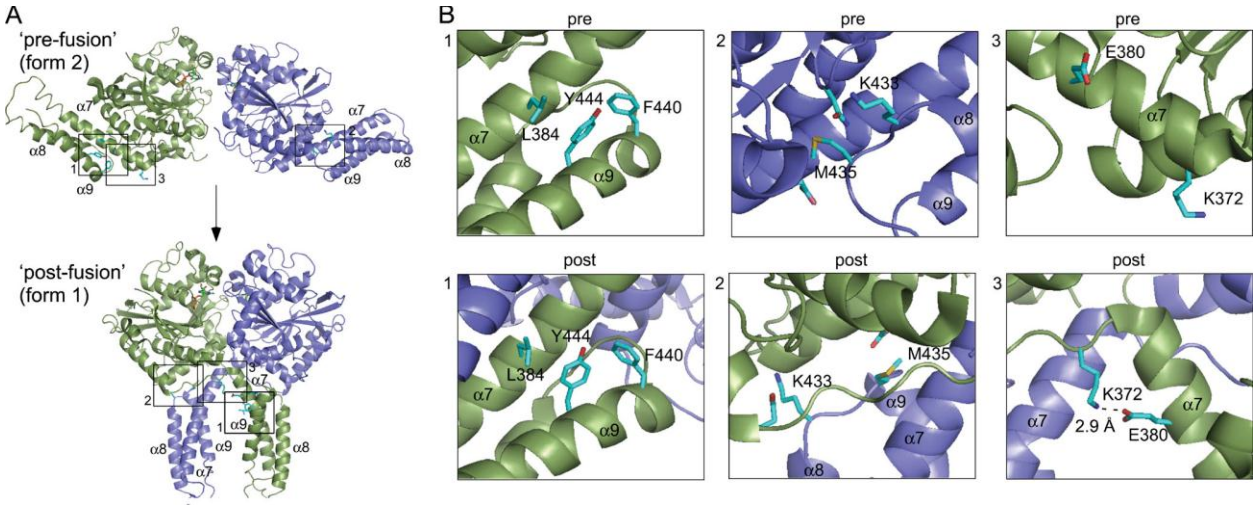

Figure 9. View of required ATL2 residues in the prefusion and postfusion conformer.

Required residues identified by knockdown replacement (Fig. 8) are shown in cartoon and stick form. The Protein Data Bank coordinates for the prefusion (3QOF) and postfusion (3QNU) ATL1 conformers were downloaded from the RCSB Protein Data Bank database (13) and rendered in PyMOL (DeLano Scientific LLC). One subunit is green, and the other is blue. Bound GDP is highlighted in sticks. (A) The location of the three categories of required residues in both pre- and postfusion dimer conformers are boxed and numbered (1–3). (B) A close-up view of the required residues boxed (1–3) in A. Key residues are numbered by

their position in the ATL2 sequence and shown in stick form. See the Results under Middle domain mutations fall into three classes for details.

A salt bridge specific to the postfusion dimer is required for ATL2 activity

To test the functional significance of the K372-E380 salt bridge seen in the postfusion structure, we first examined the effect of charge reversal of either residue on the ER network branching function of ATL2. For this, two new variants, ATL2 K372E and ATL2 E380R, were generated. Each variant was stably expressed, but neither functioned in ER network branching (Fig. 10, A and B), confirming the importance of the respective charges at the two positions. Indeed, at high expression levels, both variants exerted a dominant-negative phenotype such that an abnormal network branching pattern was seen even in the presence of endogenous ATL2/3 (Fig. 10 C). Notably, although K372 and E380 are each seen to make an additional polar contact in the postfusion dimer structure with E275 and Q376, respectively, neither charge reversal of E275 nor alanine substitution of Q376 interfered with ATL2 function (Fig. 10, A–C). Thus, the latter contacts appear dispensable. Finally, to test whether the inability of ATL2 E380R and ATL2 K372E to function might indeed be caused by their inability to form a salt bridge, the double mutant variant ATL2 K372E,E380R was constructed. We reasoned that combining the mutations in the same molecule might serve a compensatory function, restoring electrostatic attraction. Remarkably, this variant functioned indistinguishably from wild-type ATL2 in ER network branching (Fig. 10, A and B) and exhibited no dominant-negative phenotype (Fig. 10 C). Thus, the salt bridge between K372 and E380, specific to the postfusion conformer, is required for ATL2 function.

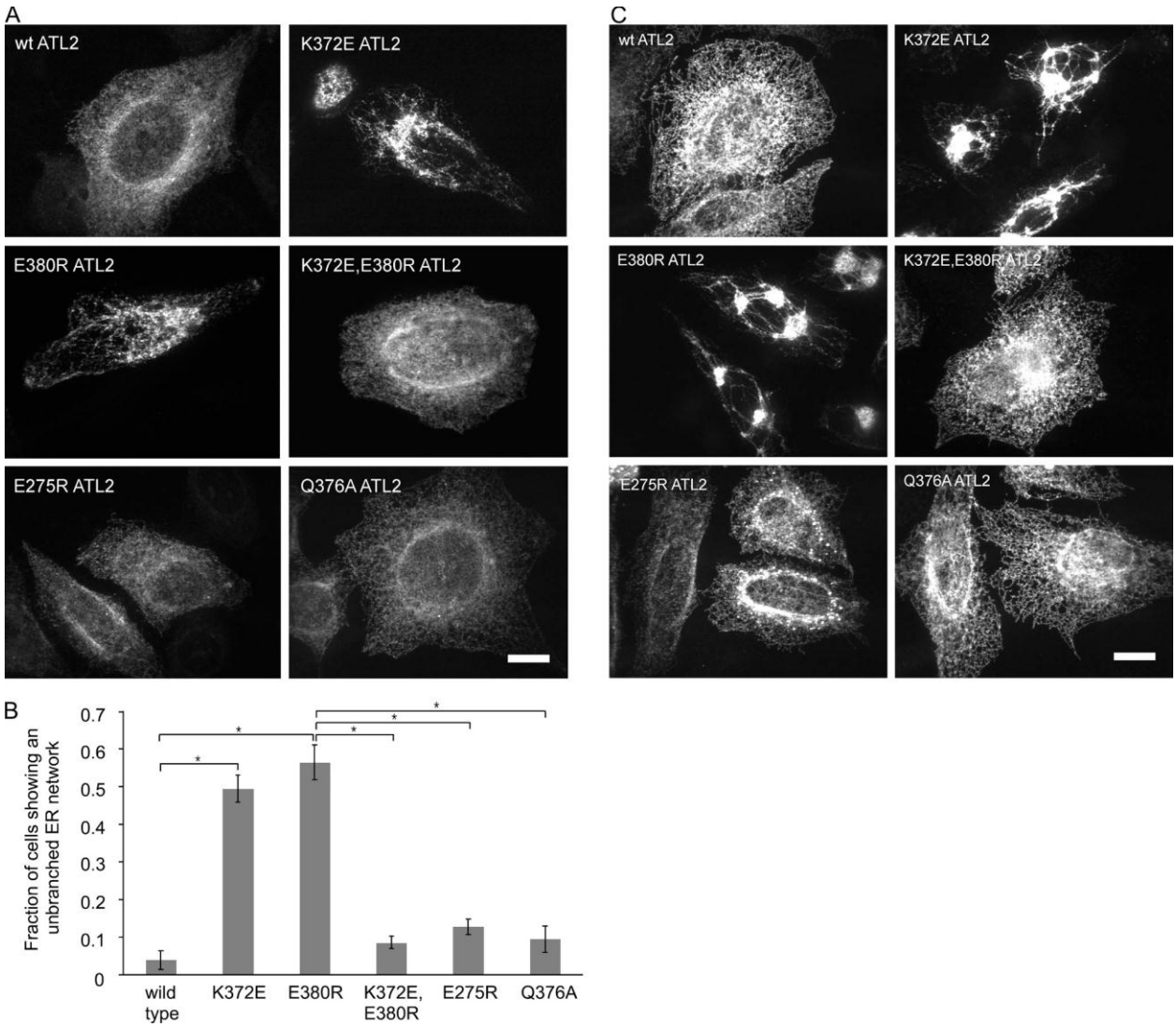

Figure 10. The K372-E380 salt bridge is required for ATL2 function.

(A) Cells transfected with the indicated HA-ATL2 variants were treated 48 h later with siRNAs against ATL2 and ATL3. 72 h after knockdown, cells were fixed and stained with antibodies against the HA epitope and viewed by confocal microscopy. (B) Quantification of the fraction of cells expressing the indicated proteins that had the unbranched ER phenotype. Values represent the means of three independent experiments ± SD. *, $P < 0.0005$. (C) High level expression of the indicated nonfunctional HA-ATL2 variants also confers a dominant-negative ER phenotype seen here even without ATL2/3 knockdown. Bars,10 μm.

The K372-E380 salt bridge is not required for either GTP binding or hydrolysis

Because the K372-E380 contact is specific to the postfusion dimer conformer, we anticipated that the most upstream steps of the proposed ATL reaction cycle, namely GTP binding, formation of the prefusion dimer, and nucleotide hydrolysis, would all be normal in the single charge reversal mutants. To assess the biochemical properties of the mutant proteins, the soluble cytoplasmic domain of the relevant ATL2 variants - wild type, K372E, E380R, and the double

mutant as well as the nucleotide binding–deficient K107A - were expressed, purified, and subjected to GTP hydrolysis assays.

Members of the dynamin superfamily of large GTPases possess a core GTPase domain with a globular fold similar to that of Ras and other small GTPases (147, 154), but their biochemical properties differ in significant ways. In contrast to Ras superfamily small GTPases that require guanine nucleotide exchange factors for GTP loading because of their high, sub-nanomolar nucleotide affinity (155), dynamin-related GTPases have a relatively low affinity for nucleotides (156). To assess nucleotide binding by ATL2 and how the K372-E380 salt bridge might influence it, the ability of each variant to bind and hydrolyze GTP was measured over a range of substrate concentrations (Fig. 11 A). When analyzed using a linearized form of the Michaelis–Menton equation (Fig. 11 B), wild-type ATL2 had an expected relatively high apparent Michaelis constant (KM) for GTP of 34 μM, well within the range of the 10–100-μM KM exhibited by other dynamin-related GTPases (155, 156). Under these conditions, K372E, E380R, and the double mutant ATL2 each exhibited a K M for GTP close to that of wild-type ATL2: 38, 35, and 44 μM for K372E, E380R, and the double mutant, respectively (Fig. 11, A and B). Therefore, the inability to form the K372-E380 contact appeared to have little impact on nucleotide binding.

Dynamin-related GTPases are also distinguished from Ras superfamily GTPases by their relatively high intrinsic catalytic activity, which renders them independent of an external GTPase-activating protein (155). In the case of dynamin, self-assembly into higher order oligomers further stimulates hydrolysis by as much as 100-fold, in a manner dependent on its associated GTPase effector domain (155, 157). Other dynamin-related GTPases, such as GBP1, have intrinsic GTPase activity but do not undergo higher order assembly (147). Consequently, these GTPases do not exhibit the dramatic assembly stimulated increase in activity that is observed for dynamin. Nevertheless, the basal GTPase activity of full-length GBP1 is stimulated three- to five-fold upon dimer formation, with a dimerization constant of 0.4 μM (147, 148). Notably, dimer-induced stimulation of GBP1 catalytic activity is observed even for truncated molecules retaining only the GTPase head domain, implying that stimulation by dimer formation requires only the head to head binding interface (148).

To assess the extent to which the ATL2 GTPase is stimulated by dimer formation, the ability of the wild-type ATL2 soluble domain to hydrolyze GTP was measured at saturated GTP concentrations under initial velocity conditions (Fig. S3 A) over a range of protein concentrations. As anticipated, the catalytic rate constant, k_{obs} , was stimulated approximately two-fold with an apparent dimerization constant of 0.2 μM (Fig. 11 C), presumably caused by enhancement of GTP binding by formation of the head to head dimer. k_{obs} began to level off at 0.3–0.5 μM ATL2, suggesting that ATL2 was largely dimeric above this concentration. No further stimulation of the GTPase activity was observed, even at concentrations as high as 30 μM ATL2 (Fig. S3 B), consistent with a lack of higher order assembly under these conditions. Next, to determine the impact of the K372-E380 salt bridge on catalytic activity, the ability of both wild-type and mutant variants to hydrolyze GTP was measured over a range of protein concentrations at which the wild-type protein was expected to be dimeric. k_{obs} for wild-type ATL2 was 6 min^{-1}, consistent with previous measurements for ATL1 (13, 14), and it did not vary significantly between 0.3 and 1.25 μM ATL2 (Fig. 11 D). As expected, the nucleotide binding–deficient K107A ATL2 exhibited only low activity, with a k_{obs} of 0.6 min^{-1}. Under these conditions, k_{obs} for K372E and E380R ATL2, as well as the double mutant variant, was indistinguishable from that of the wild type. Therefore, the ability of ATL2 to bind GTP and form a head to head dimer as well as hydrolyze GTP does not appear to depend on the K372-E380 salt bridge.

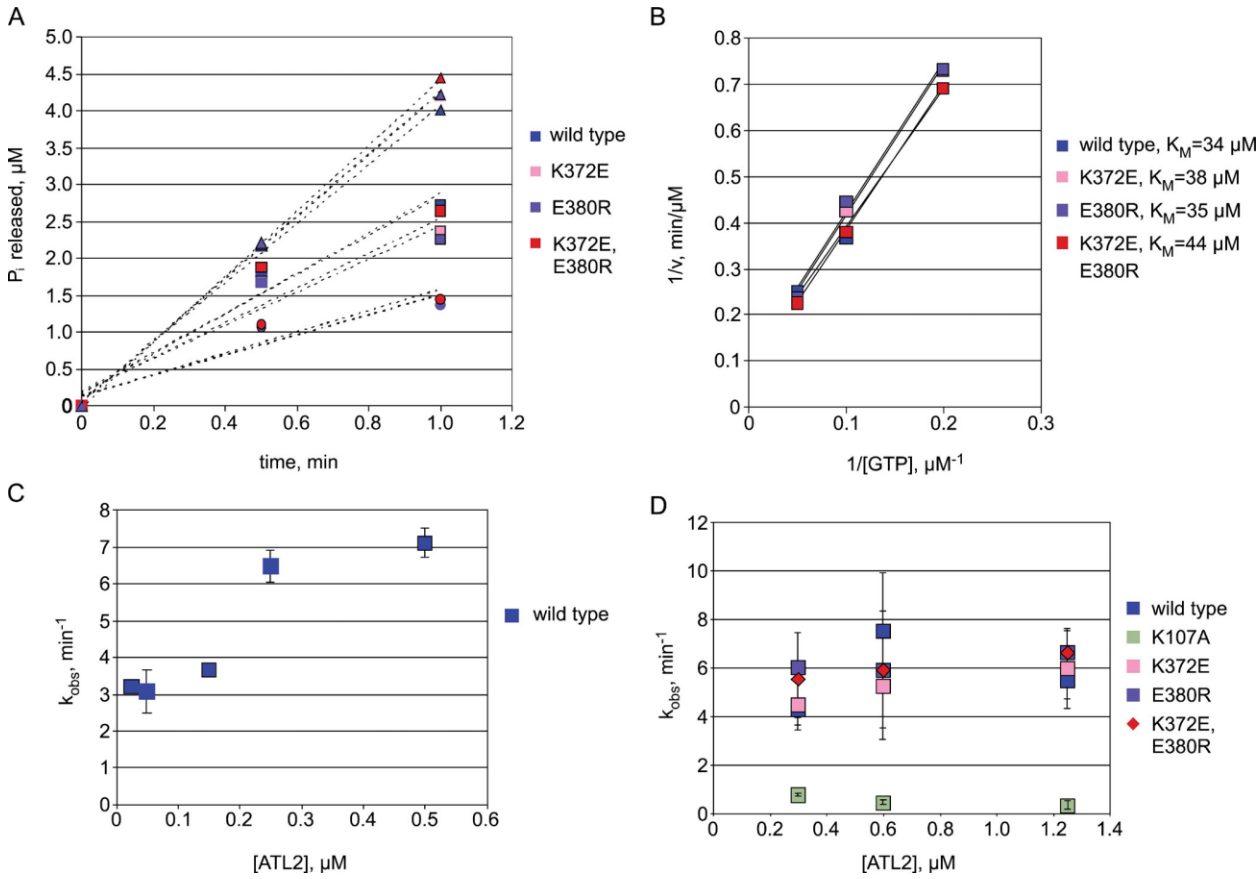

Figure 11. The K372-E380 salt bridge is not required for either nucleotide binding or hydrolysis.

(A) 1 μM of the purifi ed cytoplasmic domains (ATL2 1–467) of the indicated proteins were incubated with 5 μM (circles), 10 μM (squares), or 20 μM (triangles) GTP and assayed for phosphate release at the indicated times. Each point represents the means of two independent measurements. (B) A Lineweaver–Burk plot based on initial velocities from A was used to extract the K M of the indicated ATL2 proteins for GTP. (C) The indicated concentrations of wild-type ATL2 were incubated with 0.2 mM GTP followed by assaying for phosphate release. (D) 0.3, 0.6, or 1.25 μM of the indicated ATL2 variants was incubated with 0.2 mM GTP followed by an assay for phosphate release. Values represent the means of three independent measurements ± SD. v, initial velocity.

The K372-E380 ionic contact is required for stable dimer formation

The undiminished ability of K372E ATL2 and E380R ATL2 to bind and hydrolyze GTP suggested that prefusion (head to head) dimer formation was normal. Formation of a GMPPNP-dependent dimer, as detected by size exclusion chromatography (SEC), has been suggested previously by others to reflect formation of the GTP-bound prefusion state (13, 14). Therefore, we next subjected each variant to SEC analysis.

Consistent with previous studies (13, 14), the soluble domain of wildtype ATL2 formed dimers in the presence, but not in the absence, of GMPPNP (Fig. 12). No ATL2 dimerization was observed with GDP, consistent with previous studies for ATL1 (14, 97), though contrasting with

another (13). Also as expected, stable dimer formation was diminished for the nucleotide binding–defi cient ATL2 K107 (Fig. S4). Under these conditions, both ATL2 K372E and ATL2 E380R were expected to form stable dimers. To our surprise, the level of ATL2 K372E and ATL2 E380R in the dimer fractions was negligible, regardless of whether they had been incubated with GMPPNP (Fig. 12). Remarkably, however, the compensatory charge reversal mutation in ATL2 K372E,E380R fully restored GMPPNP-dependent dimer formation. Thus, in contrast to expectations, the K372-E380 salt bridge is required to form a stable GMPPNP dimer.

The soluble domain of ATL2 adopts the postfusion conformation in the GMPPNP-bound (GTP bound) state

The inability of ATL2 K372E and ATL2 E380R to form the GMPPNP-dependent solution dimer raised the possibility that the GMPPNP solution dimer actually corresponds to the postfusion, rather than prefusion conformer. The implications of this hypothesis are significant, as it would imply that the ATL2 soluble domain achieves the postfusion conformation in the GTP-bound state, not requiring nucleotide hydrolysis. To test this possibility, we used two independent means to probe the conformational state of ATL2 in the presence of various nucleotide analogues.

First, we attempted to visualize the GMPPNP-bound ATL2 solution dimer by single-particle EM of negatively stained samples. EM images of GMPPNP-bound ATL2 particles were processed, and a total of 571 individual particle images were boxed manually, band-pass filtered, and aligned with respect to their center of mass. To test whether GMPPNP-bound ATL2 adopts the prefusion or postfusion conformation, two 3D density maps from the same set of particle images were reconstructed using two different initial reference maps calculated from the atomic models of the prefusion (Protein Data Bank accession no. 3QOF) and postfusion (Protein Data Bank accession no. 3QNU) ATL1 conformers (shown in Fig. 9 A). The resulting 3D maps resembled the postfusion conformation more than the prefusion one (Fig. S5). Cross-correlation values between the final density maps and their respective initial references were 0.293 for the prefusion map and 0.425 for the postfusion map, indicating that the GMPPNP-bound ATL2 dimer more likely adopts the postfusion configuration.

The second method was cross-linking. Bismaleimidoethane (BMOE) is a short bifunctional sulfhydryl cross-linker capable of conjugating two cysteine residues to one another if they lie in close enough (10 Å) proximity. ATL2 has three surface-exposed cysteines. Two are in the head (C59 and C144) and one is in the middle domain (C395). Of these, only the middle domain C395 residue is in a position to mediate cross-linking of one monomer to the other to form a covalently conjugated dimer. Importantly, C395-mediated dimer conjugation is predicted to occur in the postfusion state but not in the prefusion state (Fig. 13 A). This is because the C395 residues of the two monomers are <20 Å apart in the postfusion dimer, but they are >100 Å apart in the prefusion dimer. In contrast to C395, the other two cysteines in the head are too far apart, >50 Å, in either dimer configuration. Nevertheless, they may mediate crosslinking within the monomer, likely leading to the slightly more rapidly migrating species of the monomer seen even in the absence of nucleotide. Significantly, cross-linker–dependent dimer conjugation was observed only in the presence of GMPPNP (Fig. 13 B). Dimer formation was not observed in the absence of nucleotide or in the presence of GDP or GTP, indicating that the postfusion conformation is specific to the GMPPNP-bound (or GTP bound) state. Presumably, postfusion dimer formation also occurs transiently with bound GTP, but subsequent hydrolysis returns it to the monomer state. As a control to confirm that the GMPPNP dimer is cross-linked through the middle domain C395 residue, an ATL2 variant lacking the C395 sulfhydryl (ATL2 C395N) was tested. As predicted, it failed to form dimers either in the presence or absence of GMPPNP. To further validate our assay for postfusion dimer formation, ATL2 K372E and ATL2 E380R were each subjected to the same assay. As predicted by their behavior in SEC, neither of the single mutant variants formed the GMPPNP-dependent cross-linked dimer, whereas the compensatory double mutation restored dimer formation (Fig. 6 C). These results argue that the soluble domain of ATL2 adopts the postfusion conformation exclusively in the GMPPNP-bound (or GTP bound) state. Moreover, although nucleotide hydrolysis is dispensable for achieving the postfusion state, at least for the soluble domain, formation of the K372-E380 salt bridge is not.

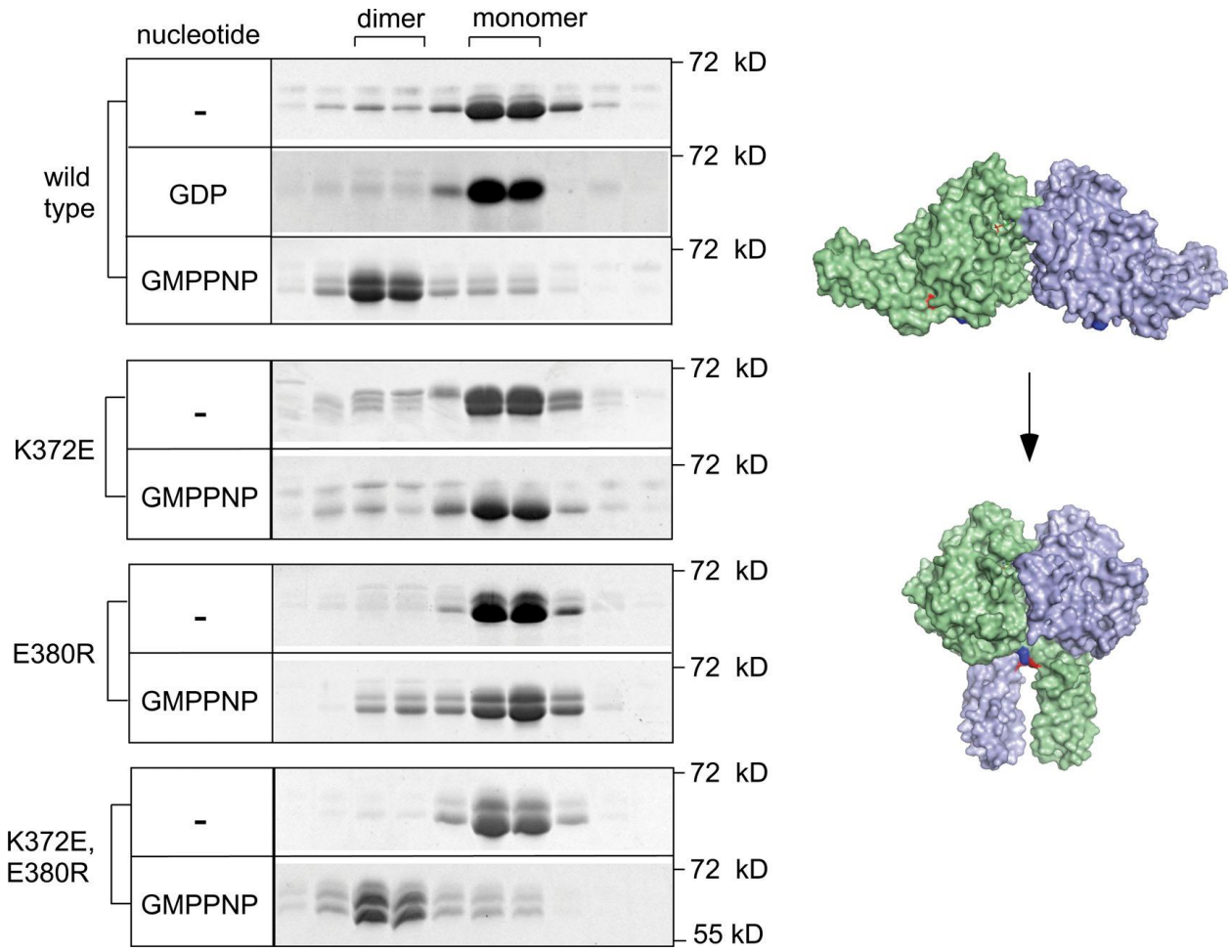

Figure 12. The K372-E380 contact is required for GMPPNP-dependent stable dimer formation.

The purified cytoplasmic domains of the indicated ATL2 variants (30 µM) were incubated with no nucleotide (-), 5 mM GDP, or 2 mM GMPPNP for 30 min at RT. Thereafter, samples were resolved on a Superdex 200 column. The Coomassie-stained proteins (~60 kD) present in monomer (~70 kD) and dimer peak (~150 kD) positions from each column run are shown after SDS-PAGE. Also shown is a surface rendering of pre- and postfusion dimer conformers with K372 and E380 highlighted in blue and red, respectively. Models were drawn in PyMOL from Protein Data Bank no. 3QOF and 3QNU.

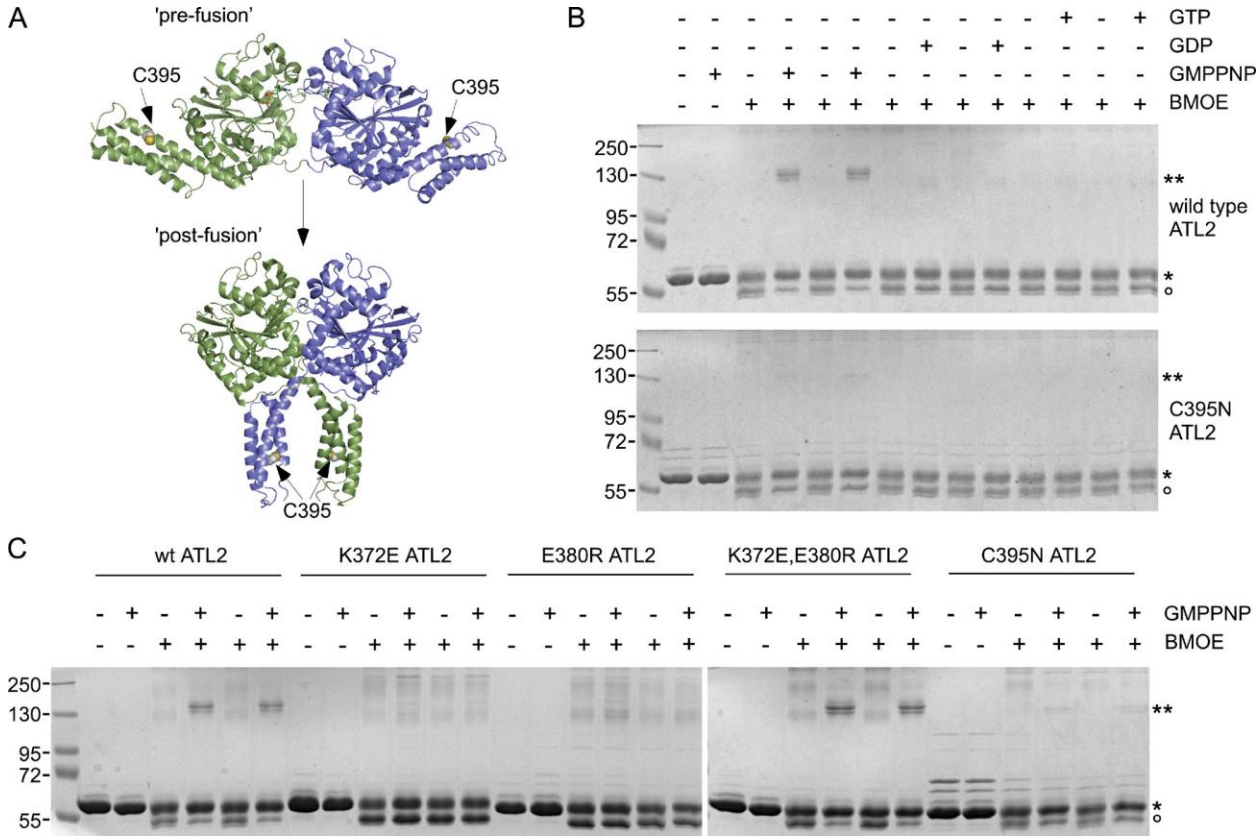

Figure 13. GTP hydrolysis is not required for the prefusion to postfusion conformational change.

(A) Location of the C395 residue in ATL2 used to report on the postfusion conformation. The C395 side chain in ATL2 is highlighted as spheres in both pre- and postfusion ATL1 dimer structures rendered as detailed in Fig. 2 . (B) The purified cytoplasmic domain of wild-type or C395N ATL2 (20 μM) was incubated in the presence or absence of the indicated nucleotides for 30 min at RT. Thereafter, samples were diluted, further incubated with or without BMOE for 1 h at RT, resolved by SDS-PAGE, and stained with Coomassie blue. The positions of non–cross-linked monomer and covalently cross-linked dimer ATL2 are indicated by single and double asterisks, respectively. The open circle indicates the position of ATL2 likely to have cysteine modifications not leading to dimer formation. (C) The purified cytoplasmic domains of the indicated ATL2 variants were subjected to the assay as described in B. Molecular masses are given in kilodaltons.

Supplemental Data

Fig. S1 shows that RNAi-mediated depletion of both ATL2 and ATL3 leads to a reduction of ER network branch points in HeLa cells. Fig. S2 shows that the middle domain ATL2 residues required for function lie near the GTPase head. Fig. S3 shows that the linearity of GTPase assay and ATL2 GTPase activity are not further stimulated at high ATL2 concentrations. Fig. S4 shows that stable formation of ATL2 soluble domain dimers depends on GTP binding. Fig. S5 shows an EM analysis of the GMPPNP-bound ATL2 solution dimer, indicating that the soluble domain of ATL2 is more likely to adopt the postfusion dimer conformation when it is bound to GMPPNP.

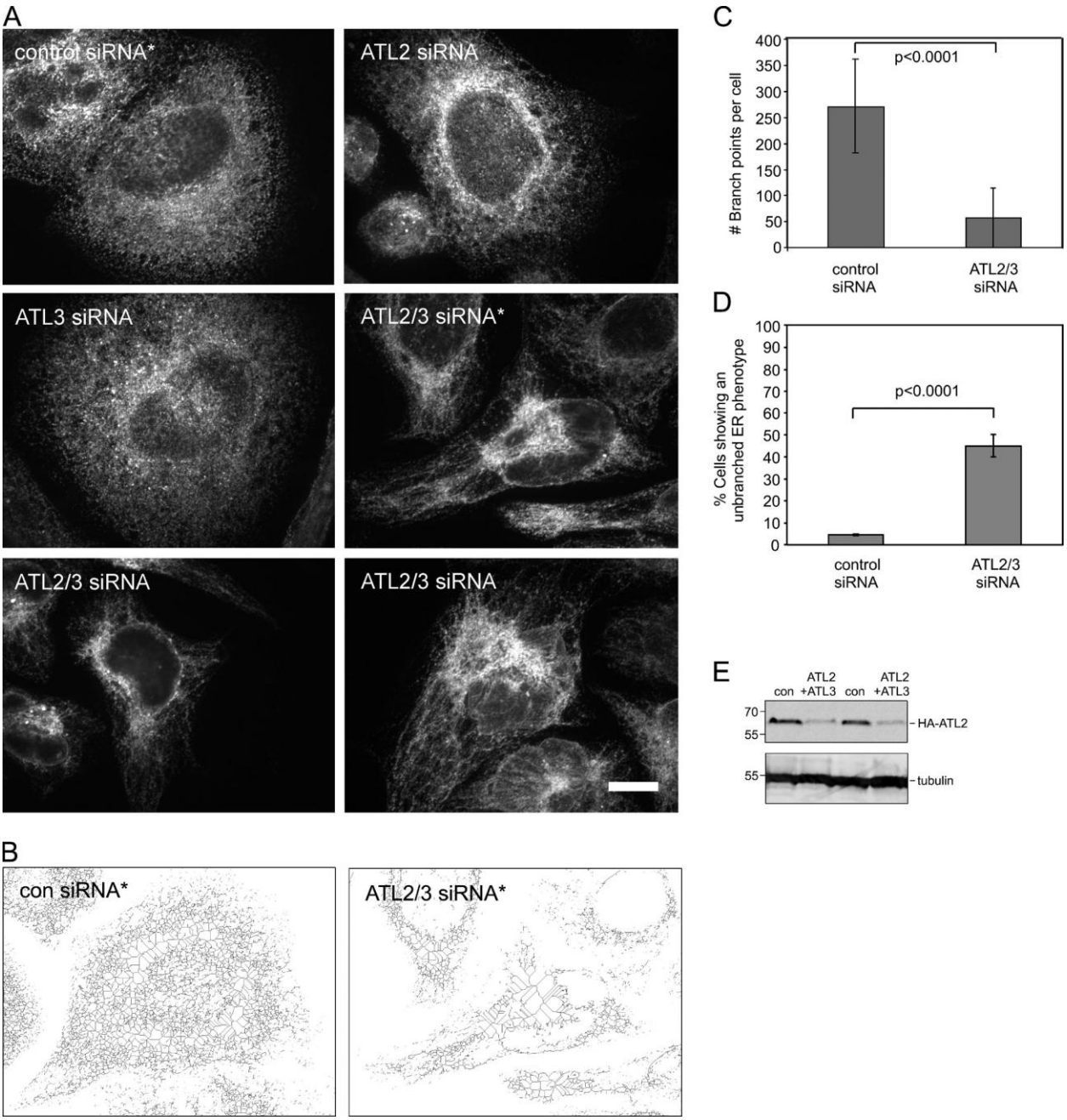

Figure S 1. Depletion of both ATL2 and ATL3 causes a reduction in ER network branch points. (A) Cells transfected with a PRA2 control (con) siRNA, ATL2 siRNA, ATL3 siRNA, or ATL2/3 siRNA were fixed, stained using an antibody against the ER marker protein disulfide isomerase, and viewed by confocal microscopy. Bar, 10 µm. (B) Maximal z projections of confocal images from A were thresholded and skeletonized in ImageJ (National Institutes of Health). Asterisks indicate corresponding images in A. (C) Quantification of the mean number of three-way junctions in 10 skeletonized images from PRA2 control and ATL2/3 siRNA–treated cells. (D) Quantification of the percentage of cells transfected with a control siRNA or ATL2/ATL3 siRNA showing the unbranched ER phenotype, defined as having <100 branch points per cell. Values represent the means of three independent experiments ± SD. (E) Immunoblot showing ATL2 knockdown. Cells transfected with an siRNA-sensitive HA-ATL2 construct were subsequently treated with a PRA2 control siRNA or ATL2/3 siRNA and processed for immunoblotting using antibodies against the HA epitope. Molecular masses are given in kilodaltons.

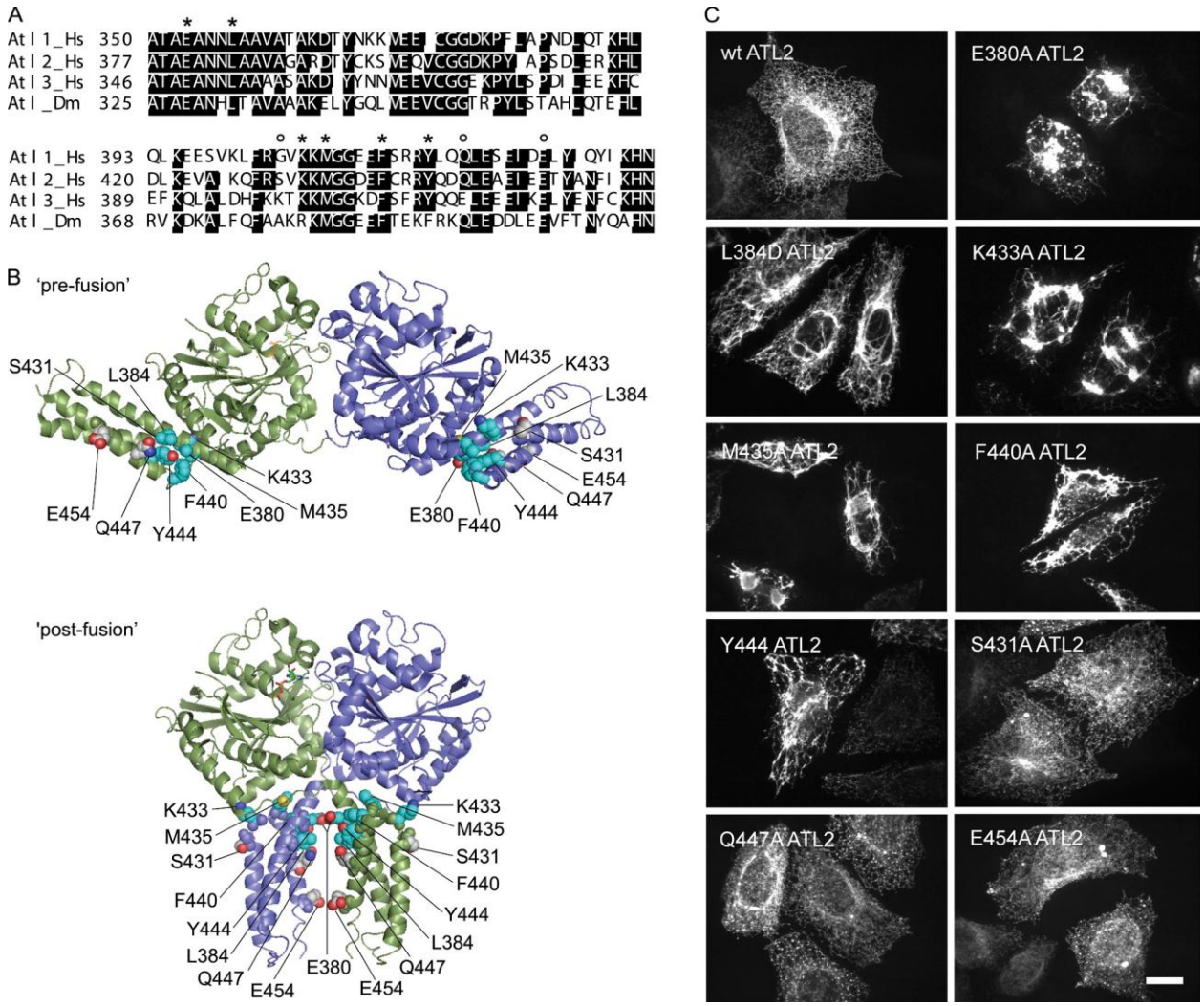

Figure S 2. Middle domain ATL2 residues required for function lie near the GTPase head. (A) Alignment of middle domain amino acids of human ATL1–3 and Drosophila ATL, with conserved residues shaded. Residues shown to be functionally required are labeled with asterisks, and residues shown to be nonessential are labeled with open circles. (B) Residues marked in A are labeled and highlighted as spheres in both prefusion and postfusion ATL1 dimer structures (L384 was an exception as it was replaced by D384). Functionally required side chains are labeled with carbon in cyan, and nonessential side chains with carbon are in gray. The numbering is according to the ATL2 sequence. The Protein Data Bank coordinates for the prefusion (3QOF) and postfusion (3QNU) ATL1 conformers were downloaded from the RCSB Protein Data Bank database (13) and rendered in cartoon form in PyMOL. One subunit is green, and the other is blue. GDP is highlighted in sticks. (C) High level expression of certain ATL2 variants with an alanine substitution in a functionally required residue results in a dominant-negative effect on ER morphology. Cells transfected with wild-type (wt) HA-ATL2 or various point mutant HA-tagged-ATL2 variants and expressing high levels of the protein were fixed, stained using an antibody against the HA epitope, and viewed by confocal microscopy. Endogenous ATL2/3 is present in these cells, as no knockdown was performed. Bar, 10 μm.

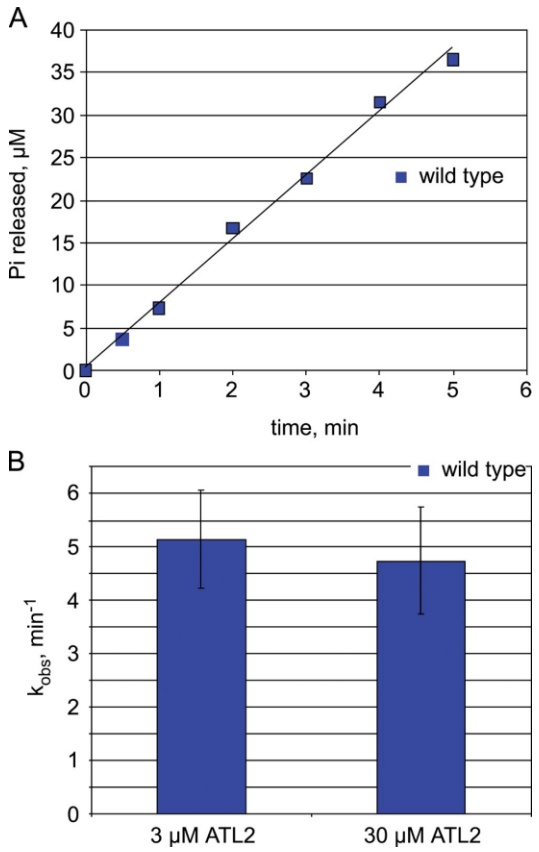

Figure S 3. Linearity of GTPase assay and ATL2 GTPase activity are not further stimulated at high ATL2 concentrations. (A) 1 µM ATL2 was incubated with 0.2 mM GTP at 37°C for the indicated times followed by quenching with EDTA and assaying for phosphate release. (B) 3 or 30 µM ATL2 was incubated with 1 mM GTP at 37°C for 1 min, quenched, and diluted 10-fold before assaying for phosphate release. Data represent the means of four independent measurements ± SD. P = 0.57.

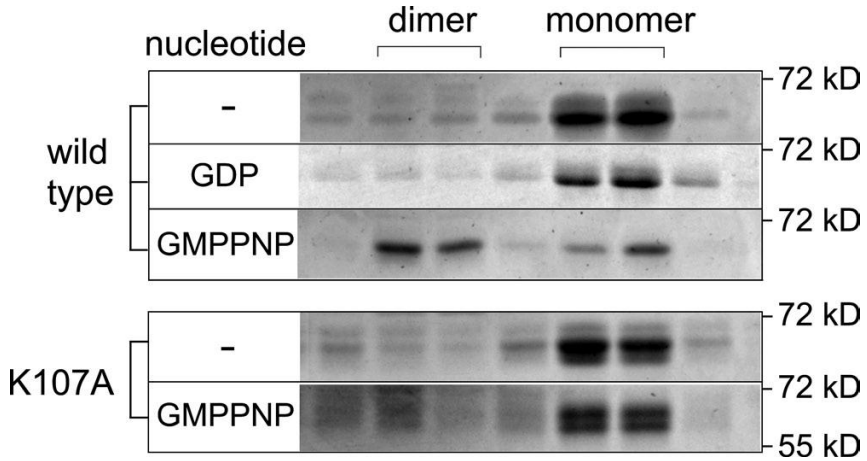

Figure S 4. Stable dimerization of the soluble domain of ATL2 depends on nucleotide binding. The purified cytoplasmic domain of wild type or the nucleotide binding–deficient K107A ATL2 variant (10 µM) was incubated with no nucleotide (-), 2 mM GMPPNP, or 5 mM GDP for 30 min at RT. Thereafter, samples were resolved on a Superdex 200 column. The Coomassie-stained proteins (60 kD) present in monomer (~70 kD) and dimer peak (~150 kD) positions from each column run are shown after SDS-PAGE.

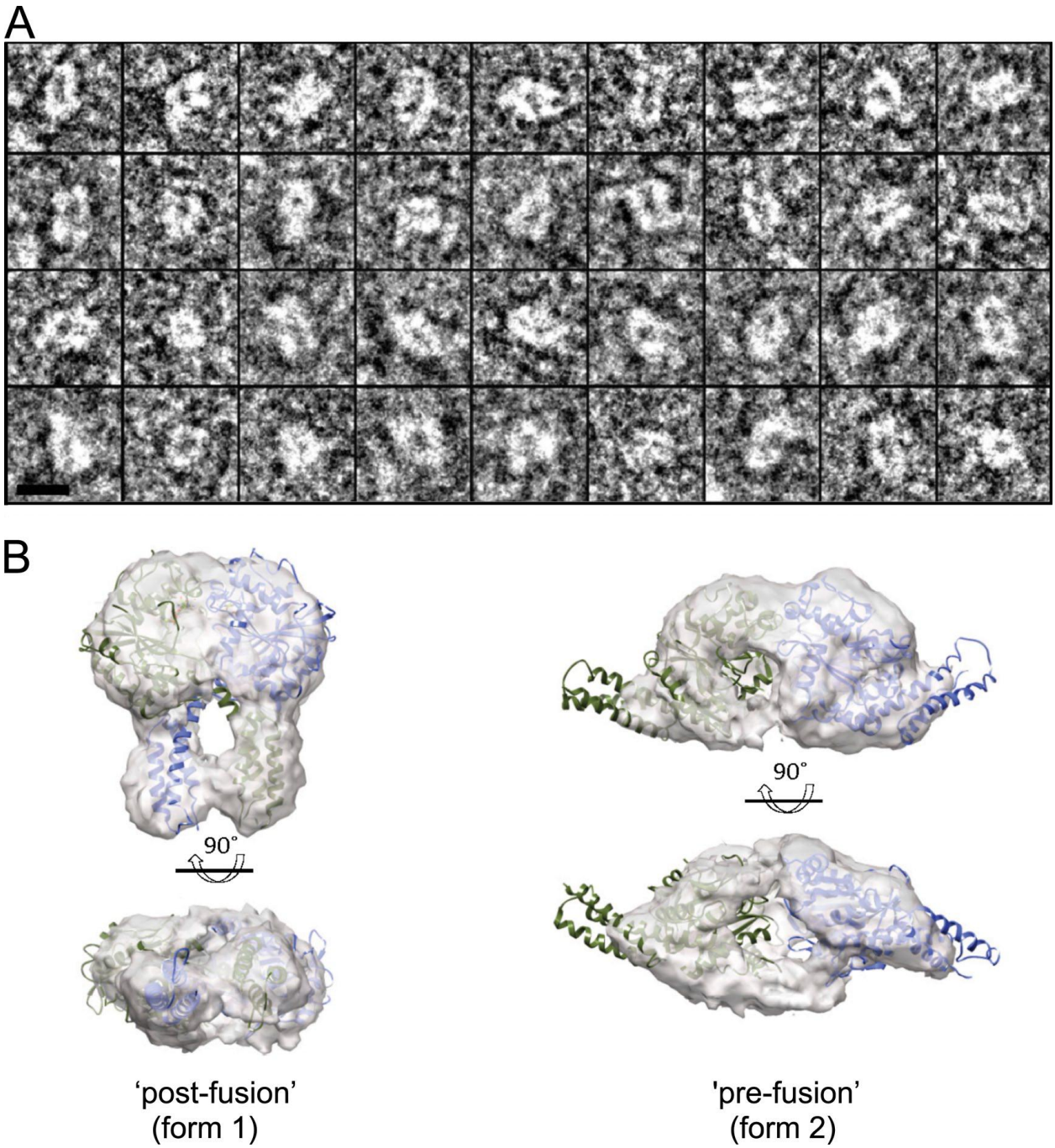

Figure S 5. EM of the GMPPNP-bound ATL2 GTPase. Representative raw particle images of GMPPNP-bound ATL2 boxed out from electron micrographs of negatively stained samples. Bar, 8 nm. (B) 3D reconstruction of dimeric ATL2 density maps using two atomic models representing the two ATL1 conformers, form 1 (Protein Data Bank accession no. 3QNU) and form 2 (Protein Data Bank accession no. 3QOF) as initial references.

3.5 Discussion

Our findings reveal an intramolecular salt bridge required for the ER network branching function of ATL2. The importance of the K372-E380 ionic interaction for ATL2 function is likely caused by its stabilization of the postfusion dimer conformation. This might seem surprising given that the charge interaction occurs intramolecularly, within each monomer subunit of the dimer. Based on the position of the salt bridge in the context of the postfusion dimer, we speculate that the ionic contact constrains the linker in a kinked conformation relative to the head and middle domains. In so doing, it may serve to position M374 and L375, two intervening nonpolar residues that need to pack extensively against the opposing head, to form the postfusion conformation. In the absence of the salt bridge, the linker may be rendered too flexible, reducing the ability of M374 and L375 to pack effectively.

Previous observations are consistent with the K372-E380 salt bridge being required for ATL-catalyzed membrane fusion. A Drosophila ATL variant bearing a mutation equivalent to E380R is significantly reduced in its ability to catalyze liposome fusion (13), though neither its GTPase activity nor its ability to dimerize has been reported. In addition, a Drosophila variant with a mutation equivalent to K372E lacks fusion activity (13). Thus, the opposing charge carried by the two residues appears functionally important. Whether the salt bridge, per se, is required for fusion activity remains to be determined. But based on the cumulative evidence, it seems likely that the ability of the two residues to engage in a salt bridge will be required for stabilizing the postfusion dimer and hence for membrane fusion, even in the more distantly related organism.

Our finding that the ATL2 soluble domain can achieve the postfusion conformation in the GMPPNP (or GTP)-bound state without nucleotide hydrolysis contrasts with the conclusions from an earlier study. In that study, biochemical analyses performed on the ATL1 soluble domain were used to arrive at the opposite conclusion: that ATL1 adopts the prefusion conformation in the GTP-bound state and the postfusion conformation in the GDP-bound state (13). This has contributed, at least in part, to the current model for ATL proposing that ATL the prefusion to postfusion conformational change is directly coupled to GTP hydrolysis and P i release. The reasons for the conflicting results and conclusions remain unclear, and further work will be needed to resolve the discrepancy. Nevertheless, the results presented herein clearly

indicate that GTP binding, in the absence of hydrolysis, is sufficient to induce the prefusion to postfusion conformational change, at least for the ATL2 soluble domain.

As shown previously for GBP1 (147, 148), we observed a modest concentration-dependent stimulation of the ATL2 soluble domain GTPase activity in the sub-micromolar range. By analogy to GBP1, this is likely caused by enhancement of GTP binding by formation of the head to head dimer. As the K372-E380 salt bridge is not present in the crystal structure of the initial nucleotide-bound prefusion dimer (13, 14), mutations hindering formation of the salt bridge would not be predicted to impair the initial dimer-induced stimulation of GTP binding and hydrolysis. As expected, neither the K372E nor E380R mutant variants were diminished in their ability to bind or hydrolyze GTP. This result underscores the specificity of the defect in the K372E and E380R mutant ATL2 they are likely able to form the initial head to head contact and bind GTP as well as the wild-type protein, yet they fail to transition to the postfusion conformation.

Our observation that GTP hydrolysis is neither required for, nor dependent on, formation of the postfusion conformation is somewhat surprising. It will be important to determine whether this behavior of the soluble domain reflects that of the full-length molecule in membranes. Finally, the interpretation of our findings with respect to the role of GTP hydrolysis in the ATL fusion mechanism also needs to be tempered by the uncertainty of whether the behavior of the ATL2 soluble domain, observed herein, reflects the behavior of the full-length, membrane-anchored protein. A possibility deserving of consideration is that membrane-anchored ATL is more conformationally constrained than its soluble counterpart. That is, whereas the soluble domain is sufficiently flexible to adopt the postfusion conformation when restricted to the GTP-bound state, membrane-anchored ATL may require an additional input of energy, provided perhaps by the hydrolysis of GTP within the prefusion dimer. A requirement for nucleotide hydrolysis for formation of the membrane-anchored postfusion dimer would serve to explain the requirement for GTP hydrolysis in ATL variants: they are likely able to form the initial head to head contact and bind GTP as well as the wild-type protein, yet they fail to transition to the postfusion conformation.

Our observation that GTP hydrolysis is neither required for, nor dependent on, formation of the postfusion conformation is somewhat surprising. It will be important to determine whether this

behavior of the soluble domain reflects that of the full-length molecule in membranes. Finally, the interpretation of our findings with respect to the role of GTP hydrolysis in the ATL fusion mechanism also needs to be tempered by the uncertainty of whether the behavior of the ATL2 soluble domain, observed herein, reflects the behavior of the full-length, membrane-anchored protein. A possibility deserving of consideration is that membrane-anchored ATL is more conformationally constrained than its soluble counterpart. That is, whereas the soluble domain is sufficiently flexible to adopt the postfusion conformation when restricted to the GTP-bound state, membrane-anchored ATL may require an additional input of energy, provided perhaps by the hydrolysis of GTP within the prefusion dimer. A requirement for nucleotide hydrolysis for formation of the membrane-anchored postfusion dimer would serve to explain the requirement for GTP hydrolysis in ATL-catalyzed liposome fusion (11). On the other hand, this scenario depends on the membrane-anchored prefusion dimer being compatible with the GTP-bound state and the postfusion dimer being compatible with the GDP-bound state. This seems counterintuitive, given that the postfusion conformation of the soluble domain is clearly compatible with the GMPPNP (or GTP)-bound state but most likely not with the GDP-bound state (Fig. 13 B).

An alternative possibility is that the behavior of the soluble domain does indeed reflect the behavior of the membrane anchored full-length protein. In the latter scenario, we would propose that nucleotide hydrolysis is not directly coupled to the prefusion to postfusion conformational change but rather that the energy released from hydrolysis is harnessed to drive another discrete step in the ATL reaction cycle. Whatever the identity of that hydrolysis-dependent step, it should explain the observed requirement for GTP hydrolysis in the in vitro fusion assay (11). Further work to determine the conformational states of GTP- and GDP-bound membrane-anchored ATL2, as well as the impact of the salt bridge identified herein on the catalytic properties of full-length and membrane anchored ATL2, promises to more clearly delineate the role of nucleotide hydrolysis in the ATL2 mechanism.

Chapter IV. Discussion

4.1 The future of atlastin

There remain a number of exciting questions to be explored as we and other labs clarify the mechanism of atlastin's action. Based on the evidence available so far, we can propose a speculative model where atlastin, bound to nucleotide, undergoes the conformational change that drives the membranes together, causing formation of the putative post-fusion conformer, and then the hydrolysis of GTP may drive the final stage of fusion while disassembling the complex, allowing GDP and Pi to be released and thus return atlastin to its unbound monomeric state. Given our data so far the first question to address is: does atlastin function in the context of membranes as it does in our experiments? That is, is hydrolysis really dispensable for the transition from the pre- to post-fusion conformer? If it is, then what is it doing? As speculated above, it may be that hydrolysis is coupled to the disassembly of post-fusion complexes. Hydrolysis is coupled through NSF to the disassembly of SNAREs, so it is not unreasonable to imagine that a comparable input of energy would be necessary to dissociate atlastin dimers.

Another important question to address is how GTP hydrolysis is regulated. We have shown that GTP hydrolysis, while it is not required to form the post-fusion dimer, it is also not dependent on the formation of the post-fusion dimer. So we can exclude that the conformational change regulates hydrolysis, which would be an obvious way for atlastin to work. But it's possible, for example, that GTP hydrolysis is relatively slow with respect to the pre- to post-fusion conformational change that is driven by GTP binding. If this is the case then if atlastin undergoes a failed attempt at the pre- to post-fusion conformational change, hydrolysis would still eventually occur, destabilizing the complex and releasing atlastin for another attempt.

The regulation of GTP hydrolysis is an exciting question, but it opens the door to an entire set of regulatory questions. Most broadly, the regulation of atlastin's fusion activity remains to be addressed. Presumably atlastin cannot be constitutively active. It is not obvious from the studies so far that atlastin is concentrated at a subdomain of ER membranes, such as growing tips of new tubules that are likely to eventually undergo a fusion event, so restriction of atlastin's localization to actively fusing membranes is unlikely to regulate atlastin's fusion activity.

Elucidation of the elements responsible for atlastin's regulation may shed light on a number of other questions. We know that Atlastin-1 can interact with Spastin, a microtubule-severing protein (158), and although that interaction has not been shown to have a regulatory role so far, and indeed it seems that atlastins 2 and 3 do not interact with Spastin, it is reasonable that there could be a mechanism for regulating ER fusion events that involves or is coupled to the regulation of growing microtubule tips, for example.

Finally, and perhaps most simply, it is going to be important to understand what all the regions of the atlastin protein are doing and how they contribute to function. So far the preponderance of data deals with the soluble portion of atlastin. The role of the c-terminus, for example, has yet to be clarified, although preliminarily it seems that it may be required for fusion *in vitro* (97). And although atlastin has two transmembrane domains, whether both are required for fusion or if one would be sufficient, or whether there are important interacting factors that have interfaces in the membrane, or if particular elements in the transmembrane domain that are important for function is not clear.

I highly anticipate the clarification of these questions and am confident that a deeper understanding of atlastin and its regulation will lead to a deeper understanding of ER structure, dynamics, and function.

References

1. Rapoport, T. A. Protein translocation across the eukaryotic endoplasmic reticulum and bacterial plasma membranes. Nature 450(7170): 663-669 (2007).

2. Voeltz GK, Rolls MM, and Rapoport TA. Structural organization of the endoplasmic reticulum EMBO reports 3, 10, 944–950 (2002).

3. Terasaki M and Jaffe LA. Organization of the sea urchin egg endoplasmic reticulum and its reorganization at fertilization. J. Cell Biol., 114, 929–940 (1991).

4. Federovitch CM, Ron D and Hampton RY. The dynamic ER: experimental approaches and current questions. Current Opinion in Cell Biology, 17, 409–414 (2005).

5. English AR, Surek N and Voeltz G. Peripheral ER structure and function. Curr. Opinion in Cell Biol. 21 596-602 (2009).

6. Vale RD and Hotani H. Formation of Membrane Networks In Vitro by Kinesin-driven Microtubule Movement. J Cell Biol 107 No. 6 2233-2241(1988).

7. Terasaki, M. et al. Microtubules and the endoplasmic reticulum are highly interdependent structures. J. Cell Biol. 103, 1557–1568 (1986).

8. Grigoriev I, Gouveia SM, van der Vaart B, Demmers J, Smyth JT, Honnappa S, Splinter D, Steinmetz MO, Putney Jr. JW, Hoogenraad CC, Akhmanova A. STIM1 Is a MT-Plus-End-Tracking Protein Involved in Remodeling of the ER Curr. Biol. 18, 177-182 200 (2008).

9. L. Dreier, T.A. Rapoport, In vitro formation of the endoplasmic reticulum occurs independently of microtubules by a controlled fusion reaction, J. Cell Biol. 148 (2000) 883–898.

10. C. Ungermann, D. Langosch, Functions of SNAREs in intracellular membrane fusion and lipid bilayer mixing, J Cell Sci 118 (2005) 3819–3828.

11. Orso , G. , D. Pendin , S. Liu , J. Tosetto , T.J. Moss , J.E. Faust , M. Micaroni , A. Egorova , A. Martinuzzi , J.A. McNew , and A. Daga. Homotypic fusion of ER membranes requires the dynamin-like GTPase atlastin . Nature . 460 : 978 – 983(2009).

12. Hu , J. , Y. Shibata , P.P. Zhu , C. Voss , N. Rismanchi , W.A. Prinz , T.A. Rapoport , and C. Blackstone . 2009 . A class of dynamin-like GTPases involved in the generation of the tubular ER network . Cell . 138 : 549 – 561

13. Bian , X. , R.W. K lemm , T.Y. L iu , M. Zhang , S. Sun , X. Sui , X. Liu , T.A. Rapoport , and J. Hu. Structures of the atlastin GTPase provide insight into homotypic fusion of endoplasmic reticulum membranes . Proc. Natl. Acad. Sci. 108 : 3976 – 3981 (2011).

14. Byrnes , L.J. , and H. Sondermann. Structural basis for the nucleotidedependent dimerization of the large G protein atlastin-1/SPG3A . Proc. Natl. Acad. Sci. 108 : 2216 – 2221(2011) .

15. L. Kapetanovich, C. Baughman, T.H. Lee, Nm23H2 facilitates Coat Protein II assembly and endoplasmic reticulum export in mammalian cells, Mol. Biol. Cell 16 835–848 (2005).

16. Rismanchi , N. , C. Soderblom , J. Stadler , P.P. Zhu , and C . Blackstone . 2008. Atlastin GTPases are required for Golgi apparatus and ER morphogenesis . Hum. Mol. Genet. 17 : 1591 – 1604

17. English AR, Surek N and Voeltz G. Peripheral ER structure and function. Curr. Opinion in Cell Biol. 21 596-602 (2009).

18. Anderson DJ and Hetzer MW. Shaping the endoplasmic reticulum into the nuclear envelope J Cell Sci 121, 137-142 (2008).

19. Schirmer E C, Florens L, Guan T, Yates J R, 3rd and Gerace L. Nuclear membrane proteins with potential disease links found by subtractive proteomics. Science 301, 1380-1382 (2003).

20. Stuurman N, Heins S and Aebi U. Nuclear lamins: their structure, assembly, and interactions. J. Struct. Biol. 122, 42–66 (1998).

21. Gruenbaum, Y. et al. The nuclear lamina and its functions in the nucleus. Int. Rev. Cyt. 226, 1–62 (2003).

22. Zastrow, M. S., Vlcek, S. & Wilson, K. L. Proteins that bind A-type lamins: integrating isolated clues. J. Cell Sci. 117, 979–987 (2004).

23. Starr, D. A. et al. unc-83 encodes a novel component of the nuclear envelope and is essential for proper nuclear migration. Development 128, 5039–5050 (2001).

24. Lee, K. K. et al. Lamin-dependent localization of UNC-84, a protein required for nuclear migration in C. elegans. Mol. Biol. Cell 13, 892–901 (2002).

25. Malone, C. J. et al. The C. elegans Hook protein, ZYG-12, mediates the essential attachment between the centrosome and nucleus. Cell 115, 825–836 (2003).

26. Zhen, Y. Y., Libotte, T., Munck, M., Noegel, A. A. & Korenbaum, E. NUANCE, a giant protein connecting the nucleus and actin cytoskeleton. J. Cell Sci. 115, 3207–3222 (2002).

27. Liu, J. et al. Essential roles for Caenorhabditis elegans lamin gene in nuclear organization, cell cycle progression, and spatial organization of nuclear pore complexes. Mol. Biol. Cell 11, 3937–3947 (2000).

28. Schirmer, E. C., Guan, T. & Gerace, L. Involvement of the lamin rod domain in heterotypic lamin interactions important for nuclear organization. J. Cell Biol. 153, 479–490 (2001).

29. Sidrauski C and Walter P. The Transmembrane Kinase Ire1p Is a Site-Specific Endonuclease That Initiates mRNA Splicing in the Unfolded Protein Response. Cell. 90, 1031–1039 (1997).

30. Federovitch CM, Ron D and Hampton RY. The dynamic ER: experimental approaches and current questions. Current Opinion in Cell Biology, 17, 409–414 (2005).

31. Friedman JR and Voeltz GK The ER in 3D: a multifunctional dynamic membrane network Trends in Cell Biology. In press. xx (1-9) (2011).

32. Milstein C, Brownlee GG, Harrison TM, Mathews MB. A possible precursor of immunoglobulin light chains. Nature: New Biology 239 (91): 117–20 (1972).

33. Walter P, Ibrahimi I, Blobel G. Translocation of proteins across the endoplasmic reticulum. I. Signal recognition protein (SRP) binds to in-vitro-assembled polysomes synthesizing secretory protein. J. Cell Biol. 91 (2 Pt 1): 545–50 (1981).

34. Blobel G, Dobberstein B. Transfer of proteins across membranes. I. Presence of proteolytically processed and unprocessed nascent immunoglobulin light chains on membrane-bound ribosomes of murine myeloma. J. Cell Biol. 67 (3): 835–51 (1975).

35. Walter P and Blobel G. Purification of a membrane-associated protein complex required for protein translocation across the endoplasmic reticulum Proc. Natl. Acad. Sci. 77:7112-7116 (1980).

36. Rapoport TA, Goder V, Heinrich SU, Matlack KE. Membrane-protein integration and the role of the translocation channel. Trends Cell Biol. Oct;14(10):568-75 (2004).

37. Stefanovic S and Hegde RS. Identification of a targeting factor for posttranslational membrane protein insertion into the ER. Cell 128, 1147–1159 (2007).

38. Schuldiner, M. et al. The GET complex mediates insertion of tail-anchored proteins into the ER membrane. Cell 134, 634–645 (2008).

39. Favaloro V, Spasic M, Schwappach B and Dobberstein B. Distinct targeting pathways for the membrane insertion of tail-anchored (TA) proteins. J. Cell Sci. 121, 1832–1840 (2008).

40. Mariappan M Li X, Stefanovic S, Sharma A, Mateja A, Keenan RJ, Hegde RS. A ribosome-associating factor chaperones tail-anchored membrane proteins Nature 466 1120-1124 (2010).

41. Dafforn TR, Della M, Miller AD. The molecular interactions of heat shock protein 47 (Hsp47) and their implications for collagen biosynthesis. J. Biol. Chem. 276 (52): 49310–49319 (2001).

42. Sargsyan E, Baryshev M, Szekely L, Sharipo A and Mkrtchian S. Identification of ERp29, an Endoplasmic Reticulum Lumenal Protein, as a New Member of the Thyroglobulin Folding Complex J. Biol. Chem. 277, 17009-17015 (2002).

43. Ruoppolo M, Orrù S, Talamo F, Ljung J, Pirneskoski A, Kivirikko KI, Marino G, Koivunen P. Mutations in domain a' of protein disulfide isomerase affect the folding pathway of bovine pancreatic ribonuclease A. Protein Sci. 12 (5): 939–52 (2003).

44. Zhang JX, Braakman I, Matlack KES, and Helenius A. Quality Control in the Secretory Pathway: The Role of Calreticulin, Calnexin and BiP in the Retention of Glycoproteins with C-Terminal Truncations Mol. Biol. Cell 8 (10) 1943-1954 (1997).

45. Selkoe DJ. Folding proteins in fatal ways. Nature 426 900-904 (2003).

46. Bernales, Papa and Walter. Intracellular signaling by the unfolded protein response. Annual Review of Cell and Developmental Biology, 22: 487–508 (2006).

47. Bernales S, McDonald KL, Walter P. Autophagy counterbalances endoplasmic reticulum expansion during the unfolded protein response. PLoS Biol. 4(12):e423. (2006).

48. Shaffer, A. L., Shapiro-Shelef, M., Iwakoshi, N. N., Lee, A. H., Qian, S. B., Zhao, H., Yu, X., Yang, L., Tan, B. K., Rosenwald, A. et al. (2004). XBP1, downstream of Blimp-1, expands the secretory apparatus and other organelles, and increases protein synthesis in plasma cell differentiation. Immunity 21, 81-93.

49. Sriburi, R., Bommiasamy, H., Buldak, G. L., Robbins, G. R., Frank, M., Jackowski, S. and Brewer, J. W. (2007). Coordinate regulation of phospholipid biosynthesis and secretory pathway gene expression in XBP-1(S)-induced endoplasmic reticulum biogenesis. J. Biol. Chem. 282, 7024-7034334, 333

50. Sriburi, R., Jackowski, S., Mori, K. and Brewer, J. W. (2004). XBP1: a link between the unfolded protein response, lipid biosynthesis, and biogenesis of the endoplasmic reticulum. J. Cell Biol. 167, 35-41.

51. Calfon, M., H. Zeng, F. Urano, J.H. Till, S.R. Hubbard, H.P. Harding, S.G. Clark, and D. Ron. 2002. IRE1 couples endoplasmic reticulum load to secretory capacity by processing the XBP-1 mRNA. Nature. 415:92–96.

52. Vembar SS, Brodsky JL. One step at a time: endoplasmic reticulum-associated degradation. Nat. Rev. Mol. Cell Biol. 9 (12): 944–57 (2008).

53. Li, M., Baumeister, P., Roy, B., Phan, T., Foti, D., Luo, S. and Lee, A. S. (2000). ATF6 as a transcription activator of the endoplasmic reticulum stress element: thapsigargin stress-induced changes and synergistic interactions with NF-Y and YY1. Mol. Cell. Biol. 20, 5096-5106.

54. Scheuner, D., Song, B., McEwen, E., Liu, C., Laybutt, R., Gillespie, P., Saunders, T., Bonner-Weir, S. and Kaufman, R. J. (2001). Translational control is required for the unfolded protein response and in vivoglucose homeostasis. Mol. Cell 7, 1165-1176.

55. Yoshida, H., Haze, K., Yanagi, H., Yura, T. and Mori, K. (1998). Identification of the cis-acting endoplasmic reticulum stress response element responsible for transcriptional induction of mammalian glucose-regulated proteins. Involvement of basic leucine zipper transcription factors.J. Biol. Chem. 273, 33741-33749.

56. West, M. et al. (2011) A 3D analysis of yeast ER structure reveals how ER domains are organized by membrane curvature. J. Cell Biol. 193, 333–346

57. Hu, J., Y. Shibata, C. Voss, T. Shemesh, Z. Li, M. Coughlin, M.M. Kozlov, T.A. Rapoport, and W.A. Prinz. 2008. Membrane proteins of the endoplasmic reticulum induce high-curvature tubules. Science. 319:1247–1250.

58. Puhka, M., H. Vihinen, et al. (2007). Endoplasmic reticulum remains continuous and undergoes sheet-to-tubule transformation during cell division in mammalian cells. The Journal of cell biology 179(5): 895-909

59. Y. Shibata, et al. Mechanisms determining the morphology of the peripheral ER. Cell, 143 (2010), pp. 774–788

60. Nikonov AV, Hauri HP, Lauring B, and Kreibich G. Climp-63-mediated binding of microtubules to the ER affects the lateral mobility of translocon complexes. J. of Cell Sci. 120, 2248-2258 (2007).

61. Nikonov AV, Snapp E, Lippincott-Schwartz J, and Kreibich G. Active translocon complexes labeled with GFP–Dad1 diffuse slowly as large polysome arrays in the endoplasmic reticulum. J. Cell Biol. 158, 497–506 (2002).

62. Shibata Y., Shemesh T., Prinz W.A., Palazzo A.F., Kozlov M.M., Rapoport T.A. 2010. Mechanisms determining the morphology of the peripheral ER. Cell. 143:774–788

63. Sparkes I, Tolley N, Aller I, Svozil J, Osterrieder A, Botchway S, Mueller C, Frigerio L, Hawes C. Five Arabidopsis reticulon isoforms share endoplasmic reticulum location, topology, and membrane-shaping properties. Plant Cell. 22:1333–1343 (2010).

64. Kuehn MJ, Schekman R. COPII and secretory cargo capture into transport vesicles. Curr Opin Cell Biol. 9(4):477-83 (1997).

65. Kaiser C, Ferro-Novick S. Transport from the endoplasmic reticulum to the Golgi. Curr Opin Cell Biol. 10(4):477-82 (1998).

66. Palade G. Intracellular aspects of the process of protein synthesis. Science. 12;189(4206):867 (1975).

67. Merisko EM, Fletcher M, Palade GE. The reorganization of the Golgi complex in anoxic pancreatic acinar cells. Pancreas. 1(2):95-109 (1986).

68. S.I. Bannykh and W.E. Balch, Membrane dynamics at the endoplasmic reticulum-Golgi interface. J. Cell Biol., 138 (1997), pp. 1–4

69. A.T. Hammond and B.S. Glick, Dynamics of transitional endoplasmic reticulum sites in vertebrate cells. Mol. Biol. Cell, 11 (2000), pp. 301

70. B.J. Bevis, A.T. Hammond, C.A. Reinke and B.S. Glick, De novo formation of transitional ER sites and Golgi structures in Pichia pastoris. Nat. Cell Biol., 4 (2002), pp. 750–756. |

71. D.J. Stephens, De novo formation, fusion and fission of mammalian COPII-coated endoplasmic reticulum exit sites. EMBO Rep., 4 (2003), pp. 210–217.

72. Mancias JD, Goldberg J. Structural basis of cargo membrane protein discrimination by the human COPII coat machinery. EMBO J. 27 (21): 2918–28 (2008).

73. Murshid A and Presley JF. ER-to-Golgi transport and cytoskeletal interactions in animal cells. Cellular and Molecular Life Sciences 61, 2 133-145 (2004).

74. Connerly PL, Esaki M, Montegna EA, Strongin DE, Levi S, Soderholm J, Glick BS. Sec16 is a determinant of transitional ER organization. Curr Biol. 15(16):1439-47 (2005).

75. R.E. Gimeno, P. Espenshade and C.A. Kaiser, COPII coat subunit interactions: Sec24p and Sec23p bind to adjacent regions of Sec16p. Mol. Biol. Cell, 7 (1996), pp. 1815–1823.

76. D.A. Shaywitz, P.J. Espenshade, R.E. Gimeno and C.A. Kaiser, COPII subunit interactions in the assembly of the vesicle coat. J. Biol. Chem., 272 (1997), pp. 25413–25416.

77. Iinuma T, Shiga A, Nakamoto K, O'Brien MB, Aridor M, Arimitsu N, Tagaya M, Tani K. Mammalian Sec16/p250 plays a role in membrane traffic from the endoplasmic reticulum. J Biol Chem. 282(24):17632-9 (2007).

78. West, M. et al. A 3D analysis of yeast ER structure reveals how ER domains are organized by membrane curvature. J. Cell Biol. 193, 333–346 (2011)

79. Anderson, D.J. and Hetzer, M.W. Reshaping of the endoplasmic reticulum limits the rate for nuclear envelope formation. J. Cell Biol. 182, 911–924 (2008)

80. De Craene, J-O. et al. Rtn1p is involved in structuring the cortical endoplasmic reticulum. Mol. Biol. Cell 17, 3009–3020 (2006)

81. Shibata, Y. et al. Mechanisms determining the morphology of the peripheral ER. Cell 143, 774–788 (2010)

82. Sparkes, I. et al. Five Arabidopsis reticulon isoforms share endoplasmic reticulum location, topology, and membrane-shaping properties. Plant Cell 22, 1333–1343 (2010).

83. Toyoshima C, Nakasako M, Nomura H, Ogawa H. Crystal structure of the calcium pump of sarcoplasmic reticulum at 2.6 A resolution. Nature 405 (6787): 647–55 (2000).

84. Walz B. Ca2+-sequestering smooth endoplasmic reticulum in an invertebrate photoreceptor. I. Intracellular topography as revealed by OsFeCN staining and in situ Ca accumulation. JCB vol. 93 no. 3 839-848 (1982)

85. D J Waxman and L Azaroff. Phenobarbital induction of cytochrome P-450 gene expression. Biochem J. 1992 February 1; 281(Pt 3): 577–592.

86. Brown, MS, Goldstein, JL. The SREBP pathway: regulation of cholesterol metabolism by proteolysis of a membrane-bound transcription factor. Cell 1997. 89:331-340.

87. Horton, JD, Shimomura, I. Sterol regulatory element-binding proteins: activators of cholesterol and fatty acid biosynthesis. Curr Opin Lipidol 1999. 10:143-150.

88. Edwards, PA, Tabor, D, Kast, HR, Venkateswaran, A. Regulation of gene expression by SREBP and SCAP. Biochim Biophys Acta 2000. 1529:103-113.

89. Sakakura, Y, et al. Sterol regulatory element-binding proteins induce an entire pathway of cholesterol synthesis. Biochem Biophys Res Commun 2001. 286:176-183.

90. Corvera S, D'Arrigo A and Stenmar H Phosphoinositides in membrane traffic Current Opinion in Cell Biology 11, 4, 460-465 (1999).

91. Carrasco S, Meyer T. STIM Proteins and the Endoplasmic Reticulum-Plasma Membrane Junctions. Annu Rev Biochem. [Epub ahead of print] (2010).

92. Csordás G, Renken C, Várnai P, Walter L, Weaver D, Buttle KF, Balla T, Mannella CA, Hajnóczky G. Structural and functional features and significance of the physical linkage between ER and mitochondria. J Cell Biol. 25;174(7):915-21. (2006).

93. Guengerich FP. Cytochrome p450 and chemical toxicology. Chem. Res. Toxicol. 21 (1): 70–83 (2008).

94. Friedman, J.R. e t al. ER sliding dynamics and ER-mitochondrial contacts occur on acetylated microtubules. J. Cell Biol. 190, 363–375 (2010)

95. Wozniak, M.J. et al. Role of kinesin-1 and cytoplasmic dynein in endoplasmic reticulum movement in VERO cells. J. Cell Sci. 122, 1979– 1989 (2009).

96. Baumann O, and Walz B. Endoplasmic reticulum of animal cells and its organization into structural and functional domains. Int. Rev. Cytol. 205, 149–214 (2001).

97. Moss, T.J., C. Andreazza, A. Verma, A. Daga , and J.A. McNew. Membrane fusion by the GTPase atlastin requires a conserved C-terminal cytoplasmic tail and dimerization through the middle domain . Proc. Natl. Acad. Sci. 108 : 11133 – 11138 (2011).

98. C. Vedrenne, H.P. Hauri, Morphogenesis of the endoplasmic reticulum: beyond active membrane expansion, Traffic 7 (2006) 639–646

96. Y. Shibata, G.K. Voeltz, T.A. Rapoport, Rough sheets and smooth tubules, Cell 126 (2006) 435–439.

97. S.L. Dabora, M.P. Sheetz, The microtubule-dependent formation of a tubulovesicular network with characteristics of the ER from cultured cell extracts, Cell 54 (1988) 27–35.

98. J.D. Lane, V.J. Allan, Microtubule-based endoplasmic reticulum motility in Xenopus laevis: activation of membrane-associated kinesin during development, Mol Biol Cell 10 (1999) 1909–1922

99. C.M. Waterman-Storer, E.D. Salmon, Endoplasmic reticulum membrane tubules are distributed by microtubules in living cells using three distinct mechanisms, Curr. Biol. 8 (1998) 798–806.

101. C. Lee, M. Ferguson, L.B. Chen, Construction of the endoplasmic reticulum, J Cell Biol 109 (1989) 2045–2055.

102. A.T. Brunger, B. DeLaBarre, NSF and p97/VCP: similar at first, different at last, FEBS Lett 555 (2003) 126–133.

103. H. Kondo, C. Rabouille, R. Newman, T.P. Levine, D. Pappin, P. Freemont, G. Warren, p47 is a cofactor for p97-mediated membrane fusion, Nature 388 (1997) 75–78.

104. M. Hetzer, H.H. Meyer, T.C.Walther, D. Bilbao-Cortes, G.Warren, I. W. Mattaj, Distinct AAA-ATPase p97 complexes function in discrete steps of nuclear assembly, Nat. Cell. Biol. 3 (2001) 1086–1091.

105. K. Uchiyama, E. Jokitalo, F. Kano, M. Murata, X. Zhang, B. Canas, R. Newman, C. Rabouille, D. Pappin, P. Freemont, H. Kondo, VCIP135, a novel essential factor for p97/p47-mediated membrane fusion, is required for Golgi and ER assembly in vivo, J Cell Biol 159 (2002) 855–866.

106. K. Uchiyama, G. Totsukawa, M. Puhka, Y. Kaneko, E. Jokitalo, I. Dreveny, F. Beuron, X. Zhang, P. Freemont, H. Kondo, p37 is a p97 adaptor required for Golgi and ER biogenesis in interphase and at the end of mitosis, Dev Cell 11 (2006) 803–816.

107. G.K. Voeltz, W.A. Prinz, Y. Shibata, J.M. Rist, T.A. Rapoport, A class of membrane proteins shaping the tubular endoplasmic reticulum, Cell 124 (2006) 573–586.

108. J. Hu, Y. Shibata, C. Voss, T. Shemesh, Z. Li, M. Coughlin, M.M. Kozlov, T.A. Rapoport, W.A. Prinz, Membrane proteins of the endoplasmic reticulum induce high-curvature tubules, Science 319 (2008) 1247–1250.

109. A. Audhya, A. Desai, K. Oegema, A role for Rab5 in structuring the endoplasmic reticulum, J Cell Biol 178 (2007) 43–56.

110. M.L. Lacombe, L. Milon, A. Munier, J.G. Mehus, D.O. Lambeth, The human Nm23/nucleoside diphosphate kinases, J Bioenerg Biomembr 32 (2000) 247–258.

111. R.P. Agarwal, B. Robison, R.E. Parks, Nucleoside diphosphokinase from human erythrocytes, Methods in Enzymology 51 (1978) 376–386.

112. H. Plutner, H.W. Davidson, J. Saraste, W.E. Balch, Morphological analysis of protein transport from the ER to Golgi membranes in digitonin-permeabilized cells: role of the P58 containing compartment, J Cell Biol 119 (1992) 1097–1116.

113. D.J. Mackay, F. Esch, H. Furthmayr, A. Hall, Rho- and rac-dependent assembly of focal adhesion complexes and actin filaments in permeabilized fibroblasts: an essential role for ezrin/radixin/moesin proteins, J Cell Biol 138 (1997) 927–938.

114. S. Rajagopalan, Y. Xu, M.B. Brenner, Retention of unassembled components of integral membrane proteins by calnexin, Science 263 (1994) 387–390.

115. P. Barraud, L. Amrein, E. Dobremez, S. Dabernat, K. Masse, M. Larou, J.Y. Daniel, M. Landry, Differential expression of nm23 genes in adult mouse dorsal root ganglia, J Comp Neurol 444 (2002) 306–323.

116. V.P. Pinon, G. Millot, A. Munier, J. Vassy, G. Linares-Cruz, J. Capeau, F. Calvo, M.L. Lacombe, Cytoskeletal association of the A and B nucleoside diphosphate kinases of interphasic but not mitotic human carcinoma cell lines: specific nuclear localization of the B subunit, Exp Cell Res 246 (1999) 355–367.

117. J. Biggs, E. Hersperger, P.S. Steeg, L.A. Liotta, A. Shearn, A Drosophila gene that is homologous to a mammalian gene associated with tumor metastasis codes for a nucleoside diphosphate kinase, Cell 63 (1990) 933–940.

119. F.R. Frankel, Organization and energy-dependent growth of microtubules in cells, Proc Natl Acad Sci U S A 73 (1976) 2798–2802.

120. T.W. Keenan, D.J. Morre, Phospholipid class and fatty acid composition of Golgi apparatus isolated from rat liver and comparison with other cell fractions, Biochemistry 9 (1970) 19–25.

121. G. Blin, E. Margeat, K. Carvalho, C.A. Royer, C. Roy, C. Picart, Quantitative analysis of the binding of ezrin to large unilamellar vesicles containing phosphatidylinositol 4,5 bisphosphate, Biophysical journal 94 (2008) 1021–1033.

122. J.E. Harlan, P.J. Hajduk, H.S. Yoon, S.W. Fesik, Pleckstrin homology domains bind to phosphatidylinositol-4,5-bisphosphate, Nature 371 (1994) 168–170.

123. T.P. Levine, S. Munro, Targeting of Golgi-specific pleckstrin homology domains involves both PtdIns 4-kinase-dependent and-independent components, Curr Biol 12 (2002) 695–704.

124. V. Papayannopoulos, C. Co, K.E. Prehoda, S. Snapper, J. Taunton,W. A. Lim, A polybasic motif allows N-WASP to act as a sensor of PIP (2) density, Mol Cell 17 (2005) 181–191.

125. R.F. Epand, U. Schlattner, T.Wallimann, M.L. Lacombe, R.M. Epand, Novel lipid transfer property of two mitochondrial proteins that bridge the inner and outer membranes, Biophysical journal 92 (2007) 126–137.

126. O. Lambert, N. Cavusoglu, J. Gallay,M. Vincent, J.L. Rigaud, J.P. Henry, J. Ayala-Sanmartin, Novel organization and properties of annexin 2-membrane complexes, J Biol Chem 279 (2004) 10872–10882.

127. S.G. Taneva, P.J. Patty, B.J. Frisken, R.B. Cornell, CTP: phosphocholine cytidylyltransferase binds anionic phospholipid vesicles in a cross-bridging mode, Biochemistry 44 (2005) 9382–9393.

128. H. Hama, N. Almaula, C.G. Lerner, S. Inouye, M. Inouye, Nucleoside diphosphate kinase from Escherichia coli; its overproduction and sequence comparison with eukaryotic enzymes, Gene 105 (1991) 31–36.

129. T. Fukuchi, J. Nikawa, N. Kimura, K. Watanabe, Isolation, overexpression and disruption of a Saccharomyces cerevisiae YNK gene encoding nucleoside diphosphate kinase, Gene 129 (1993) 141–146.

130. T. Ouatas, B. Abdallah, L. Gasmi, J. Bourdais, E. Postel, A. Mazabraud, Three different genes encode NM23/nucleoside diphosphate kinases in Xenopus laevis, Gene 194 (1997) 215–225.

131. H.N. Fournier, C. Albiges-Rizo, M.R. Block, Newinsights into Nm23 control of cell adhesion and migration, J Bioenerg Biomembr 35 (2003) 81–87.

132. N. Kimura, N. Shimada, Y. Ishijima, M. Fukuda, Y. Takagi, N. Ishikawa, Nucleoside diphosphate kinases in mammalian signal transduction systems: recent development and perspective, J Bioenerg Biomembr 35 (2003) 41–47.

133. K.S. Krishnan, R. Rikhy, S. Rao, M. Shivalkar, M. Mosko, R. Narayanan, P. Etter, P.S. Estes, M. Ramaswami, Nucleoside diphosphate kinase, a source of GTP, is required for dynamindependent synaptic vesicle recycling, Neuron 30 (2001) 197–210.

134. F. Palacios, J.K. Schweitzer, R.L. Boshans, C. D'Souza-Schorey, ARF6-GTP recruits Nm23-H1 to facilitate dynamin-mediated endocytosis during adherens junctions disassembly, Nat Cell Biol 4 (2002) 929–936.

135. G. Baillat, S. Gaillard, F. Castets, A. Monneron, Interactions of phocein with nucleoside-diphosphate kinase, Eps15, and Dynamin I, J Biol Chem 277 (2002) 18961–18966.

136. N. Kimura, N. Shimada, Membrane-associated nucleoside diphosphate kinase from rat liver. Purification, characterization, and comparison with cytosolic enzyme, J Biol Chem 263 (1988) 4647–4653.

137. M.H. Bosnar, J. De Gunzburg, R. Bago, L. Brecevic, I. Weber, J. Pavelic, Subcellular localization of A and B Nm23/NDPK subunits, Exp Cell Res 298 (2004) 275–284.

138. A. Godi, A. Di Campli, A. Konstantakopoulos, G. Di Tullio, D.R. Alessi, G.S. Kular, T. Daniele, P. Marra, J.M. Lucocq, M.A. De Matteis, FAPPs control Golgi-to-cell-surface membrane traffic by binding to ARF and PtdIns(4)P, Nat Cell Biol 6 (2004) 393–404.

139. M. Krauss, V. Haucke, Phosphoinositide-metabolizing enzymes at the interface between membrane traffic and cell signalling, EMBO Rep 8 (2007) 241–246.

140. S. Taneva, J.E. Johnson, R.B. Cornell, Lipid-induced conformational switch in the membrane binding domain of CTP:phosphocholine cytidylyltransferase: a circular dichroism study, Biochemistry 42 (2003) 11768–11776.

141. D. Arac, X. Chen, H.A. Khant, J. Ubach, S.J. Ludtke, M. Kikkawa, A.E. Johnson,W. Chiu, T.C. Sudhof, J. Rizo, Close membrane-membrane proximity induced by Ca(2+)-dependent multivalent binding of synaptotagmin-1 to phospholipids, Nature structural & molecular biology 13 (2006) 209–217.

142. C. Vedrenne, D.R. Klopfenstein, H.P. Hauri, Phosphorylation controls CLIMP-63-mediated anchoring of the endoplasmic reticulum to microtubules, Mol Biol Cell 16 (2005) 1928–1937.

143. I. Grigoriev, S.M. Gouveia, B. van der Vaart, J. Demmers, J.T. Smyth, S. Honnappa, D. Splinter, M.O. Steinmetz, J.W. Putney Jr., C.C. Hoogenraad, A. Akhmanova, STIM1 is a MT-plus-end-tracking protein involved in remodeling of the ER, Curr Biol 18 (2008) 177–182.

144. Zhu, P.P., A. Patterson, B. Lavoie, J. Stadler, M. Shoeb, R. Patel, and C. Blackstone. 2003. Cellular localization, oligomerization, and membrane association of the hereditary spastic paraplegia 3A (SPG3A) protein atlastin . J. Biol. Chem. 278 : 49063 – 49071

145. Praefcke , G.J. , and H.T. McMahon . 2004 . The dynamin superfamily: universal membrane tubulation and fission molecules? Nat. Rev. Mol. Cell Biol. 5 : 133 – 147.

147. Prakash, B., G.J. Praefcke , L. Renault, A. Wittinghofer , and C. Herrmann. 2000. Structure of human guanylate-binding protein 1 representing a unique class of GTP-binding proteins . Nature . 403 : 567 – 571

148. Ghosh , A. , G.J. Praefcke , L. Renault , A. Wittinghofer , and C. Herrmann . 2006 . How guanylate-binding proteins achieve assembly-stimulated processive cleavage of GTP to GMP . Nature . 440 : 101 – 104 .

149. Chappie , J.S. , S. Acharya , M. Leonard , S.L. Schmid , and F. Dyda . 2010 . G domain dimerization controls dynamin's assembly-stimulated GTPase activity. Nature . 465 : 435 – 440

150. Daumke , O. , and G.J. Praefcke . 2011 . Structural insights into membrane fusion at the endoplasmic reticulum . Proc. Natl. Acad. Sci. USA . 108 : 2175 – 2176 .

151. Ludtke , S.J. , P.R. Baldwin , and W. Chiu . 1999 . EMAN: semiautomated software for high-resolution single-particle reconstructions . J. Struct. Biol. 128 : 82 – 97

152. Tang , G. , L. Peng , P.R. Baldwin , D.S. Mann , W. Jiang , I. Rees , and S.J. Ludtke . 2007 . EMAN2: an extensible image processing suite for electron microscopy. J. Struct. Biol. 157 : 38 – 46

153. Pieper , U., B.M. Webb, D.T. Barkan, D. Schneidman-Duhovny , A. Schlessinger , H. Braberg , Z. Yang , E.C. Meng , E.F. Pettersen , C.C. Huang , et al . 2011 . ModBase, a database of annotated comparative protein structure models, and associated resources . Nucleic Acids Res. 39 (Suppl. 1): D465 – D474

154. Niemann , H.H. , M.L. Knetsch , A. Scherer , D.J. Manstein , and F.J. Kull . 2001 . Crystal structure of a dynamin GTPase domain in both nucleotidefree and GDP-bound forms . EMBO J. 20 : 5813 – 5821.

155. Neal , S.E. , J.F. Eccleston , A. Hall , and M.R. Webb . 1988 . Kinetic analysis of the hydrolysis of GTP by p21N-ras. The basal GTPase mechanism . J. Biol. Chem. 263 : 19718 – 19722

156. Song , B.D. , and S.L. Schmid . 2003 . A molecular motor or a regulator? Dynamin's in a class of its own . Biochemistry . 42 : 1369 – 1376

156. Song , B.D. , M. Leonard , and S.L. Schmid . 2004 . Dynamin GTPase domain mutants that differentially affect GTP binding, GTP hydrolysis, and clathrinmediated endocytosis . J. Biol. Chem. 279 : 40431 – 40436 .

157. Stowell , M.H. , B. Marks , P. Wigge , and H.T. McMahon . 1999 . Nucleotidedependent conformational changes in dynamin: evidence for a mechanochemical molecular spring . Nat. Cell Biol. 1 : 27 – 32

158. Sanderson CM, Connell J, Edwards TL, Bright NA, Duley S, Thompson A, Luzio P, Reid E. Spastin and atlastin, two proteins mutated in autosomal dominant hereditary spastic paraplegia, are binding partners. Hum Mol Genet. 2006 15(2): 307–318.